EUROPEAN ORGANIZATION FOR NUCLEAR RESEARCH
PS DIVISION

THE STUDY OF A EUROPEAN NEUTRINO FACTORY COMPLEX

P. Gruber[a] (ed), M. Aleksa[a], J. F. Amand[a], B. Autin[a], J. L. Baldy[a], M. Benedikt[a], R. Benett[b], A. Bernardon[a], A. Blondel[l], K. Bongardt[c], R. Cappi[a], M. Castellano[d], E. Chiaveri[a], J. P. Delahaye[a], C. J. Densham[b], P. Drum[b], R. Edgecock[ab], A. Fabich[a], G. Franchetti[c], J. Gareyte[a], R. Garoby[a], U. Gastaldi[f], F. Gerigk[b], S. Gilardoni[al], M. Giovannozzi[a], S. Hancock[a], K. Hanke[a], H. Haseroth[a], Ch. Hill[a], I. Hoffman[e], B. Holzer[a], K. Hübner[a], A. Jansson[j], C. D. Johnson[a], C. Johnstone[g], D. Küchler[a], J. Lettry[a], M. Lindroos[a], A. Lombardi[a], M. Martini[a], F. Meot[h], E. Metral[a], M. Migliorati[d], D. Möhl[a], A. S. Müller[a], D. Neuffer[g], L. Palumbo[d], J. Pasternak[a], A. Perrin[a], W. Pirkl[a], M. Poehler[a], C. Prior[b], H. Ravn[a], G. Rees[b], A. Riche[a], S. Russenschuck[a], R. D. Ryne[i], K. Schindl[a], H. Schönauer[a], S. Schriber[j], R. Scrivens[a], Yu. Senichev[k], P. Sievers[a], M. Silari[a], F. Tazzioli[d], H. Ullrich[a], N. Vassilopoulos[a], A. Verdier[a], M. Vretenar[a], F. Wenander[a], E. J. N. Wilson[a], C. Wyss[a], M. F. Zimmermann[a], M. Zisman[i], P. Zucchelli[a]

ABSTRACT

The Neutrino Factory is a new concept for an accelerator that produces a high-intensity, high-energy beam of electron and muon neutrinos – the ultimate tool for neutrino oscillation studies and the only machine conceived up today that could help detect CP violation of leptons.

The basic concept of the Neutrino Factory is the production of neutrinos from the decay of high-energy muons. Due to their short lifetime, these muons have to be accelerated very fast. Several new accelerator techniques, like a high-intenstiy proton linac, high-power targets, ionization cooling or recirculating muon linacs are required. This paper presents a snapshot of the accelerator design at CERN. Although some aspects of this European Neutrino Factory Scheme have been optimised for the CERN site, the basic principle is site-independent.

[a] CERN, [b] RAL, [c] FZ Jülich, [d] INFN Frascati, [e] GSI, [f] INFN Legnaro, [g] FNAL, [h] Saclay, [i] LBNL, [j] LANL, [k] University of Aarhus, [l] University of Geneva

CONTENTS

1 Executive Summary

The Neutrino Factory is a new concept for an accelerator that produces a high-intensity, high-energy beam of electron and muon neutrinos, first proposed by S. Geer [Geer98]. With the first experimental evidence of neutrino oscillations at Super-Kamiokande [suk98] in Japan, the neutrino puzzle is now one of the most interesting topics in particle physics. Oscillations are directly linked to a non-zero mass for at least one of the neutrinos, requiring an extension of the Standard Model. Furthermore, these oscillations could violate CP conservation. CP violation is known in the hadronic sector, but has not yet been seen for leptons. Neutrinos are the only candidates for CP violation in the leptonic sector, which could explain the anti-symmetry between matter and antimatter in the universe. Finally, the extremely low neutrino mass could provide insight into an extremely large mass scale through the so-called 'see-saw' mechanism.

This paper presents the current status of the accelerator design at CERN. The design has been optimised for the CERN site, making use of existing hardware and infrastructure. The proton driver of the Neutrino Factory could even contribute to a possible upgrade of the LHC beam brilliance. The basic principle of the European Neutrino Factory scheme is, however, site-independent. There have been other intensive studies on this subject in the USA [fer00, bnl01] and Japan[Mor02].

The Neutrino Factory will increase the precision of the mass differences Δm^2_{13} and Δm^2_{12} from 10% (planned MINOS and KAMLAND experiments) to 1%. It will dramatically increase the sensitive region for the mixing angles $\sin^2\theta_{13}$ (see Fig. 1.1) and $\sin^2\theta_{23}$. Moreover, the Neutrino Factory is the only machine that can discover a possible CP-violation and measure the phase δ.

The Neutrino Factory has many features that allow a big step forward in neutrino physics:

- **High intensity** Its intensity is 10^3 times greater than current man-made neutrino beams.

- **High energy** As the number of neutrino interactions increases linearly with the beam energy, the Neutrino Factory features a very high beam energy of 20-50 GeV.

- **Two flavours** Perfectly suited for oscillation physics, the Neutrino Factory delivers a beam of two flavours (muon neutrino and electron anti-neutrino) at the same time.

- **Two charges** In the Neutrino Factory, the muon sign can be selected. Thus it is possible to deliver the anti-particles of the above, allowing the search for CP-violation.

The basic concept of the Neutrino Factory is the production of muon neutrinos and electron antineutrinos from muon decay. An intense proton beam is delivered to a target, where pions are produced. These pions are collected in a magnetic field, selecting one charge sign. In a 30 m long decay channel the pions decay into muons. At this stage, the beam has an enormous energy spread and transverse emittance. The first is reduced using phase rotation, the second with ionisation cooling. The cooled beam is accelerated in one linac and two recirculating linacs to energies of 20 to 50 GeV and injected into a storage ring. This storage ring has two long straight sections that point towards two neutrino detectors. Whenever muons decay in one of the straight sections, each of them produces two neutrinos, which are directed to one of the detectors, thus forming an intense neutrino beam.

Apart from neutrino physics, the Neutrino Factory complex could be used for muon and kaon physics as well as for studies of the quark structure through deep inelastic scattering of neutrinos. The proton driver could be used as an injector for the PS to increase the average proton current for fixed-target experiments and the brilliance of the beam provided by the PS for LHC. It could also be shared with other planned facilities such as the EURISOL radioactive ion-beam facility or a spallation neutron source.

This paper demonstrates that the European Neutrino Factory seems to be feasible and concepts exist to deliver the 10^{21} muons per year defined as a target number by the physics community. The current Neutrino Factory scenario has been driven by the aim to reach the target number and is far from being optimised. Further research – especially to increase the muon transmission –. can increase the intensity or relax some parameters. Some novel technologies, such as ionisation cooling, have yet to be proven. Serious efforts are needed to make this machine more efficient and affordable. Considering the time horizon of other neutrino activities around the world, the time is now ripe to enter into a detailed study of this machine.
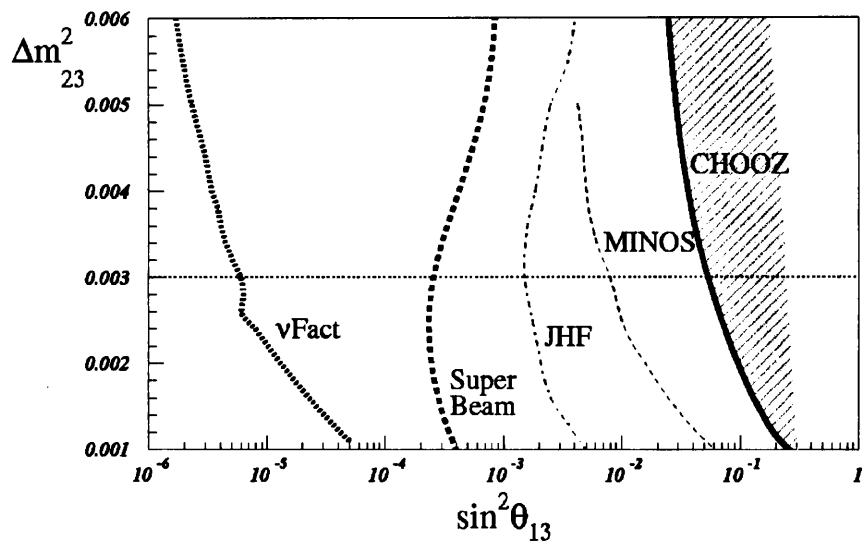
Fig. 1.1: Comparison of reach in the $\nu_\mu \to \nu_e$ oscillations. The Neutrino Factory has by far the largest discovery potential. Right to left: present limit from the CHOOZ experiment; expected sensitivity from the MINOS experiment; from the 0.75 MW JHF to Super-Kamiokande project with an off-axis narrow-band beam; from a possible neutrino superbeam from the 4 MW CERN-SPL to a 400 kton water Cerenkov detector in the Fréjus tunnel; and from a Neutrino Factory with a 40 kton large magnetic detector. The dashed horizontal line is the current best estimate for the mass difference from Super-Kamiokande.

2 The Neutrino Factory

2.1 Introduction

The recent discovery of neutrino oscillations at Super-Kamiokande [suk98] has brought a lot of attention to neutrino physics. While observing solar neutrinos can help to solve the puzzle of neutrino physics, solar neutrino physics suffers from low detection cross-sections because of the low energy of the solar neutrinos and from uncertainties about the neutrino source – the sun. Ultimate answers to the questions on neutrino oscillations and CP violation with neutrinos can only be found with an intense, high-energy, man-made beam.

Of the many neutrino sources, muons are the most promising mother particles. They have a moderately short lifetime of 2.2 µs that still allows the manipulation of a muon beam while delivering the decay neutrinos sufficiently fast. The muon decay produces two neutrinos of different flavours, which allows for crosschecking and the elimination of beam systematics. If muons are mass-produced, accelerated, and injected into a storage ring, where they decay, they can produce an intense, well-controlled neutrino beam. This is the concept of the Neutrino Factory [Geer98].

Unfortunately, muons cannot be produced directly, so a precursor particle, the pion has to be produced. The first stage of any neutrino factory is thus a high-power proton driver that shoots protons onto a target, where – among other particles – pions are produced. These pions have to be collected and transported. After about 20m, most pions have decayed into muons. At this stage, the muon beam has a low phase space density and resembles more a cloud than a beam. Its transverse emittance is huge and it has an energy spread from zero to almost the maximum proton energy. The next step is to create a useable muon beam. Longitudinally, phase rotation is applied to reduce the energy spread. As it is not possible to completely eliminate it, the phase rotation is optimised to flatten out the most important part of the energy spectrum, while particles outside the 'momentum bite' are lost. Transversally, ionisation cooling is applied to reduce the emittance by a factor of 4 per plane. Once the beam is cooled, it can be accelerated to a final energy of 30–50 GeV (this is the optimum energy range to allow the detection of neutrino oscillations). This acceleration has to be very fast in order to avoid unnecessary muon decay losses. In the final stage of the Neutrino Factory, the accelerated muons are injected into a storage ring with long straight sections. They decay all over the storage ring and whenever they decay in one of the two long straight sections, their decay products contribute to the neutrino beam. In the decay ring, the muons have a relativistic γ of 300–500, so their lifetime in the laboratory frame is 0.7–1.1 ms. After a few lifetimes, all muons have decayed and the storage ring is free for the next bunch of muons. This implies a rather high repetition rate of the overall machine, in the range of several tens to hundreds hertz. There are three possible geometries for the decay ring: a racetrack, a triangle, and a bow-tie. The first has only one downhill straight section and can thus serve only one far detector. The two latter ones can serve two detectors, possibly located at two different distances to provide complementary results. The bow-tie is the more efficient geometry, while the triangle is easier to build. For the moment, the CERN scenario is based on a triangular decay ring with two detectors at distances of about 700 km and 3000 km.

The detectors need to have a large mass, as the number of events observed is proportional to the product of the beam intensity times the detector mass.

From the very description of this type of neutrino factory, it is apparent that such a machine is a very complex project that needs many years of R&D before approval. If the scenario presented here has reasonable technical grounds, several major areas, especially pion production and collection, muon cooling and fast acceleration, can still be improved and the goal is to arrive at a design that is both robust and affordable.

2.2 The goal of this study

This study is aimed at reaching the target intensity of 10^{21} muons/year using existing or realistic technologies. Currently, the design is consistent but not optimised. This paper aims at giving a snapshot of the current CERN research activities. It presents what the Neutrino Factory Working Group has so far identified as the 'baseline scenario'. There are five chapters, following the five main areas of research, which are proton driver, pion production, muon cooling, muon acceleration, and the storage ring. In each chapter, the current state of the baseline scenario is presented, followed by a brief discussion of alternative scenarios. These alternative

scenarios have been studied or might become necessary if some of the assumptions that this study is based on have to be modified.

As this is a report about work in progress, a list of open questions as well as the next R&D steps needed form the end of each chapter.

2.3 Physics motivation and requirements for a high-intensity neutrino machine

After the exciting results of the Super-Kamiokande experiments, the flavour changing processes in neutrino propagation (neutrino oscillation) is a phenomenon with solid experimental evidence [suk98].

$$
\begin{pmatrix} v_e \\ v_\mu \\ v_\tau \end{pmatrix} = \begin{pmatrix} 1 & 0 & 0 \\ 0 & c_{23} & s_{23} \\ 0 & -s_{23} & c_{23} \end{pmatrix} \begin{pmatrix} c_{13} & 0 & s_{13}e^{-i\delta} \\ 0 & 1 & 0 \\ -s_{13}e^{-i\delta} & 0 & c_{13} \end{pmatrix} \begin{pmatrix} c_{12} & s_{12} & 0 \\ -s_{12} & c_{12} & 0 \\ 0 & 0 & 1 \end{pmatrix} \begin{pmatrix} v_1 \\ v_2 \\ v_3 \end{pmatrix}
$$

Neutrino oscillations arise from the fact that the Standard Model describes the interaction between massless neutrinos of different flavours (electron-neutrino, muon-neutrino, tau-neutrino), and if the masses are measured to be non-zero, there is no reason for flavours and mass eigenstates to coincide. The latter appear in the Schrödinger equation that describes the neutrino propagation in space. From the hypothesis that the flavour base does not correspond to the mass bases, one can express a flavour state as a linear combination of mass eigenstates. As measured at LEP [lep01], there are only three active neutrino flavours; hence the matrix that describes the relation between neutrino flavour and mass states has to be 3×3, where e, μ, τ are the flavour states, 1 2 3 the mass states associated to the mass m_1, m_2 and m_3, $c_{ij} = \cos\theta_{ij}$ and $s_{ij} = \sin\theta_{ij}$ with θ_{ij} the mixing angle, δ the CP violation phase.

In total, as free parameters to measure, there are three mixing angles, one CP phase, and two squared mass differences.

Once a neutrino is produced, it is in one of the flavour states, but as it propagates, it can turn into another flavour state, according to the probability computed from the Schrödinger equation and quantum mechanics. For example, the probability for a muon neutrino of energy E to turn into a tau neutrino after a distance L in vacuum is equal to:

$$
P(v_\mu \rightarrow v_\tau) = \sin^2 2\theta_{23} \sin^2 \left(\frac{\Delta m_{13}^2 L}{4E_v}\right)
$$

being $\Delta m_{13}^2 = m_1^2 - m_3^2$. This probability is non-zero only if the mixing angle and the square mass difference are both non-zero: neutrinos mix and they have mass (see Ref. [cgg02] for a review).

Considering a given distance L between source and detector and a given energy spectrum, Nature provides a source for measuring θ_{23} via atmospheric neutrinos (v_μ disappearance) and θ_{12} from solar neutrinos (v_e disappearance). The only existing limit for the third mixing angle θ_{13} comes for the CHOOZ reactor experiment [apo99] but there is still no experimental evidence that this angle has to be different from zero. If this were the case, solar ($v_e \rightarrow v_{\mu,\tau}$) and atmospheric ($v_\mu \rightarrow v_\tau$) would be two separate oscillation regimes.

A number of experiments in the near future will increase the precision in the measurement of the mixing matrix parameters, but still, some important questions will remain unsolved, namely:

- Which is the sign of the mass differences Δm_{23}^2?
- What is the exact value of the angle θ_{13}?
- Does the CP violation in the leptonic sector exist? And if yes, what is the value of the violating phase delta?

None of the existing available neutrino sources, natural or man-made, has or will have the possibility to provide answers to these questions as precisely as the neutrino factory, mostly because one needs a high-energy electron neutrino source known with high precision.

A neutrino beam produced from muon decay $\mu^+ \to e^+ + \nu_e + \bar{\nu}_\mu$ ($\mu^- \to e^- + \bar{\nu}_e + \nu_\mu$) at high energy (tens GeV range) and under controlled conditions, as in the case of the neutrino factory, would offer the following advantages:

- electron neutrinos at high energy,
- the neutrino spectrum is known precisely from the muon energy and polarisation;
- the beam is pure since there are two neutrino flavours at the same time but with different leptonic charges.

The parameters of the neutrino factory and the detector baselines can be optimised for the maximum number of oscillation events. The cross-section σ_ν for neutrino interactions grows linearly with energy E while the oscillation probability is a function of $\sin^2 L/E$ with L being the baseline length. Supposing L/E constant to optimise the oscillation probability P, the number of events is calculated as follows:

$$N_{osc} \sim \text{Flux} \times \sigma_\nu \times P(\nu_\alpha \to \nu_\beta) \sim \frac{E_\nu^3}{L^2} \sin^2 \frac{L}{E_\nu} \propto E_\nu$$

which means that the higher the energy E, the more statistics one would have for the measurements. However, once the neutrino energy is fixed, the choice of the distance comes from the maximum of the oscillation probability for a given mass difference ($\Delta m^2_{13} \sim 3 \cdot 10^{-3}$ eV^2), and the baseline is limited by the Earth's diameter. A good compromise for the neutrino energy seems to be 30–50 GeV and for the baseline lengths around 2500 and 7000 kilometres to get the right sensitivity to the oscillation parameters.

The signal for oscillations to be looked at in the detector is clear: if the neutrino factory produces positive muons, they will decay into electron neutrinos and muon antineutrinos. In the far detector, the charged-current interaction of muon antineutrinos will again produce positive muons, while electron neutrinos oscillated into muon neutrinos will produce negative muons. In this way, one can simply separate the number of negative and positive muons and extract the oscillation parameters. The technique of counting the 'wrong sign muons' will permit the measurement of [cer00]:

- θ_{13} and θ_{23} with the precision of 0.1% or down to limit of about 10^{-3};
- CP violation with good sensitivity over the complete LMA (Large Mixing Angle) solution for solar neutrinos;
- the sign of the squared mass difference via the MSW effect (see below).

The CP-violation phase can be extracted from the difference between the two probabilities $P(\nu_e \to \nu_\mu)$ and $P(\bar{\nu}_e \to \bar{\nu}_\mu)$ by changing the sign of the muons produced by the neutrino factory [jbc01]. The advantage of a source like the neutrino factory is that both of the neutrinos of same flavour but opposite helicity are produced in the same condition, cancelling the systematic errors due to limited knowledge of the beam properties.

The sign of the Δm^2_{13} would be extracted from the electron neutrino oscillation. In fact, electron neutrinos interact in matter in a different way than the other flavours, since ordinary matter contains electrons (MSW effect, named after the physicists S. P. Mikheev, A. Yu. Smirnov and L. Wolfenstein). Matter would act on electron neutrinos as a birefringent medium would act on one component of polarised light, inducing an extra phase in the neutrino propagation formula, and varying the oscillation probability in vacuum. The effect induced strongly depends on the material density, the distance between source and detector, and on the sign of Δm^2_{13}.

The physics requirements can be translated into a table of desired machine parameters as expressed in the NuFact'99 workshop at Lyon [ICFA00]:

Parameter	Value	Reason
Intensity	10^{21} v/yr	Low neutrino cross-section
Min. energy	30 GeV	Low neutrino cross-section at low energies
Max. energy	50 GeV	Oscillation maximum must be smaller than Earth's diameter; CP violation effect is covered by matter effect
Precision beam parameters	1%	To avoid systematic errors. Emittance, divergence, and intensity must be known to better than 1%

7

2.4 The basic concept of the CERN Neutrino Factory scenario

The reference scenario described here is based on the particular situation at CERN. It is intended as a working hypothesis that is in part CERN, specific, while being dominated by the wish to achieve the required high muon flux [Pal99].

The present CERN accelerators cannot meet the requirements stated in Section 2.3 and are not suited to easy upgrade of the available beam power. However, a proposal [Gar99] has been made to replace the CERN PS injector complex (50 MeV linac and 1.4 GeV booster) by a linear accelerator, destined primarily as injector into the PS for the LHC beam. It was intended to offer a higher brilliance LHC beam from the PS. The basic idea in proposing to build this linac is to re-use the cavities, klystrons, and auxiliary equipment from LEP. The average beam power of 4 MW appears to be feasible. In this scenario it is envisaged to use this linac with beam energy of 2.2 GeV. This linac could also be used for the pion production of the neutrino factory. The results of the HARP experiment [Dyd99], will measure the production cross-section in this energy range and will produce data by the end of 2002. These results will be crucial in the final assessment of the choice of proton driver.

Protons hitting a target produce pions, which decay very rapidly into muons. The pions do not form a beam in the usual meaning of the word, but depart from the target in all directions and with a very large energy spread. To make efficient use of the produced pions, it is necessary to collect them. After the pion decay, it is necessary to reduce the muon energy spread and to modify their angular distribution so that they fit into a smaller aperture. Only in this way can one produce a beam, which can be accelerated and stored in a technically reasonable machine.

Reducing the energy spread is called 'phase rotation' and is basically the acceleration of low energetic muons and the deceleration of high-energy muons. This can be achieved by conventional rf cavities if a phase-energy correlation in the muon beam can be built up, because the acceleration (deceleration) depends on the phase. This is possible with all non-relativistic beams.

Reducing the transverse phase space is called 'cooling', which is achieved by slowing down the muons and accelerating them in the forward direction with rf cavities. Ideally one would stop the muons completely and accelerate them, which would result in the best beam. However, the muon lifetime is only 2.2 μs and most of the muons would decay before being accelerated. For the very same reason, fast acceleration using high gradients is necessary to benefit from the relativistic increase of their lifetime in the laboratory frame.

To allow for phase rotation, the neutrino factory requires the production of beam pulses consisting of relatively short trains of very short proton bunches. This makes it possible to use bunch rotation to reduce the large energy spread within the muon bunches. The pulse repetition rate must not be too high; otherwise the energy consumption of the subsequent accelerators becomes too high. Also it would be wasteful if a new injection into the storage ring took place before the previous batch had decayed (the ring design employs full-aperture kickers and so injection would kill the previous circulating muon beam). The linac cannot directly provide a suitable beam; hence it will operate with H⁻ ions and inject into an accumulator ring, using charge-exchange injection to achieve a large circulating proton current. Bunches will be formed in this ring with suitable rf cavities. They will be transferred into a compressor ring for further shortening of their length. The linac will operate at 50 Hz and initial pulse duration of 2.8 ms at a mean current of 13 mA during the pulse. After accumulation and compression the resulting beam pulse, now shortened to 3.2 μs – the revolution period in the accumulator and compressor rings – contains a bunch train comprising 140 bunches spaced at 44 MHz frequency. It is assumed that the accumulator and compressor rings will be accommodated in the old ISR tunnel.

This beam will irradiate the production target. Furthermore about 10–20% of the 4 MW beam power is transferred as heat to the target. Currently, it is planned to use a liquid mercury jet as a target. This jet explodes after the passage of the beam and thus the heat load is carried away with the material while induced activity can be distilled away.

It is necessary to capture the pions produced in the target. At CERN there is considerable experience with magnetic horns for the collection of antiprotons and in the production of (conventional) neutrino beams. It is therefore worth while to investigate the possibility of using a magnetic horn also for the neutrino factory.

Because of the high repetition rate and the large number of bunches, an rf system is proposed for the manipulation of the muons after the pion decay. The rf system will capture and phase-rotate the muon

bunches, and it will also be used in the ionisation cooling of the muon beam in order to compensate the loss of energy of the muon due to ionisation when passing through matter. Further acceleration of the muons to 2 GeV is performed in a special linac with solenoid focusing, followed by more conventional quadrupole focusing. Subsequent acceleration takes place in two Recirculating Linacs (RLAs) to an energy of 50 GeV. The muons are then injected into a storage ring (decay ring) where they decay completely. (At 50 GeV, the muon lifetime is 1 ms and the next beam is injected after 20 ms.) The muons decaying in the long straight sections of this ring produce the required neutrino beams. A schematic layout of this CERN reference scenario is presented in Fig. 2.1. Figure 2.2 shows a possible layout of the neutrino factory on the CERN site. Note that the muon storage ring (MSR) needs to be properly aligned once the detector sites are fixed.
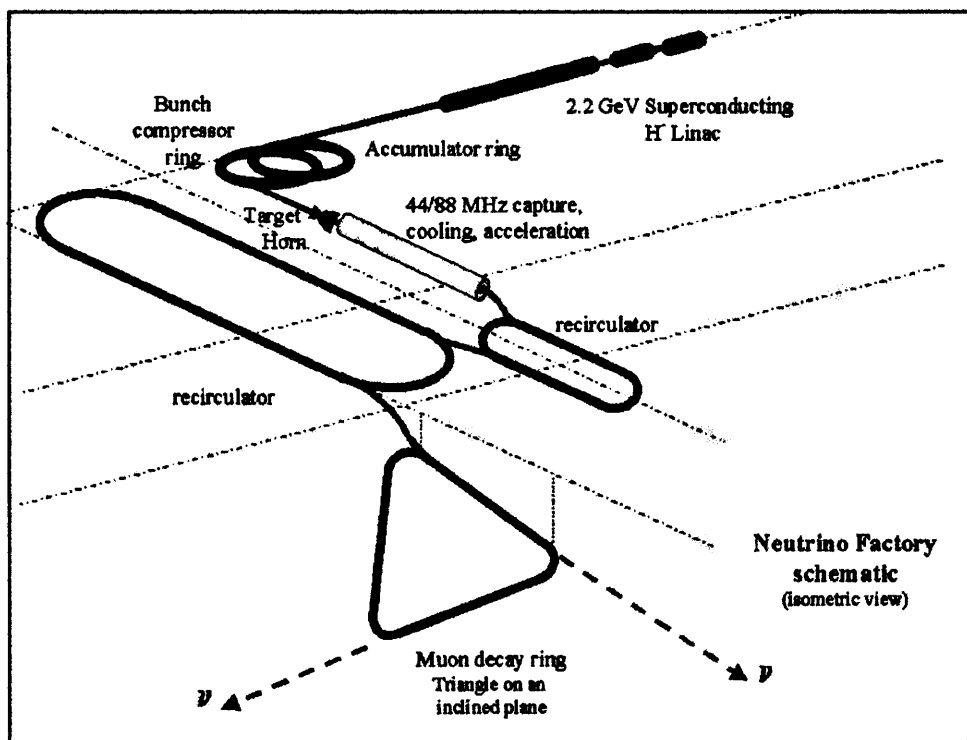

Fig. 2.1: Schematic of Neutrino Factory showing a triangular decay ring

2.5 Other possible uses of a neutrino factory

There are several other uses of the neutrino factory that could come as a by-product.

- The Neutrino Factory can be envisaged as a part of a multipurpose facility, sharing the proton driver with other users such as the EURISOL radioactive ion beam facility or a spallation neutron source.

- Slow muons that cannot be used for neutrino production can be used for stopped muon experiments [stop].

- Kaons that are produced as a by-product from the pion production can be used for Kaon physics [kaon].

- Neutrinos could be used for deep inelastic scattering experiments in a facility close to the decay ring [dis]
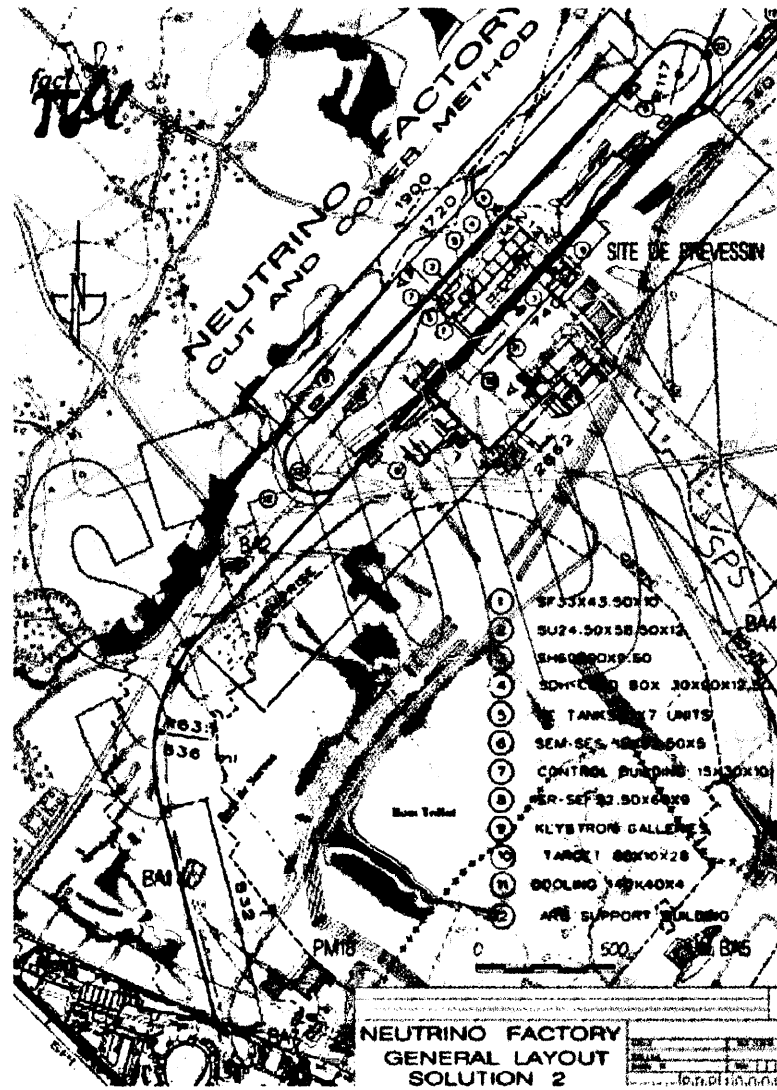
9

Fig. 2.2: Possible layout of a Neutrino Factory on the CERN site. The SPL and the accumulator ring can be seen at the lower left on the Meyrin site, while target station, cooling, recirculating linacs, and decay ring could be situated on the Prévessin site.

2.6 Parameter list

Table 2.1 Overall Neutrino Factory parameters

Proton beam power	4 MW
Repetition rate	50 Hz
Target material	Hg
Magnet. horn current (inner/outer)	300/600 kA
Phase rotation	with rf
Absorber material	liquid H_2
Muons in storage ring	10^{21}/yr

Table 2.2 Overview of the geometry and the beam parameters of all subsystems. Note that over 90% of the muons are lost (see column 'intensity')

Part	Geometry			Beam (at the end of the part)						RF system		Magn. system	
	Size	Turns	$\alpha_\perp$ rms [cm mrad]	Particle	E [GeV]	Intensity [particles/s]	$\varepsilon_\perp^N$ (rms)[1] [cm mrad]	Total ΔE [MeV]	Bunch length	Freq. [MHz]	Real estate gradient/ tot. voltage	Focus	B[T]
SPL	$l = 691$ m	–	–	p	2.2	1.1×10^{16}	–	0.4	–	352.2	3.5 .... 9 MV/m	quad	
Accumulator	$c \approx 942$ m	≈ 1000	–	p	2.2	1.1×10^{16}	–	0.4	17 ns	44	0.3 MV	quad	
Compressor	$c \approx 942$ m	7	–	p	2.2	1.1×10^{16}	–	0.4	6 ns	44 (88)	2 (0.35) MV	quad	
After the horn	–	–	–	π	0...1	2.2×10^{15}	$2000\pi^2$	>1000	6 ns	–	–		
Decay channel	$l = 30$ m	–	–	$\pi \to \mu$	0.2	2.15×10^{15}	3080π	>1000	>6 ns	–	–		
Phase rotation	$l = 30$ m	–	3080π	μ	0.2	1.14×10^{15}	3080π	80	5.6 ns[3]	–	–	solenoid	1.8 T
Cooling I	$l = 46$ m	–	3080π	μ	0.2	3.96×10^{14}	2230π	80	5.6 ns	44	2 MV/m	solenoid	1.8 T
Acceleration	$l = 32$ m	–	2230π	μ	0.28	3.96×10^{14}	2230π	80	5.6 ns	44	2 MV/m	solenoid	2.0 T
Cooling II	$l = 112$ m	–	2230π	μ	0.3	2.42×10^{14}	910π	80	2.8 ns	88	4 MV/m	solenoid	5.0 T
Acceleration IIa	$l = 500$ m	–	1500π	μ	≈ 2	1.54×10^{14}	$>910\pi$[4]	80	2.8 ns	88	4 MV/m	solenoid	5.0 T
Phase rotation II	$l \approx 200$ m	–	1500π	μ	≈ 2	1.54×10^{14}	$>910\pi$	400	0.5 ns	220	4 MV/m	...[5]	...[e]
Acceleration IIb	$l \approx 250$ m	–	1500π	μ	3	1.54×10^{14}	$>910\pi$	400	0.5 ns	220	4 MV/m	...[e]	...[e]
RLA I (w/o arcs)	$l = 350$ m	4	1500π	μ	11	$>10^{14}$	$>910\pi$	800	0.5 ns	220	4 MV/m	quad	0.5 T
RLA II (w/o arcs)	$l = 1900$ m	4	1500π	μ	50	$>10^{14}$	$>910\pi$	>800	0.5 ns	352	4 MV/m	quad	0.5 T
Decay ring	$c = 2075$ m	<500	1500π	$\mu \to \nu$	≤ 50	$>10^{14}$	$>910\pi$	>800	0.5 ns	352	(100 MV)	quad	0.5 T

[1] In this design, the ideal aperture limit is 3σ, implying a 2D-acceptance α = 9ε. This value is *not* always achieved. In these cases particles are (deliberately) lost.
[2] Emittance for particles within the energy range of 0.1...0.3 GeV; normalized to the reference energy of 0.2 GeV.
[3] The actual bunch is longer. The length of the captured bunch is 5.6 ns. All other particles are lost.
[4] Simulations show small transverse emittance growth in the accelerator parts after the end of cooling. Detailed numbers are not available.
[5] To be determined

3 Proton driver

3.1 Introduction

A high-power proton beam is used in the neutrino factory to produce pions that decay into muons and later into neutrinos. The layout of the CERN Neutrino Factory baseline design leads to a number of requirements for the proton driver:

Power In order to produce the target number of 10^{21} muons/year in the decay ring, current estimates (based on current capture efficiencies and losses) show that a beam power of 4 MW is required.

Proton energy Currently, the pion production cross-section is not very well known, and above a threshold energy of 2 GeV the useful pion spectrum seems to depend only on the proton beam power and not on the proton energy. For the moment, any energy can be chosen. The HARP experiment at the CERN PS currently measures pion production cross-sections for proton energies in the range of 2–15 GeV. One possible outcome of HARP is a preference for a certain proton driver energy.

Bunch length and spacing As the CERN scenario is based on the bunch-to-bucket principle (one proton bunch produces particles that fill one rf bucket at 44 MHz), a very short bunch length of 1 ns rms is needed. The bunch spacing has to match the rf frequency of the downstream phase rotation and cooling. Furthermore, the train of proton bunches must be shorter than the decay ring.

Repetition rate Muon lifetime at 50 GeV allows a repetition rate of <100 Hz, although the pulsed magnetic horn and the pulsed cavities in the front end make lower rates of <50 Hz desirable. Power consumption in the front end is largely dominated by the repetition rate, as the rise time of the pulsed cavities is two orders of magnitude longer than the beam length.

If the above requirements are met, any proton driver design can be chosen. In the following section, the CERN baseline design – based on a 2.2 GeV superconducting linac – and three alternative designs based on Rapid Cycling Synchrotrons (RCSs) are presented. The final choice of proton driver will be influenced by the results of HARP and considerations of other possible uses of the proton drivers. The parameters for these four choices are summarised in Table 3.1.

Rapid cycling synchrotrons are favoured for kinetic energies above ~3 GeV. The repetition rate is inversely proportional to the energy (from 50 Hz at 5 GeV to 25 Hz at 15 GeV [Pri00] and 8.33 Hz at 30 GeV [Sch00, Sch00a]). An attractive feature is the possibility to have a large distance between bunches.

For energies below 3 GeV, a linac complemented with storage rings is sufficient. In order to achieve short pulses, the cycling rate must be rather large, and 50 Hz is the minimum to achieve 4 MW at 2.2 GeV.

This scenario is based on the bunch-to-bucket principle, which means that all pions/muons generated by one proton bunch are collected in one rf bucket of the front end. This implies that the distance between the bunches has to be matched to the front end. Furthermore, to achieve both a high bunching factor in the Proton Driver Accumulator-Compressor (PDAC) and a low energy spread at the end of bunch compression, a short distance between bunches is preferred.

Table 3.1 Comparison of proton drivers

	Beam power	Repetition rate	Bunches per train	Bunch distance
Linac + storage rings [Sch00]	Potential for >4 MW	50 Hz	140	22.7 ns
5 GeV RCS [Pri00]	4 MW	50 Hz (2 × 25Hz)	4	340 ns
15 GeV RCS [Pri00]	4 MW (up to 6 MW)	25 Hz (2 × 12.5Hz)	18	130 ns
30 GeV RCS [Sch00, Sch00a]	4 MW	8.33 Hz	8	400 ns

The Linac solution is presently preferred at CERN [Sch00, Vre00] because of its potential for other uses, for example as a potential injector of the CERN PS, because of the advantage of re-using a substantial

amount of the LEP hardware, and because of its capability to be extended to higher beam powers. This low-energy scenario combines a 2.2 GeV, 50 Hz superconducting H⁻ linac (called Superconducting Proton Linac – SPL – for historical reasons) with an accumulator and a compressor ring: PDAC – the Proton Driver Accumulator-Compressor. This would fit well into the ISR tunnel of circumference 948 m. A 44 MHz rf system in both rings of the PDAC matching the muon rotation and cooling system is a natural choice, alleviating at the same time the bunch compression task. This choice, which is referred to as the reference scenario, will be reviewed at the end of 2002, using the results from the HARP experiment [Dyd99], which will measure the production of π^+ and π^- from different proton beam energies and different types of targets.

Meanwhile, in order to cope with a possible evolution in the neutrino factory design, the use of rapid cycling synchrotrons for the 4 MW proton drivers has also been studied. In collaboration with RAL, two site-independent 5 GeV, 50 Hz and 15 GeV, 25 Hz drivers have been investigated. In the case that slow repetition rates are finally preferred, we opted to study a 30 GeV, 8.33 Hz synchrotron (upgradeable to 8 MW, 15 Hz by adding a second ring), again using the ISR tunnel. RAL also designed a 180 MeV, 56 mA linac, derived from the ESS study [ESS96], which would be the injector in all three synchrotron-based scenarios.

The lower repetition rate of the RCS has a number of advantages. The average power dissipated in the magnetic horn is substantially reduced, the horn lifetime is increased, and the design of its power supply is simplified; the reduction of the pulsing rate of the large superconducting rf system in the Recirculating Linear Accelerator (RLA) is very welcome as it reduces the power consumption considerably.

3.2 Baseline design: The SPL scenario

The baseline proton driver scenario consists of a superconducting H⁻ linac (SPL) [Vre98, Gar99] that delivers 4 MW of 2.2 GeV protons at 50 Hz repetition rate. In order to achieve a short beam with short pulses, the protons are accumulated in an accumulation ring and then bunch-compressed in a second bunch compressor ring. These two rings have been designed to fit into the old ISR tunnels at CERN.

3.2.1 The Superconducting Proton Linac (SPL)

The proposed 700 m long SPL [Vre00a, Vre00a] makes extensive use of the large inventory of rf equipment from the dismantled LEP to accelerate H⁻ ions up to a kinetic energy of 2.2 GeV (Fig. 3.1). Room-temperature rf structures are used up to 120 MeV, and superconducting resonators from 120 to 2200 MeV. The main parameters of the SPL are listed in Table 3.2.

Table 3.2 SPL main parameters

Ions	H⁻
Kinetic energy	2.2 GeV
Mean beam power	4 MW
Repetition rate	50 Hz
Beam pulse length	2.8 ms
Mean current during the pulse	13 mA
Number of ions per pulse	2.27×10^{14}
Number of ions per second	1.1×10^{16}
rf and bunch frequency	352.2 MHz
Overall length	691 m
Peak rf power	37 MW
Mean grid power consumption	38 MW
Transverse normalised rms emittance	<0.6 μm
Bunch length at the entrance of the accumulator (total)	0.13 ns
Energy spread at the entrance of the accumulator (total)	0.4 MeV
Energy jitter at the entrance of the accumulator (max.)	± 2 MeV

13

Supplied by an H⁻ ion source at 45 keV potential, the beam is bunched and accelerated to 3 MeV in an rf quadrupole (RFQ) operating at 352 MHz. At this energy, a fast chopper eliminates the unwanted bunches and provides the proper time structure for an optimum longitudinal capture in the accumulator synchrotron after the Linac (see Section 3.2.2). A second RFQ brings the energy up to 7 MeV. Between 7 and 18 MeV, conventional Drift Tube Linac (DTL) structures are used, with quadrupole magnets housed in the drift tubes, inside the rf resonators. Above 18 MeV and up to 120 MeV Coupled Cavity Drift Tube Linac (CCDTL) structures are employed, with quadrupoles outside the resonators. Between 120 and 389 MeV, new modules containing multi-cell superconducting cavity modules are needed. From 389 MeV to 2.2 GeV, 128 new $\beta = 0.8$ five-cell cavities are fitted inside 32 LEP cryostats (see Fig. 3.1).
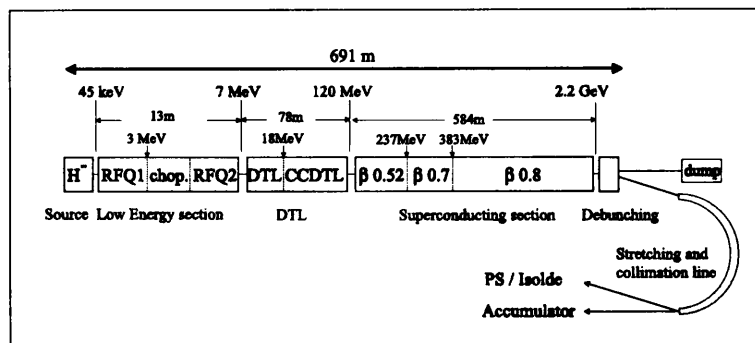

Fig. 3.1: SPL block diagram

A total of 46 LEP klystrons are employed for rf power generation (as many klystrons as in LEP2), as well as 32 LEP 4 cavities modules refurbished with new cavities (out of the 68 formerly used in LEP2).

Radiation handling is a key concern at such a high beam power. In order to permit hands-on maintenance, losses must be kept below 1 W/m, a challenging figure that requires an adequate machine design with a careful control of beam halo as well as an effective collimation system. Simulations predict that the current design fulfils this requirement. The large aperture of the LEP2 cavities is an advantage in this respect because most of the halo particles that develop after the initial collimation are transported to the end of the linac and dumped in collimator dumps so that radiation issues are localised and properly addressed.

Although a significant fraction of the total hardware is already available, some development effort is needed for all equipment of the 120 MeV room-temperature linac as well as for the low-beta superconducting cavities. The machine layout will be refined using the results of these hardware developments and the outcome of extended beam dynamics studies including the analysis and minimisation of halo. Conventional but important design and construction work will also be needed for the focusing, diagnostic and control equipment, the cryoplants, and the civil engineering of the 700 m accelerator tunnel and technical gallery.

3.2.2 Accumulator and compressor rings

In order to serve the neutrino factory, the 2.7 ms long pulse of low average current (13 mA) from the SPL needs to be converted into a train of short (1 ns rms) bunches. That is why an accumulator and a compressor ring are required. The length of the train must be below the circumference of ~2 km of the muon storage ring. A ring fitting into the existing ISR tunnel (C = 942 m, 15 m wide) is a possible choice for accumulating 2.3×10^{14} protons at 50 Hz (see Figure 3.2). The 2.2 GeV H⁻ ions from the linac pass through a stripping foil at the entrance of the accumulator ring where they lose both electrons. The resulting protons are efficiently accumulated over 845 turns in small emittance buckets in the accumulator ring. 140 of the 146 buckets generated by the 44 MHz rf system are progressively populated by up to 1.6×10^{12} protons/bunch. At the end of accumulation, the bunches are fast ejected and transferred into the compressor ring, where bunch compression by bunch rotation takes place in 7 turns, with 2 MV at 44 MHz and 350 kV at 88 MHz. The bunches of 1 ns rms are then ejected onto the pion production target.
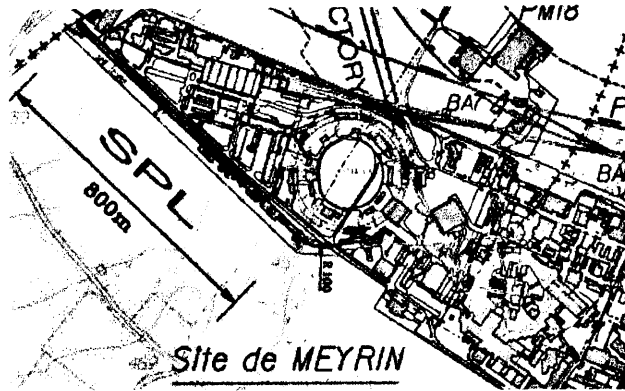
14

Fig. 3.2 Possible location of the proton driver complex on the CERN Meyrin site. SPL and accumulator/compressor rings in the ISR tunnels (in the center of the map).

An initial attempt to design a single ring with a nearly isochronous lattice at 2 GeV ($\gamma = 3.1$, $\gamma_t = 3.13$), capable of performing both accumulation and the bunch rotation with modest rf voltage, was discarded. It soon became clear that space charge causes blow-up of the <0.2 ns long linac micro-bunches, *and* requires high rf voltage for macro-bunch compression. Moreover, there is a strong non-linear effect of space charge on momentum compaction such that transition energy varies over the bunch. Much more robust appears a layout with *two* rings of *high* transition energy, separating the functions of accumulation and bunch rotation, as depicted in Figs. 3.3 and 3.4.
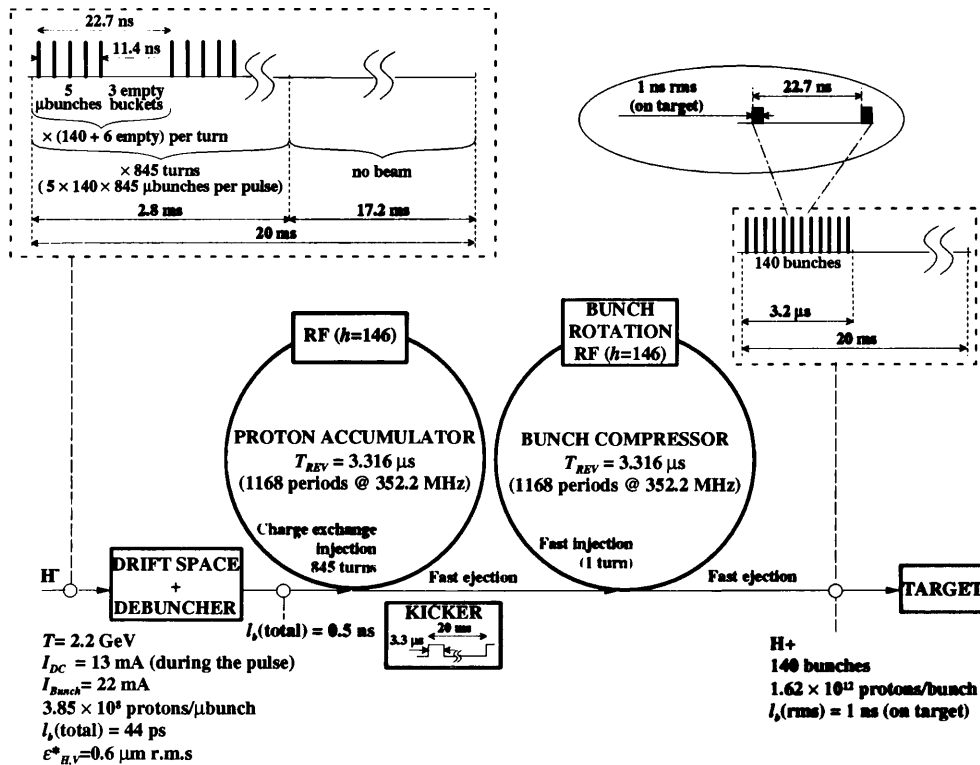

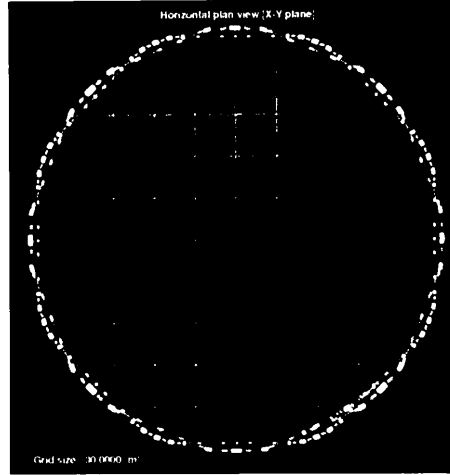**Fig. 3.3** Accumulator and compressor scheme for the Neutrino Factory

15

Fig. 3.4 The CERN reference proton driver: Accumulator/
compressor in the ISR tunnel. Grid size 30 m.

Owing to the high γ_t, the microbunches in the accumulator debunch quickly. Space charge has little influence on the linearity of the lattice, and the high synchrotron tune in the accumulator produces a smooth distribution in longitudinal phase space, which is a good start for the rotation. The latter requires more rf voltage, but the critical issue of fast cavity filling is circumvented. The pre-detuned, filled, compressor cavities minimise transient beam loading. The ring parameters are listed in Table 3.3.

Table 3.3 Parameter list for the 2.2 GeV proton driver accumulator-compressor

Parameter	Unit	Accumulator	Compressor
Beam			
Kinetic energy, T	GeV	2.2	
Pulse frequency	Hz	50	
Revolution period	μs	3.32	
Number of bunches		140	
Pulse intensity	p/pulse	2.3×10^{14}	
Bunch spacing	ns	22.7	
Bunch intensity	p/bunch	1.6×10^{12}	
Bunch length (4σ)	ns	14-17	6
Rel. momentum spread (2σ)		1.5×10^{-3}	5×10^{-3}
Norm. trans. emittance (1σ)	μm	55π	
Rings			
Radius, R	m	151	151
Main dipole magn. field, B	Tesla	0.69	0.49
Number of injected turns		845	1
η		-0.085	-0.086
γ-transition		14.84	15.09
Q_x, Q_y		11.23, 13.30	17.18, 16.40
RF			
rf voltage, V_{rf}(44 MHz)	MV	0.3	2
rf voltage, V_{rf}(88 MHz)	MV	-	0.35
Harmonic number, h (44 MHz)		146	
Harmonic number, h (88 MHz)		292	
rf frequency, f_{rf}	MHz	44.02	44.02 + 88.04
Synchrotron frequency, f_s	kHz	3.3	~11.3

For the proposed implantation of the SPL on the site, part of the debunching section and a 250 m long collimator achromat need also to be installed in the ISR tunnel. Figs. 3.5a, 3.5b shows a super period of the accumulator with a long dipole at the centre of a dispersion bump, which is absent in the compressor lattice (Figs. 3.6a, 3.6b). This low-field dipole bends the trajectory of the injected beam towards the foil with a minimum of excited H^0 states. The technique of ramping of the linac energy for horizontal 'painting' by placing the foil at a point of large dispersion (anti-correlated with a vertical orbit bump to produce a Kapchinsky–Vladimirsky-like ('hollow') transverse distribution) has been proposed for a number of high-intensity machines, notably ESS. With an average of 4–5 foil traversals of the circulating beam, the carbon foil temperature may exceed 2300 K, an issue that needs to be carefully studied.

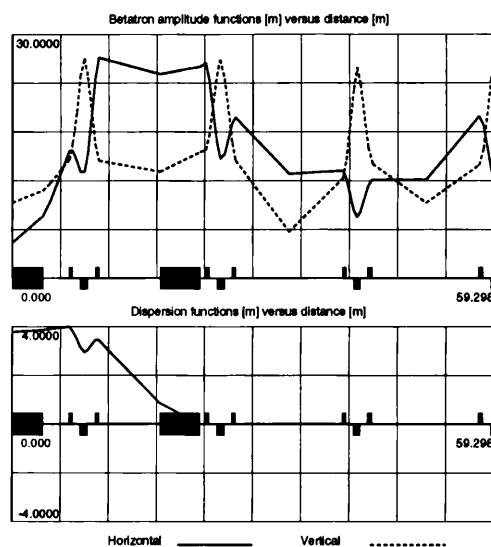**Fig. 3.5a** Structure of a superperiod of the accumulator

Fig. 3.5b Lattice functions β_H, β_V and D_H for one half-accumulator superperiod
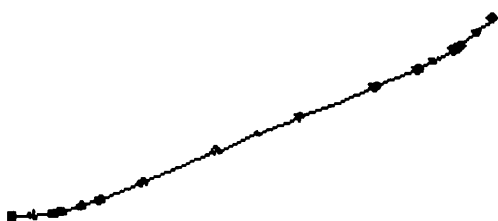

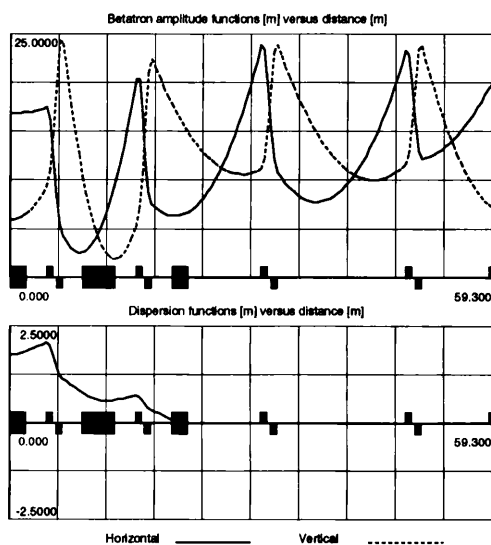**Fig. 3.6a** Structure of a superperiod of the compressor

Fig. 3.6b Lattice functions β_H, β_V and D_H for one half-compressor superperiod

17

In order to produce well confined bunches, only five out of the possible eight 352 MHz microbunches are accelerated in the linac and injected into the 44 MHz bucket, the others are removed by the chopper at the linac front-end. The rf voltage is raised linearly from 30 to 300 kV to maintain the bunch approximately matched in the presence of the increasing space charge. Owing to the high transition-γ, about six full synchrotron periods are completed during accumulation, yielding a smooth ellipse-like phase space distribution (Fig. 3.7a), and ensuring the desired bunch confinement before starting the rotation in the compressor (Fig. 3.7b).

Amongst the effects of space charge and collective instabilities in the accumulator, only the microwave instability raises concern. Its calculated growth time of 0.6 ms for a broadband impedance of $(Z/jn) = 1 \, \Omega$ is of the order of the accumulation time of 2.8 ms. A more detailed simulation predicts stability by Landau damping due to the tails of the distribution. Even the Laslett tune shift in the compressor at the end of bunch rotation is not more than $\Delta Q \sim -0.2$.
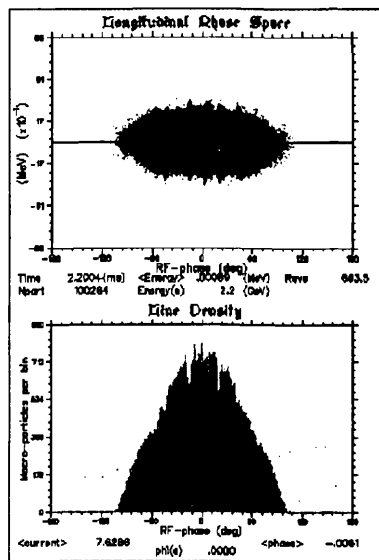

Fig. 3.7a Bunch after 845 turns (end) of accumulation / start of rotation. The horizontal scale is the phase in degrees.
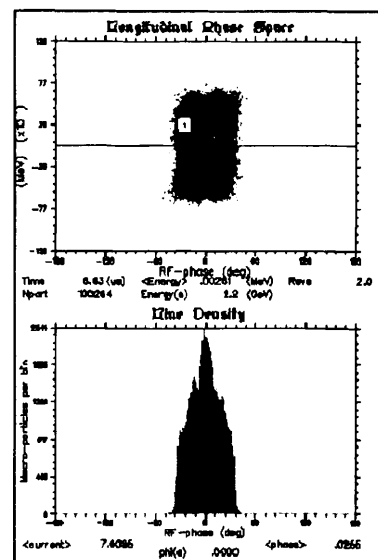
Fig. 3.7b Bunch after 7.5 turns (end of rotation) in the compressor. The horizontal scale is the phase in degrees. Note the different vertical scales.

3.2.3   Other uses of the SPL

Although designed for the needs of a neutrino factory, the SPL can replace the present injectors of the PS and improve its performance [Vre98]. The location of the SPL has been carefully chosen for an easy transfer of the beam to the PS and ISOLDE with minimum civil engineering (see Fig. 3.2).

The brilliance of the proton beam for LHC can be doubled. For the needs of users of high beam intensity, like the CERN Neutrino to Gran Sasso experiment (CNGS), a study group has identified the possible scenarios, the necessary upgrades in the PS and SPS, and quantified the potential improvements in performance [Capp01]. The present ISOLDE facility can be supplied with a beam, which is up to five times more intense (up to 10 μA, limited by the present ISOLDE lay-out) and better matched to the target capabilities, without interfering with the PS needs. In a future stage, the next generation ISOL facility, which will need a current of up to 100 μA, can also be satisfied.

In a staged approach, before the muon part of the neutrino factory is available, the 2.2 GeV/4 MW proton beam from the accumulator or the compressor ring can also be used to generate a conventional neutrino beam from pion decay. The interest for physics of such an intermediate facility is being actively investigated.

3.3 Rapid-cycling synchrotrons

3.3.1 Introduction

In case higher proton energies and/or lower repetition rates are desired, three scenarios of rapid cycling synchrotrons (RCS) have been studied. On two of them (the 5GeV and 15GeV machines), the ISIS Accelerator Group at the Rutherford Appleton Laboratory (RAL) has been actively collaborating with CERN. All machines are based on a 180 MeV injector linac designed by RAL.

3.3.2 Injector linac

Common to all RCS scenarios is a 180.2 MeV H⁻ injector linac operating at a mean current during pulse of 57 mA. The overall length is 129 m and the injector consists of a 2.493 MeV, 280 MHz radiofrequency quadrupole linac (RFQ), a chopper section, and an eight-tank, 280 MHz Alvarez linac. A 3 MW peak power rf generator is required by each of the eight tanks, including 25% additional power for field control. The chopping section provides a 70% beam duty cycle at a sub-harmonic of 280 MHz, which is close to the RF frequency of the booster rings at injection. Levels of transverse space charge are acceptable and full modelling of the linac has been carried out using the Los Alamos code PARMILA [path90].

The beam line between the linac and rings provides some debunching of the linac microbunches, subsequent momentum reduction, collimation and ramping, and vertical beam separation for each booster synchrotron. Separate 280 MHz cavities are required for each stage. A four-period, 41.6 m, achromatic collimator bends the H⁻ beam through 180° and includes reverse bends and two buncher cavities. The reverse bends enable the high normalised dispersion needed for momentum collimation to be achieved. A range of fractional momentum ramping up to 4×10^{-3} is provided for injection painting, with normalised transverse rms emittances of approximately 0.26 (π) μ rad.m.

3.3.3 The 5 GeV/25 Hz (Driver I) and 15 GeV/12.5 Hz (Driver II) rapid-cycling synchrotrons

Both scenarios consist of two boosters and two RSC rings that are stacked in order to increase the repetition rate on target. Two sets of design parameters are under consideration for the synchrotron-based models. The first option (Driver I, Fig. 3.8) uses four proton bunches per pulse at a final energy of 5 GeV and repetition rate of 50 Hz. The other (Driver II, Fig. 3.9) is at 25 Hz with six bunches per pulse at 15 GeV. Both scenarios aim to provide 4 MW of beam power, though Driver II has the potential to upgrade to 6 MW.
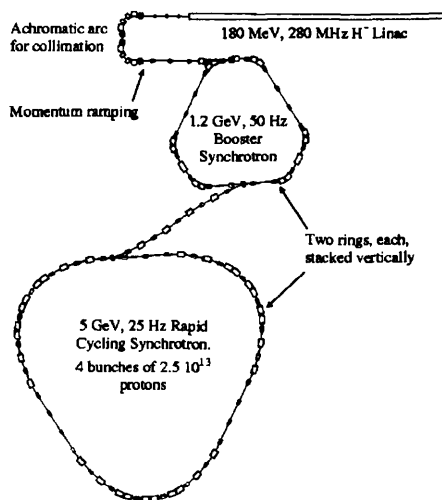

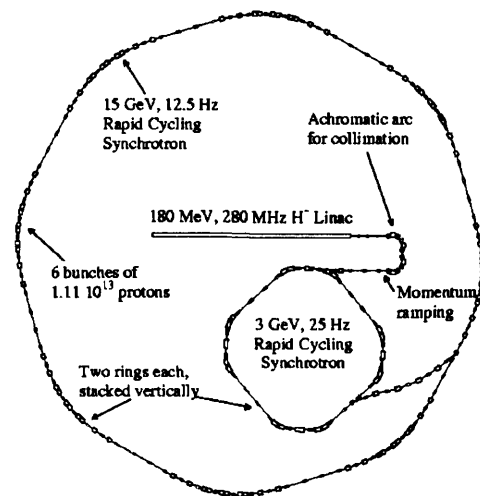Fig. 3.8 Layout of the 5 GeV, 50 Hz, 4 MW proton driver (Driver I).

Fig. 3.9 Layout of the 15 GeV, 25 Hz, 4 MW proton driver (Driver II).

The development of the designs has been influenced by two main factors. The aim is to generate final output bunches of high intensity and very short (1 ns rms) bunch lengths at the pion target. Achievement of the required intensity, via accumulation in the rings, presents different problems from final bunch compression, and no satisfactory common solution has been found. Each synchrotron scenario therefore uses separate booster rings for injection and a first stage of acceleration, followed by main rings for acceleration to full energy and compression. The short final bunch durations require a small final longitudinal emittance of the order of only 1 eVs if unacceptably high-energy spreads are to be avoided. From the equation for the longitudinal bucket area

$$A = \frac{8R\alpha}{hc} \sqrt{\frac{2\gamma(1-\eta_{sc})VE_0}{\pi h|\eta|}}$$

A will be minimised if γ, $1/h$, and $1/|\eta|$ are minimised and η_{sc} is a maximum. Here η is the slip factor $1/\gamma_t^2$-$1/\gamma^2$, α is the standard normalised Hamiltonian integrals and

$$\eta_{sc} = \frac{Negh^2}{2\varepsilon_0 RF\gamma^2 V}$$

is the ratio of the longitudinal space charge voltage to the applied cavity voltage. An upper limit of $\eta_{sc} = 0.4$ is taken to avoid the microwave instability. These conditions are most conveniently met with low injection energy, and a value in the range 150–200 MeV is preferred.

In view of these considerations, both schemes use a 180 MeV H$^-$ linac. In the case of Driver I the linac feeds two 50 Hz, 1.2 GeV synchrotrons, operating almost in phase. The rings are likely to be stacked one above the other. Together these feed in alternate cycles two 25 Hz, 5 GeV rings, also stacked vertically. The combined output, after bunch compression, is 5 GeV and 50 Hz. The final energy of 5 GeV has been selected for this study, as this is the lowest energy at which it appears practical to achieve the specified final synchrotron bunch lengths. For Driver II, the basic scheme remains the same but the two booster synchrotrons are now at 25 Hz and 3 GeV, and the main rings at 12.5 Hz and 15 GeV, with a combined output at 25 Hz.

3.3.3.1 Ring injection, trapping and acceleration

The use of booster and main rings allows the different requirements of injection and bunch compression to be treated separately. Triplet lattices, developed over a period of time for use in the European Spallation Source (ESS) [Bau96], have been adopted for the boosters, and provide both regions of high dispersion for injection and momentum collimation, and long dispersion-free straights for the rf systems, betatron collimation and fast extraction. The lattice functions and superperiod structure for the booster of Driver I are shown in Fig. 3.10; those for the booster of Driver II are similar. Booster I has three superperiods and mean radius 32.5 m, and Booster II has four superperiods and mean radius 50 m.

Injection of the chopped beam is via an Al$_2$O$_3$ stripping foil in a low-field dipole ($B(t)$~0.05 T) positioned at a point in the rings where the normalised dispersion $D_x/\sqrt{\beta_x}$ is in the range 1.6–1.8. One hundred and sixty turns are injected into Driver I over 200 μs and 70 turns into Driver II over 134 μs. The intervals are timed symmetrically about the minimum of an accelerating sinusoidal waveform $B(t) = B_0 - B_1\sin(2\pi ft)$. Thus injection is into a decelerating bucket at the start of injection and into an accelerating bucket at the end. The rf cavity voltages are carefully programmed so that the entire beam is injected into stable regions of longitudinal phase space, particularly in the latter stages of injection. Momentum painting of longitudinal phase space improves the accumulated beam distribution and enhances the bunching factor.
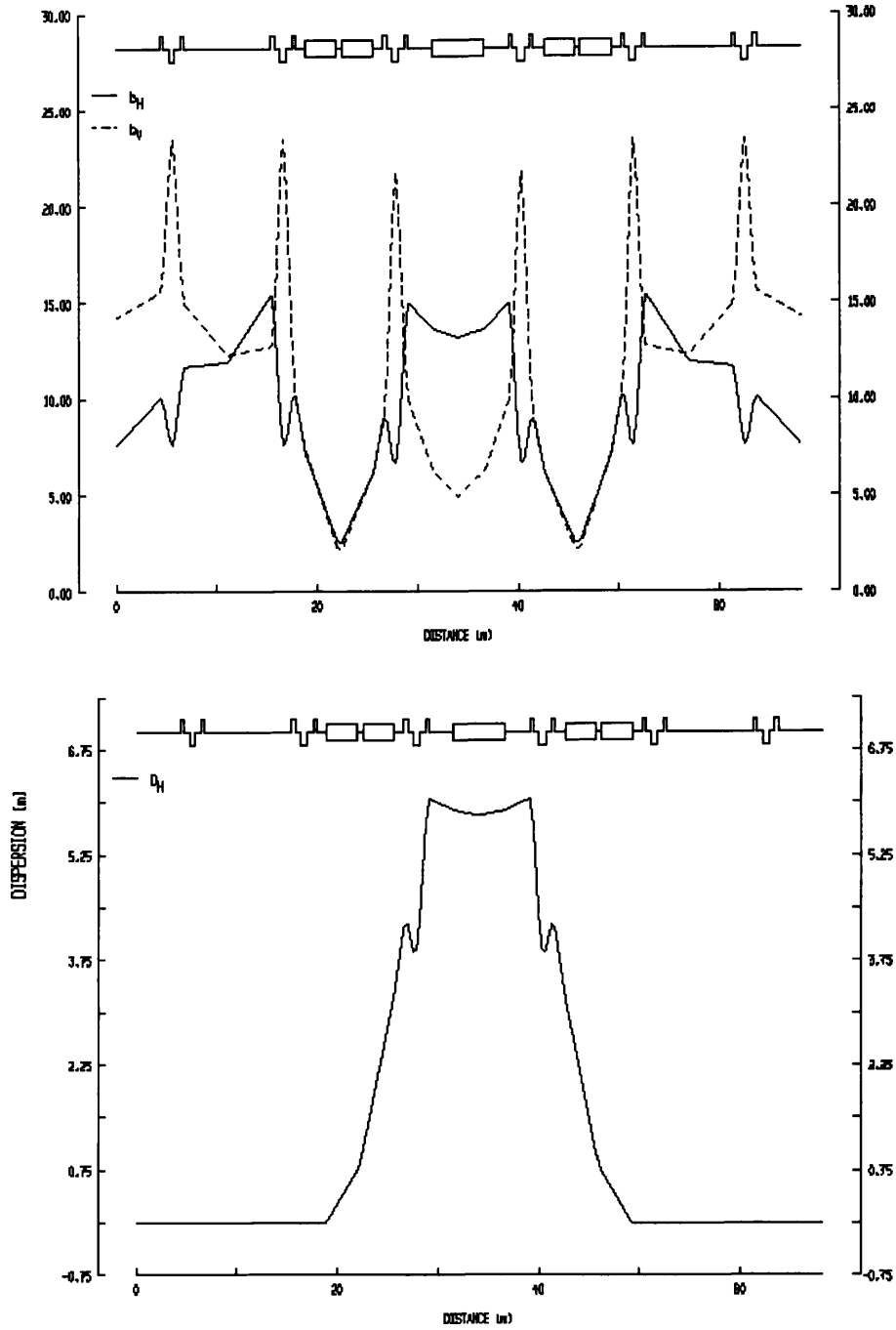
Fig. 3.10 Lattice functions for the booster synchrotron of Driver I

Transversely, the distribution is controlled by four vertical orbit bump magnets and coupling of the momentum painting into the horizontal plane via dispersion. The system is optimised with the aim of reducing subsequent traversals of the stripping foil by recirculating protons, thereby avoiding excessive temperatures in the foil.

In order to permit hands-on maintenance in the rings, low loss levels are required of the order of 10^{-3}. Some of this is accounted for by H^- and proton interactions with the foil, making it important that further losses, which occur mainly during trapping in the first stages of acceleration, are avoided. This is achieved using a suitably programmed system of rf voltages, with a radio frequency range allowing limited radial steering after injection. A single harmonic $h = 2$ system with maximum peak voltage $\hat{V} = 0.28$ MV is used in Booster I, while Booster II has $h = 3$ and $\hat{V} = 0.4$ MV. Two bunches each of 2.5×10^{13} protons and three of 1.11×10^{13} protons are accumulated in the boosters respectively. At ejection, the respective bunch durations are 100 ns and 50 ns.

3.3.3.2 Final bunch compression

For each driver, the bunches in the two vertically-stacked booster rings are extracted and transferred together to either the upper or the lower of the two main synchrotrons in alternate cycles. Each transfer line contains a pulsed dipole magnet to provide vertical beam splitting.

The requirements of the final 1 ns rms bunch compression have, to a large extent, dictated the main ring designs. Separate simulation studies indicate that the compression can be achieved by working close to transition energy. Crossing transition and subsequent instabilities need to be avoided; thus the lattice requirement that γ approaches from below to within about 5% of γ_t at top energy has been adopted. As bunches compress, however, γ_t will in general be reduced, and there is a risk that transition may be crossed nevertheless. A feature of the ring design is therefore that transverse space-charge tune shifts are small and the dispersion functions resist depression of γ_t. Simple doublet lattices have been adopted and the shape of the resulting dispersion function, the β-functions and the superperiod structure for Driver I are shown in Fig. 3.11. Here the effect of over 1200 A of peak beam current is merely to depress γ_t from 6.50 to 6.47. Inductive impedances $|Z/n| \sim 5$-10 Ω are envisaged for the metallic and ceramic vacuum chambers to help reduce longitudinal space-charge effects.

3.3.3.3 Parameters of the RAL RCS scenarios

A summary of the main parameters of the two RAL drivers is given in Table 3.4. The initial study of both scenarios is complete and remaining work on the drivers will rely on the use of three-dimensional tracking codes for refinement of the systems.

Table 3.4 Parameters of the synchrotron drivers

Parameter	Driver I	Driver II
Booster synchrotrons:		
Kinetic energy (MeV)	180–1200	180–3000
Number of bunches	2	3
Bunch intensity	2.5×10^{13}	1.1×10^{13}
Number of injected turns	160	70
Injection period (μs)	200	134
Mean radius (m)	32.5	50.0
γ-transition	4.73	5.97
Normalised dispersion $D_h/\sqrt{\beta_h}$ at foil ($m^{1/2}$)	1.6	1.8
Q_h, Q_v	4.24, 4.35	5.70, 4.32
rf harmonic number	2	3
Peak rf voltages (MV)	0.28	0.40

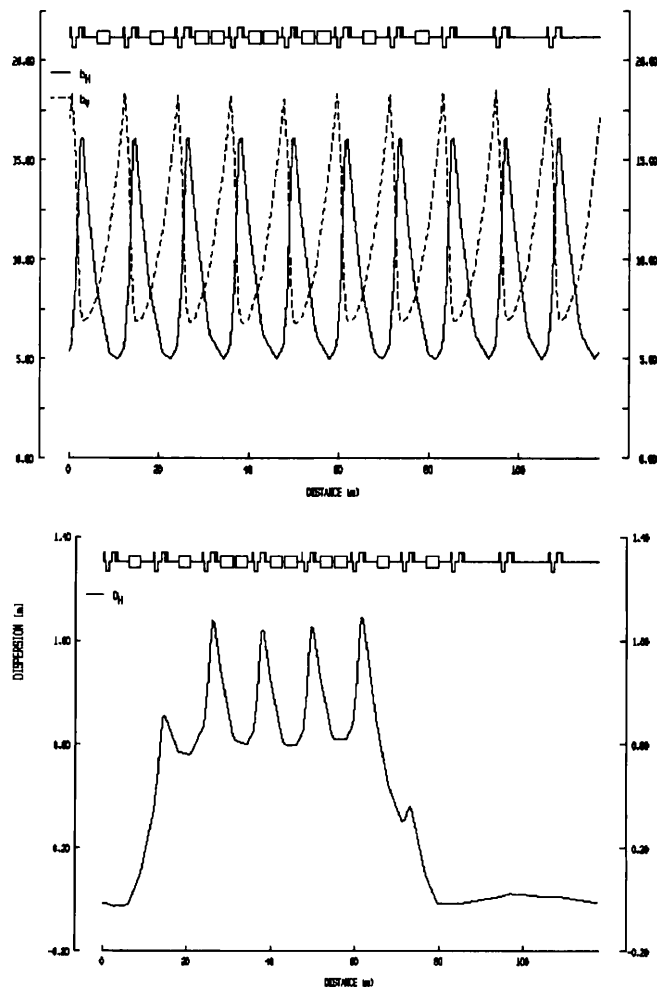| Parameter	Driver I	Driver II
MAIN SYNCHROTRONS:		
Kinetic energy (GeV)	1.2–5.0	3.0–15.0
Number of bunches	4	6
Mean radius (m)	65.0	150
γ-transition	6.50	17.14
γ	2.28–6.33	4.20–16.99
Q_h, Q_v	7.78, 5.80	20.41, 15.24
ΔQ_h, ΔQ_v	–0.07, –0.13	–0.02, –0.02
Chromaticities	–1.15, –1.21	–1.15, –1.31
Harmonic numbers	8 and 24	36
Peak rf voltages (MV)	0.58 and 0.5	1.7

Fig. 3.11 Lattice functions for the main synchrotron of Driver I

Acceleration is achieved by cavities with programmed rf fields. For Driver I, where the rings contain four bunches, these use the harmonic number $h = 8$ with maximum $\hat{V} = 0.575$ MV, providing some compression. Additional $h = 24$ cavities are brought into play over the last 1 ms of the cycle to reach the 1 ns rms length required. The peak total voltage necessary from these additional cavities is 0.5 MV. Simulations show a final bunch with peak momentum spread $\Delta p/p \sim 1.6\%$ and longitudinal emittance $\varepsilon_L \sim$ 1.0 eVs. In the case of Driver II, $h = 36$ cavities with $\hat{V}$ rising to 1.7 MV in mid-cycle, then falling to 0.6 MV, give similar results with the final conditions achieved by adiabatic bunch compression.

3.3.4 The 30 GeV/8 Hz rapid-cycling synchrotron (Driver III)

This scenario is not matched to the 44 MHz muon collection system, but a 40.27 MHz collection system could handle the bunch structure from this proton driver. The driver synchrotron, also using the ISR tunnel, is filled on a 2.2 GeV, 60 ms, flat bottom by four batches of two bunches each from a 1/4-size 50 Hz booster (similar to the AUSTRON RCS design [Bry95]). At the end of the booster cycle these bunches are pre-compressed to fit into the buckets of an $h = 32$ rf system of the driver, which accelerates the eight bunches in 45 ms to top energy. The necessary peak voltage of 3.8 MV is delivered by 22 cavities of a novel design [Pir00]. An external mechanical tuner, coupled to the cavity by 31/8" cables produces the required frequency variation of ~4%. Each cavity ($L = 1.8$ m, $r/Q = 42\ \Omega$, $Q = 5000$–10000) contributes 175 kV. The high peak rf voltage can provide naturally short bunches without compression at top energy, if the transition energy is chosen to be not too far above it, and if the vacuum chamber impedance does not exceed $(Z/jn) = 2\ \Omega$. These criteria are met by the present design.

The feasibility of the approach has been demonstrated by tracking studies, including a broadband resonator or a set of equivalent high-Q resonant longitudinal impedances. For a top energy of 30 GeV, the optimum γ_t is ~40. A "resonant" lattice, similar to that proposed earlier for high γ-transition values [Ili91], was designed, which has excellent dynamic apertures. It was a big design challenge to concurrently fulfil the needs for long dispersion-free straight sections, chromaticity correction, limited dispersion, and linearity of momentum compaction, when more than half of the circumference is taken up with bending magnets. In fact, a limit to the quadratic term $|\alpha| \leq 0.01$ of the momentum compaction was found by simulation. This condition is in general not met by a resonant lattice, except for a region of partially-compensated chromaticity around $\xi_{x,z} \sim -6$, a value which is just acceptable. Tables 3.5 and 3.6 summarise the main parameters of the booster and the driver synchrotrons. A possible topology, where the complete injector is inside the ISR tunnel, is shown in Figure 3.12.

Furthermore a different, more conventional lattice of γ_t ~30, limiting the top energy to 25 GeV (still above transition of the SPS), is being studied.

Table 3.5 Booster beam and machine parameters for Driver III

Parameter	Unit	Value
Kinetic energy	GeV	2.2
Pulse frequency	Hz	50
Pulse intensity	protons	2.5×10^{13}
Number of bunches		2
Circumference	m	238
Number of injected turns (56 mA)		100
rf harmonic number		2
rf frequency	MHz	1.38–2.42
rf peak voltage	MV	0.35
Space-charge tune shift at injection		–0.18

Table 3.6 Driver output and machine parameters for Driver III

| Parameter	Unit	Value
Mean beam power	MW	4
Kinetic energy	GeV	30
Pulse frequency	Hz	8.33
Pulse intensity	protons	10^{14}
Number of bunches		8
Bunch length (1σ)	ns	1
Momentum spread (2σ)		0.008
Transverse emittances, norm. (2σ)	μm	150π
Longitudinal emittance/bunch	eVs	2
Circumference	m	952
rf harmonic number		32
rf frequency	MHz	9.7–10.2
rf peak voltage	MV	3.8
Transition energy γ_t		39
Tune shift on flat bottom		−0.22
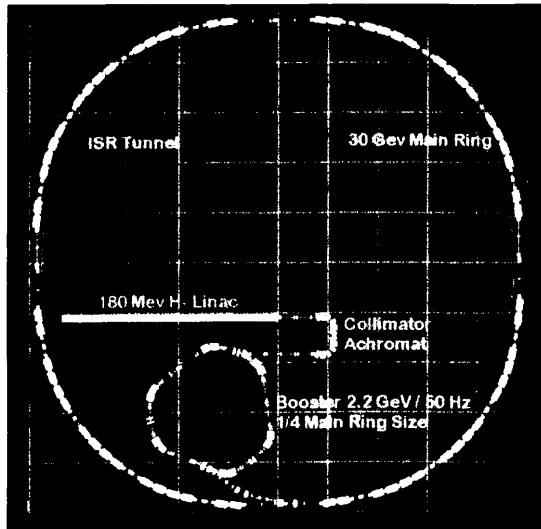
Fig. 3.12 The CERN 30 GeV, 8 Hz proton driver (Driver III) in the ISR tunnel with its injector. Grid size 30 m.

The study of the 8 Hz synchrotron scenario will be complemented by the evaluation of a 25 GeV driver with a more conservative lattice, a more detailed assessment of the coherent effects, and a study of halo development during the up to 60 ms long stacking. The study will then be suspended. It will resume if a future evolution shows that the RCS approach appears more promising.

3.4 Comparison of proton drivers

As it cannot be excluded that the calculated pion production at 2.2 GeV needs to be corrected in view of the results of the HARP experiment [Dyd99] at the CERN PS, higher beam energies of 5–30 GeV may be desirable. Actually, the approach of having a chain of Rapid Cycling Synchrotrons (RCS) could be more economic than the combination of high-energy linac plus accumulator and compressor rings. Injector linac energies not exceeding 150–180 MeV facilitate the handling of the RF capture loss, which is very difficult to suppress completely. This approach has been pursued in the RAL scenarios in a site-independent optimisation. For a CERN-specific scenario, a driver synchrotron of 30 GeV is desirable, as this machine could inject into the CERN SPS above transition energy (the SPS transition is at $\gamma_t = 22$), substantially upgrading its performance for fixed-target physics and the LHC [Aut97]. ISOLDE would profit from the 440 kW beam power of the 2.2 GeV booster synchrotron.

Table 3.7 Proton Drivers with 4 MW power and their Bunch Compression Technique studied at CERN and RAL

Philosophy	High energy linac + accumulator-compressor	DTL (180 MeV) + 2 stages of RCS (rapid cycling synchrotrons)		
Scenario	Reference	Driver I	Driver II	Driver III
	2.2 GeV/50 Hz	5 GeV/50 Hz	15 GeV/25 Hz	30 GeV/8 Hz
	CERN-specific	Site-independent	Fits ISR tunnel	CERN-specific
Rings	Accumulator + Compressor	2 RCS 1.2 GeV/50 Hz 2 RCS 5 GeV/25 Hz	2 RCS 3 GeV/25 Hz 2 RCS 15 GeV/12.5 Hz	1 RCS 2.2 GeV/50 Hz 1 RCS 30 GeV/8.3 Hz
Bunches	140	4	6	8
ε_L [eVs]	0.1	1	2	2
rf compression	$h = 146$; 44 MHz; 2 MV	$h = 4$; 3 MHz; 2 MV; 2 harmonics ($h = 8$, 24)	$h = 36$; 11 MHz; 1.7 MV	$h = 32$; 10 MHz; 3.5 MV
Compression method	$\eta \sim -0.1$ bunch rotation in 7.5 turns	$\eta \sim -0.0013$ 'at end of cycle, bunch rotation	$\eta \sim -0.00006$ adiabatic compression	$\eta \sim -0.0002$ adiabatic compr. for $Z/jn < 2\Omega$!
Critical features	Laslett ΔQ: ~-0.2, but <-1 for small number of turns	Space charge > chamber impedance Rotation delicate	Space charge = chamber impedance ΔQ dependence of α_1	Limits to α_1 in conflict with high-χ lattice

3.5 Collaborations

- **CEA**
  CEA collaborates with CERN on the low-energy part of the SPL.

- **IN2P3**
  IN2P3 collaborates with CERN on the low-energy part of the SPL.

- **RAL**
  The ISIS Accelerator Group at the Rutherford Appleton Laboratory has been actively collaborating with CERN on proton driver designs, target geometry and construction, and the front end of a possible neutrino factory. The proton driver work has concentrated mainly on the use of rapid cycling synchrotrons but RAL has also contributed to the CERN scenario based on a high-energy superconducting linac feeding accumulator and compressor rings. The ISIS

Accelerator Theory Group performed the design of the accumulator ring. Injection studies have been carried out, and a lattice suitable for the final bunch compression was also identified.

- **TRIUMF**
  S. Koscielniak, F. Jones and R. Baartman have collaborated with CERN on the proton driver scheme.

- The support of various scientists from Los Alamos (USA) and Jülich (D) is gratefully acknowledged.

3.6 Research needed

- Continuation of the SPL studies.

- Refinement of the design of the accumulator for the SPL and its collimators.

- Detailed tracking studies of the RCS drivers.

- Results of HARP to help decide the proton driver.

3.7 Conclusions

It seems feasible to meet the required 4 MW proton beam power at 1 ns rms bunch length with both the baseline design and rapid cycling synchrotrons. All scenarios work on paper and in the simulation and will have to be refined in future. Results from HARP will give an important input for the choice of the optimum proton driver energy. The final decision for a proton driver will be based on cost, the pion yield, and possible alternative uses of such a machine in the CERN accelerator chain.

3.8 WWW-links

http://cern.web.cern.ch/CERN/Divisions/PS/SPL_SG/
The SPL study group.

http://hos.home.cern.ch/hos/NufactWG/Pdrwg.htm
The proton driver rings working group.

4 Target Station and Support Facility

4.1 Introduction

We describe a target station in which pions are abundantly produced in order to serve as precursors of muons. It consists of a complete high-level radioactivity laboratory with the technical support equipment needed to operate and service the high-power production target, the spent beam absorber, and the first particle collection and focusing device.

It is planned to build it in a modular way so that its individual parts can be rapidly replaced and serviced by means of remote handling. This should allow flexibility in the choice of equipment and allow a stepwise approach in which lower-power conventional techniques are used in an early phase and later exchanged against better performing high-power targets when developed. This approach is compatible with the idea of the beta-beam, based on short-lived beta-unstable nuclei as neutrino sources (see Section 8.1).

The deleterious effects on the equipment and its surroundings caused by the megawatt-scale power and radiation dissipated by the high-intensity proton beam is the major challenge which identifies the target and pion capture system as one of the most crucial items of the neutrino factory. A molten metal-jet target located inside the neck part of a magnetic horn for pion collection has been chosen as the scenario for further investigation of the CERN muon neutrino factory production system. The tentative layout of such a system is shown in Fig. 4.1 [Ravn01] and will be described in detail below. The system is quite similar to the scenario chosen by the US partners in the Muon Collaboration who favour a 20 T superconducting solenoid as pion collector [Kirk00].
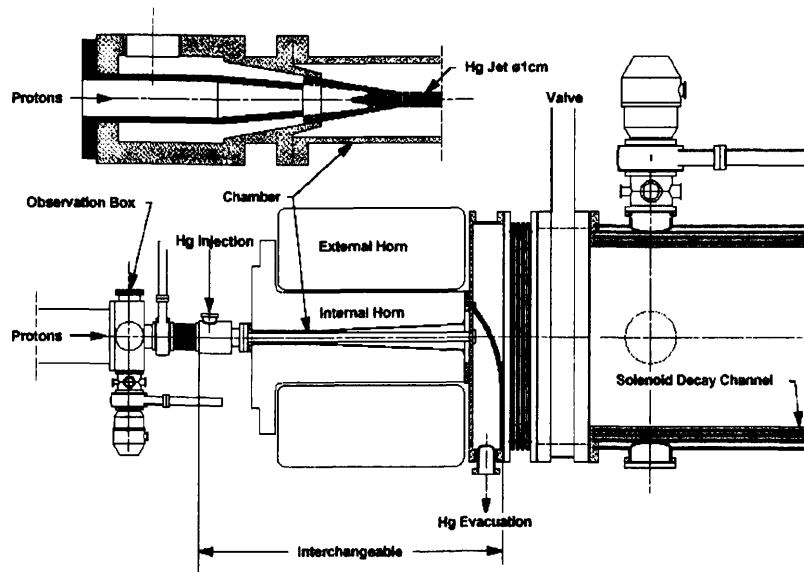

Fig. 4.1 Layout of a target and magnetic horn module in which a jet of mercury is directed into the neck region of the horn. The mercury is injected via an annular nozzle that allows coaxial injection of the proton beam. Also indicated is the double horn structure that serves to reduce the stress on the critical neck region.

4.2 Pion production system

The generation of pions in targets at high power gives rise to – or even exceeds – similar requirements that are considered in a number of other planned facilities. The spallation neutron sources [Bauer96, Mansur01], Accelerator Production of Tritium (APT), Accelerator Driven Systems (ADS) and energy production may ease their heat transfer problem by depositing the beam power in large amounts of target material. However, the neutrino factory, like the planned facilities for acceleration of Radioactive Ion Beams (RIB)

needs orders of magnitude smaller volume targets in order to efficiently release the charged particles to be captured and accelerated. The key problem is the initial pressure waves induced in any condensed matter by the microsecond short proton pulse, which deposits about 100 kJ. They eventually exceed the yield strength of any solid target or tubes containing liquid ones and cause them to break mechanically after a short time.

New innovative techniques may be needed in order to dispose of the power generated in the small volume of a pion production target where local densities up to 100 kW cm^{-3} may be encountered. At present two concepts seem to be viable in which either solid or liquid metal target material is recirculated rapidly in the beam.

A number of such ideas were presented at the NuFact'99 workshop [NIM00] and are now under laboratory tests in order to verify the simulations and determine engineering parameters. They should in principle allow the use of pulsed proton driver beams with 4 MW average power and may possibly be extended to 20 MW but a considerable R&D effort is needed in order to select the future directions from among the many ideas.

4.2.1 Baseline design: molten metal jet

Since equipment and expertise on liquid metal technology already exists at CERN and molten metal targets have been chosen by most of the above-mentioned projects, we believe this is the most promising direction. The essential feature of the jet is that it is rapidly re-formed after each proton pulse that only scatters the liquid because of the above-mentioned thermal expansion wave. Moreover, the heat is carried away with the material. As in spallation neutron sources, mercury has been chosen as the most promising high-Z target and coolant material while several other metals or alloys including low-Z elements could be considered, as well. Other advantages of a mercury-jet target should be noted:

1. High pion yield (high-Z)
2. High source brightness (high density)
3. Flowing liquids have excellent power handling capabilities
4. No water radiolysis
5. Liquid at ambient temperature (no liquid-to-solid phase change issues)
6. Minimal waste stream (compared to solid alternatives) since the mercury is continuously reused
7. The majority of the radioactive reaction products may be concentrated and removed from the mercury by distillation
8. Passive removal of decay heating
9. No confinement tubing (free flowing jet)
10. No need for nearby beam windows (differential pumping confinement)

4.2.1.1 Recent R&D work on the Hg jet

A molten metal laboratory has been commissioned and a prototype Hg jet was injected into a 13 T solenoid at Grenoble [Debray01]. The experience gained was used in continuation of the tests in a 20 T solenoid as well as to start designing a pilot set-up to be tested in the PS-Booster/ISOLDE beam. Such tests will allow the simulation of power densities of only a factor 5 below those expected in the SPL-generated beam.

In addition a static Hg-filled test chamber with a high-speed digital camera often referred to as the thimble test has been constructed for systematic on-line tests in the 1.4 GeV ISOLDE beam. Because of scheduling constraints, the in-beam tests with this chamber were first done in the 24 GeV BNL beam within the Muon Collaboration experiment E951 [Fabich00]. As seen in Fig. 4.2, the disruption of the metal bath already noted in ISOLDE liquid Pb targets [Lettry97a] could be confirmed and recorded. The test was performed with only a few proton bunches and gave valuable data on in-beam Hg handling and proton-beam-induced pressure wave propagation in a liquid metal.
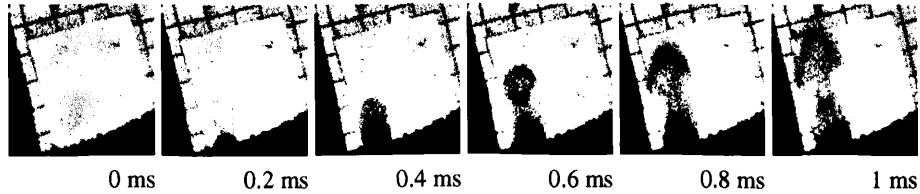
Fig. 4.2 Reaction of a ~1 cm³ thimble partly filled with mercury to the impact of a 24 GeV proton bunch of 4.0 × 10¹² particles and 100 ns duration. The protons enter at the lower left corner where the thimble is located. The picture series shows that within 1 ms after the hit, the Hg is ejected as a fountain. The squares in the pictures are 1×1 cm.

This experiment was followed by on-line tests of a scaled-down version of the Hg jet in the BNL test beam. The series of pictures displayed in Fig. 4.3 shows the break-up of the free flowing Hg jet as a result of one proton bunch impact. The data, which are still in the analysis stage, suggest the following tentative conclusions: There is no visible propagation of the expansion wave in the axial jet direction outside the short length of maximum power deposition. The droplet speed was lower than in the thimble test (~20 m/s) but seemed to be proportional to the number of protons in the bunch over the short intensity range studied.

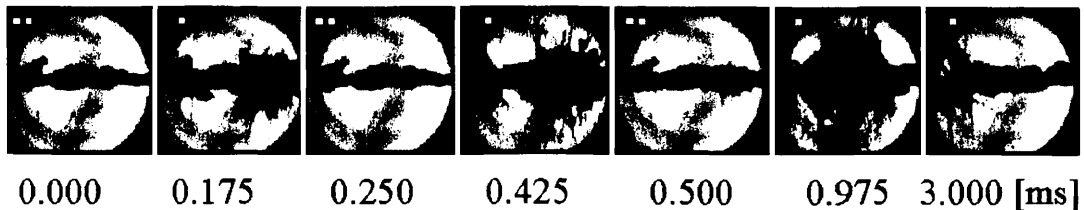**Fig. 4.3** Break-up of an Hg jet coaxial to the proton beam both entering from the right. The jet parameters were: diameter ~1cm and jet velocity ~3 m/s. The proton beam parameters were 24 GeV, 3.8 × 10¹² ppb, pulse length 100 ns and radius 1 mm.

In conclusion the BNL–CERN thimble and jet test at 1/100 of the design power density and 1/10 of the needed jet speed revealed no showstopper for the Hg target concept.

4.2.2 Alternative designs for the pion production system

4.2.2.1 Water or gas-cooled solid, granular target

In addition, recent ideas of direct water- or gas-cooled granular metal targets, based on more conventional techniques, have received attention [Sievers01]. The beam-induced thermal shocks are expected to be grossly reduced in the small granules of the target (spheres of 2 mm diameter, see Fig. 4.4). Moreover, the very high surface-to-volume ratio of the ensemble of the granules provides for efficient cooling to evacuate the high power densities. A high capacity helium gas cooling circuit may be envisaged in an initial approach. The target is calculated to accept a beam power of 3 MW. The crucial problems are heat transfer, material stress, fatigue, radioactivity, radiation damage, in particular of the front and end windows of the target container, and cooling media confinement. Some of these issues, like heat transfer, are being addressed experimentally in off-beam tests and technical solutions to alleviate radiation damage in the beam windows are being worked out.

Thus, in addition to the mercury jet target, a path towards a stationary target is being exploited for which the integration into a horn or solenoid collector system seems readily feasible. Moreover the R&D investment for a granular target and its infrastructure are within accessible limits and the performance is predictable with good reliability.
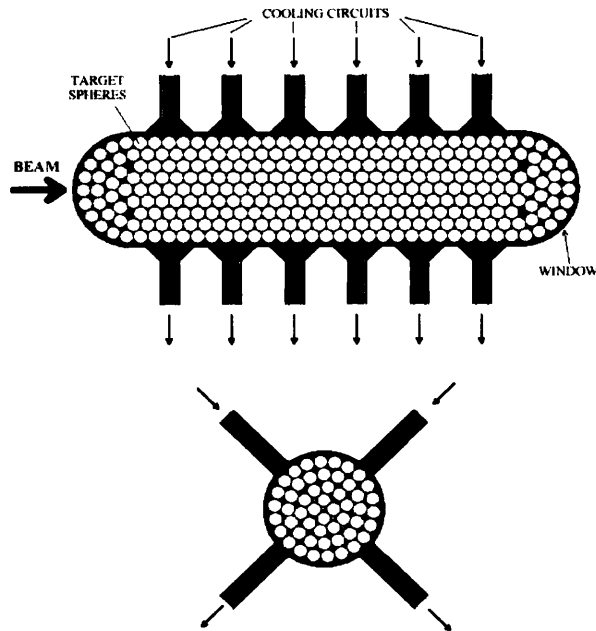
Fig. 4.4. Principle of a more conventional target consisting of cooled beads of solid tantalum

4.2.2.2 Conducting target

The mercury jet and the granular target have to be integrated into the horn, as well. Target and pion collector can be dissociated by pulsing an extremely high current into the target [Autin01]. This way, the pions are focused at the time of their creation and their phase space distribution is much denser in the centre. Seen from the collector, such a target looks like a thin brilliant disk, which can be put at the focus and thus outside of the collector. A consistent set of parameters has been derived for a conducting mercury target. The current needed is of the order of 2 MA. Such a device would be built using the technology of the 1.3 MA lithium lenses developed for the antiproton beams [Bellone]. The main difference lies in the high repetition rate (50 Hz), and the electrical power reaches 3.5 MW. The deposited heat would be evacuated by letting the mercury flow inside a closed circuit cooled with a heat exchanger.

4.3 Pion collection system

In order to maximise the secondary pion collection efficiency, the target needs to be surrounded by a large-acceptance pion collection and focusing system.

4.3.1 Baseline design: magnetic horn

Since one is interested in the production of one sign of pions for any given proton bunch, it is planned to use a pion collection system based on the azimuthal magnetic fields generated between the coaxial conductors of a magnetic horn. This technology has a long tradition at CERN for the focusing of secondary particles [Vdm61] and has the advantage that the parts exposed to the beam are rather simple and inexpensive and they can be radiation hard. The horn design is rather different from those used for high-energy beams, such as CNGS [CNGS98] and NuMI. In fact, the horns for conventional neutrino beams focus pions or kaons point-to-parallel because one is not particularly interested in the spot size dimension at the exit of the focusing system, while a transverse momentum reduction is more relevant for the final neutrino beam at the detector site. In the case of the Neutrino Factory, the beam coming from the horn

enters directly into the 60 cm diameter solenoid of the decay channel. While reducing the transverse momentum is still a desired feature for the Neutrino Factory, the horn has to be matched to the downstream beam optics.

The horn [Ball99] is compact in the longitudinal dimension (1 m), while the large radial dimensions are quite remarkable compared to traditional designs. This choice was dictated by the particular pion spectrum produced by the 2.2 GeV proton beam. Most of the useful particles exit the target radially, with a typical transverse momentum of 250 MeV/c. One needs to bend these particles as soon as possible, which means a small radius of the horn neck, and for a long transverse distance. Since the magnetic field in the horn decreases as $1/R$, where R is the distance between a point in space and the horn axis of symmetry, the focusing effect decreases with the distance. The maximum current is fixed by mechanical and thermal constraints; a reduction of the pulse length and thus of the horn inductance is a key condition for maximising the current. Limiting the magnetic volume limits the inductance of the device; a good solution is then to split the horn into two radial sections. A current of 300 kA flows in the inner horn section, which has a conical shape. This part focuses most of the low-energy particles and the high-energy pions emitted at small angles. The outer horn section, which is a hollow cylinder surrounding the first horn, is excited by a current of 600 kA. The higher field generated at large radii captures the high-energy pions leaving at large angles. The performance of this horn is currently under study, but preliminary results show that, the collection efficiency is comparable to that of a 20 T solenoid.

A preliminary technical study of the 1m long triangular shaped horn pulsed at 50 Hz has been started [Mau80].

Limiting factors for this technology are found in the waist region of the inner conductor. It needs to have a minimum diameter of 5–8 cm in order to accommodate the target and its plumbing. There are two challenges: the Joule losses in a waist of this diameter raise concerns about cooling, and the lifetime is limited by stress due to the magnetic forces as well as material weakening through radiation damage. A new cooling system is shown in Fig. 4.5, where the traditional conductor is divided into three layers. Starting from the horn axis, the first skin is an aluminium layer without current; the second is a water flowing layer, which cools the third layer. It is this inner aluminium layer, where the current flows. The current is confined by the eddy current effect. A good compromise between the radial dimension of the conductors, the water channels and supports, and the pion absorption is still under study. Usual water spraying of the third current-carrying layer (i.e. inner conductor) is kept in addition. A cooling water flow between the inner conductor at high voltage and the target chamber is prohibited because of the need for electrical insulation.
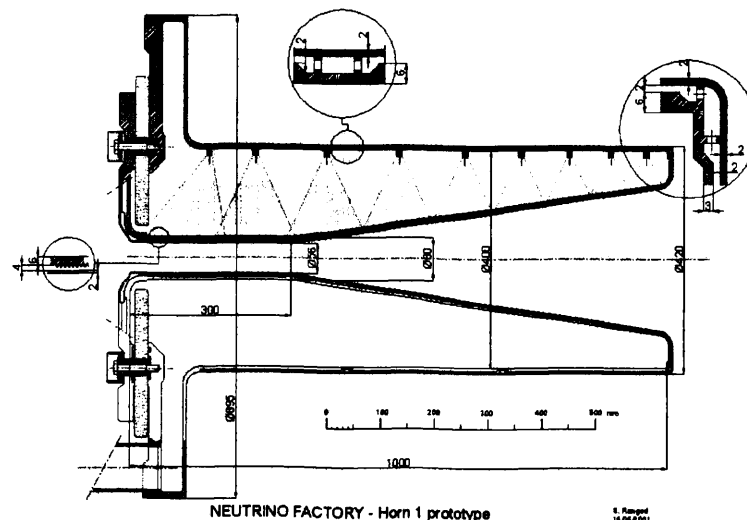

NEUTRINO FACTORY - Horn 1 prototype

Fig. 4.5: Design of a prototype of the magnetic horn.

4.3.2 Alternative designs: superconducting solenoid and conducting target

4.3.2.1 Superconducting solenoid

In the US projects the pion capture is based on the utilisation of a 15 cm bore, 20 T peak field superconducting solenoid which has the advantage of providing adequate space for the metal jet, the spent beam absorber, and their plumbing. The 20 T field is followed by a long section where the field decreases adiabatically from 20 T to 1.25 T [Weg99] and the beam pipe dimension increases to 60 cm diameter. The effect of the field reduction of a factor sixteen is translated into an increase of the beam radius by a factor of four, but also into a reduction of the same amount for the transverse momentum. In fact, if the longitudinal component of the B-field follows a slow reduction along the z axis according to Eq. (4.1):

$$B_z(z) = \frac{B_0}{1 + \alpha * z} \qquad (4.1)$$

where $B_0 = 20$ T and α is the adiabatic parameter, one can show [Jack75] that the magnetic flux across the transverse orbit is conserved (namely $Br^2 = $ const), and the angular momentum is also conserved (namely $B/p_t^2 = $ const). Replacement costs and the radiation hardness of such a sensitive magnet are the issues here.

4.4 Spent beam absorber

The pion production target absorbs only 25% of the 4 MW beam power while the remaining beam needs to be absorbed in a suitable beam stopper, which could be accommodated in the downstream part of the horn. Although heat transfer techniques similar to those used in the target may be applied, the material and cooling of the dump has to be studied in view of a low-Z material. An alternative could be a carbon–iron assembly cooled by helium and water. However, it is not an ideal location since apart from increasing the complexity of the horn it will also absorb some pions. A location somewhere after the decay channel is under study but no satisfactory solution has yet been found.

4.5 Target station and support laboratory

The housing and operation of the above-mentioned equipment requires a substantial laboratory infrastructure very similar to that found in the planned spallation neutron sources ESS [Bau96] and SNS [Man01]. In order to assure a staged approach to more and more powerful target techniques and to allow frequent service, a modular system in which individual components can rapidly be exchanged by remote control is envisaged. Such systems have been used at ISOLDE and constructed for high-intensity use at the ISAC project at TRIUMF. In this system [ISAC] the in-beam equipment is mounted at the bottom of a long plug as seen in Fig. 4.6. These plugs are loaded into the beam tunnel from above. The plugs have enough shielding to allow hands-on work at the upper end when the beam is off. The plugs may now be transported to storage locations or maintenance hot cells via the crane bay that forms the third floor in the target station as seen in Fig. 4.7.
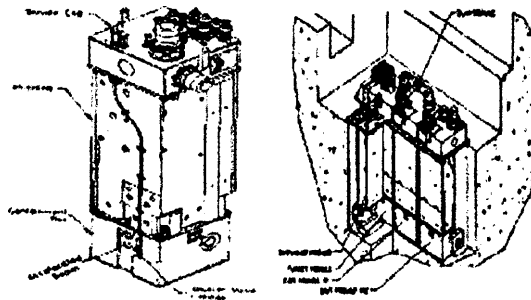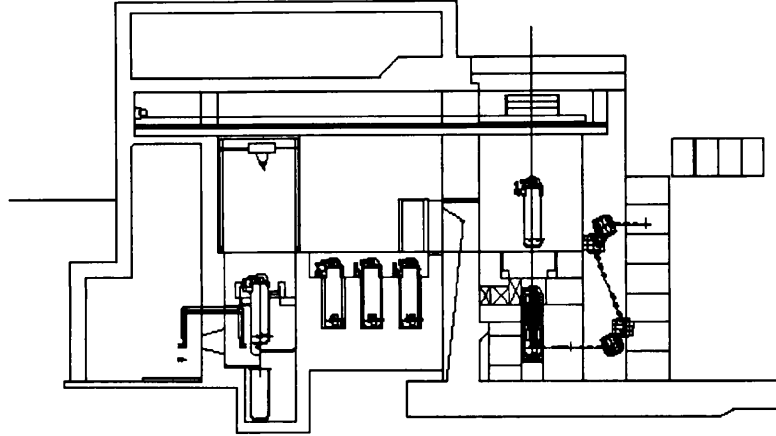

Fig. 4.6 ISAC target plugs

Fig. 4.7 Principle of top-loading active equipment into the beam tunnel or the hot cells

4.6 Collaborations

Contacts with the community of people and laboratories outside CERN who have expressed interest in participating in a variety of high-power target, pion collection, and beam-dump developments is maintained and is being extended to new laboratories.

At present the collaborations with BNL, LCMI Grenoble, and RAL are actively producing data.

4.7 Research needed

Within the existing resources a programme for further development of the chosen concept has been set up. On the experimental side the programme is as follows:

- Test of the 15 m/s 'old' Hg jet in the 20 T field
- Experimental studies of the turbulence effects in the high-speed jet with Reynolds number $Re = 5 \times 10^6$
- Response of a static Hg sample to proton bunches up to 8×10^{12} ppB
- Response of a static Hg sample to proton beam-size and energy
- Response to a multibunch pulse (CERN scenario)
- Response to a bunch length reduced to 3–5 ns
- Response to other dE/dx at other proton energies
- Building and testing of a horn prototype

For the simulation and development of models, which allow the extrapolation of the test results at CERN by a factor of 5 in beam power at the future SPL, the situation is less clear. At the moment capabilities outside CERN and resources within the fields listed below are actively being sought.

- Hydrodynamic design of Hg jet and nozzle at a jet speed of ~30 m/s and 20 mm diameter [Farhat]
- Pumping system for continuous Hg jet at ~30 m/s and 20 mm diameter
- Modelling of the proton-beam-induced expansion wave on a liquid Hg column [Hassein01, Samulyak]
- Modelling of the magneto-hydrodynamic effects on a liquid Hg column [Hassein01, Samulyak]
- Calculation and measurement of heat transfer coefficient of the water-cooled granular target consisting of solid spheres [Thome]
- Assessment of the effect of vibrations and radiation damage in the windows of the water-cooled target container
- Assessment of the corrosion effect caused by the water-radiolysis products

4.8 Conclusions

A molten-metal jet target with a horn has been chosen as baseline scenario for the Neutrino Factory. It involves advanced new techniques that have to be developed. Alternative designs have been discussed. A target and horn working group has been formed at CERN in which many of the skills needed for designing a 4 MW target station are represented. It should serve as interface to the much more powerful molten-metal target collaborations existing within the communities of spallation neutron sources and accelerator-driven systems. Discussions of possible joint target developments have started. Laboratories for molten-metal technology and horn development have been set up at CERN. The first European in-beam experiments aimed at determining crucial engineering parameters that will allow a choice among the various proposed technologies have started. A satisfactory solution to the location and type of the beam dump that does not cause excessive losses of muons or unnecessary amounts of radioactive waste remains to be found.

4.9 WWW links

http://nfwg.home.cern.ch/nfwg/nufactwg/nufactwg.html

The CERN Neutrino Factory homepage.

5 Layout of the front-end of the decay and cooling section

5.1 Introduction

After the target pions decay in a 30m long channel focused by a 1.8 T solenoid, with a transverse radius of 30 cm. The result is a beam with enormous transverse and longitudinal dimensions. The normalised rms transverse emittance is 3000 πcm mrad. There are particles of virtually all energies from close to zero up to the maximum proton energy. In order to turn these muons into a workable beam and to increase the number of muons that fit into the acceptance of the downstream accelerators, two techniques have to be used:

- In the **longitudinal plane**, phase rotation is applied. Phase rotation is the exchange of an energy spread into a phase spread. This is possible, whenever an energy–phase correlation builds up. It is done by properly tuned rf that decelerates high-energy particles and accelerates low-energy particles and thus reduces the energy spread. The longitudinal emittance is (to a first approximation) not changed in this process.
- In the **transverse plane**, emittance reduction is possible by using ionisation cooling. This is a two-step process. First, particles pass through an absorber with a low-Z material (liquid hydrogen in this case). Here, the particles' momenta are reduced uniformly. Next, the particles are re-accelerated in an rf cavity, where only the longitudinal component of the momentum is restored. Thus, transverse momentum and with it $x' = \text{arc } \tan(p_t/p_l)$ is reduced.

A main feature of the CERN baseline scenario is the bunch-to-bucket principle. There is no rebunching throughout the whole neutrino factory complex. One proton bunch of 1 ns *rms* length produces a pion and subsequently a muon bunch that debunches to a length of about 20 ns. This fits into one 44 MHz rf bucket in the phase rotation and cooling. From here on, the particles are always kept in the rf bucket.

5.2 Baseline scenario: the 44/88 MHz channel

At the beginning of the phase rotation and cooling channel, particles with a kinetic energy in the range 100–300 MeV are captured in a series of 44 MHz cavities at a phase of -90° [1], and their energy spread is reduced by a factor two. At this point a first cooling stage, employing the same rf cavities, reduces the transverse emittance in each plane by 40% while keeping the average energy constant. After the first cooling stage the beam is accelerated to an average energy of 280 MeV. At 300 MeV the beam is injected into an 88 MHz cavity cooling system. In this second part, rematching cells are periodically inserted to control the longitudinal dynamics. At the end of the second cooling stage the emittance is reduced by a factor of 4 in each transverse plane [Lom00]. Subsequently, the muons are accelerated with a linac operating at 88 MHz and 220 MHz until the final energy of 3 GeV – suitable for injection in the first muon recirculating linear accelerator (μRLA) – is reached.

Note that 44 MHz is a subharmonic of the subsequent rf frequencies of 88, 220 and 352 MHz. The latter has been chosen for the μRLAs in this study because the re-use of LEP cavities is assumed. The key parameters of the front-end are presented in Table 5.1.

Tab. 5.1 Components of the 40–80 MHz scheme and their characteristics

	Decay	**Rotation**	**Cooling I**	**Accel**	**Cooling II**	**Accel**
Length [m]	30	30	46	32	112	~450
Diameter [cm]	60	60	60	60	30	20
B-field [T]	1.8	1.8	2.0	2.0	5.0	5.0
Frequency [MHz]	–	44	44	44	88	88–220
Gradient [MV/m]	–	2	2	2	4	4–10
Kinetic energy [MeV]	–	200	200	200–280	280–300	300–3000

---

[1] All phases in this Section are given in the linac definition with 0° being the rf on crest.

5.2.1   Simulation of the beam dynamics in the front/end

A pion beam is generated from a 2.2 GeV proton beam ($dp/p = 1.2 \times 10^{-2}$, $\varepsilon_x = 50 \, \mu$ m) instantly impinging on a 26 mm mercury target immersed in a 20 T solenoid. (Note that the CERN baseline scenario features a magnetic horn. For reasons of practicality, pions generated in a solenoid have been used. This does not change the following results.) The data have been extrapolated (linearly) to a 260 mm long target. These particles have been used for all the simulations presented here, notwithstanding further optimisation of the target and the subsequent focusing system. The beam dynamics of the pion–muon system from the decay channel up to the injection into the μRLA was studied with the program PATH (CERN version) [path90]. All the particles produced from the target were tracked through the system; cuts in longitudinal phase space have been made at the interface of each section for the sake of clarity in the presentation and accuracy in the simulation.
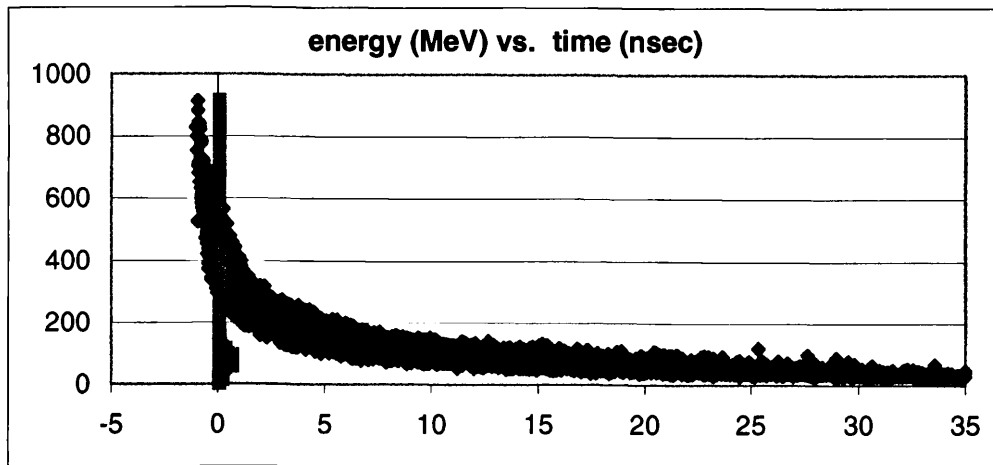

Fig. 5.1a Distribution of particles at the input (bright) and output of the decay channel plotted in longitudinal phase space [MeV, ns]. Only muons in the admittance (0.1 eVs) of the downstream system will be captured.
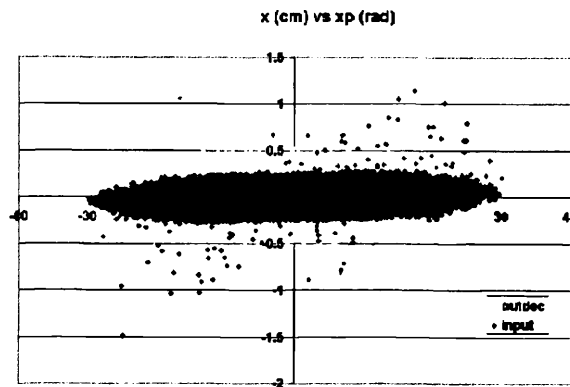

Fig. 5.1b Distribution of particles at the input (dark) and output (bright) of the decay channel plotted in transverse phase space [rad, cm]. The emittance blow-up is due to the pion decay.

Simulations have been performed with idealised rf cavities, in particular the 44 MHz cavities for phase rotation and cooling have been assumed to be 1 m long, and the 88 MHz cavities have been assumed to be 0.5 m long. Provided the 'real estate' gradient and the bore aperture are kept the same (2 MV/m, 30 cm at 44 MHz and 4 MV/m, 15 cm at 88 MHz), the cavity geometry (gap length, total length, shape) can be modified without fundamentally affecting the results reported in the following. A different cavity shape

involves some re-matching of the transverse plane as the distance between adjacent solenoids is probably bound to change. This generic cavity design has been used to decouple the beam dynamics work from the cavity design (see Section 5.4).

The input and output longitudinal and transverse phase spaces of the decay channel are reported in Figs. 5.1a and 5.1b. Work has started towards limiting the transverse emittance increase during the decay process in a magnetic field [holz01]. There is an increase in transverse emittance of a factor of ~1.5 due to the decay kinematics of the low-energy pions.

Only a subset of the muons surviving at the end of the decay channel can be captured in a 44 MHz rf structure because of the enormous energy spread. Assuming a realistic gradient of 2 MV/m, and in order to keep the phase rotation section within a length of approximately 50 m, only the particles within an energy spread of ±100 MeV can be successfully captured. An energy range of 100 MeV to 300 MeV is chosen as a compromise between the density of the muon spectrum (favouring lower energies) and the requirement that the (relativistic) Δβ must be small to avoid further debunching (favouring higher energies). Muons with momenta lower than 100 MeV debunch faster than a 2 MV/m field can rotate them and thus they cannot be successfully rotated if we assume a limit gradient of 2 MV/m. Should future rf tests demonstrate a higher field available at 44 MHz, the system will be reviewed. In Fig. 5.2 the terms of the trade-off are schematised: the higher the energy, the smaller the variation of relativistic beta (de-bunching not too severe); the lower the energy, the higher the density of muons. The energy band chosen is shown in grey.

For the reference scheme the phase rotation system is optimised for muons with kinetic energies between 100 and 300 MeV. More than 50% of the muons arriving at the end of the decay fit in the energy acceptance of the phase rotation system. This fraction cannot be improved unless pions are pre-rotated immediately after production or higher rf gradients become available. A set-up composed of 30 cavities at 44 MHz, each 1 m long with a gradient of 2 MV/m and an aperture radius of 30 cm is proposed. A solenoid around the vacuum chamber has been employed, giving the results reported in Fig. 5.3. The cavities do not need to be closed with a beryllium window. Particles have been tracked through a calculated field, with and without windows, showing little difference in the outcome. The rotation is very gentle, about 3 degrees per cell, thus limiting the transverse emittance increase due to rf defocusing to some 10%.

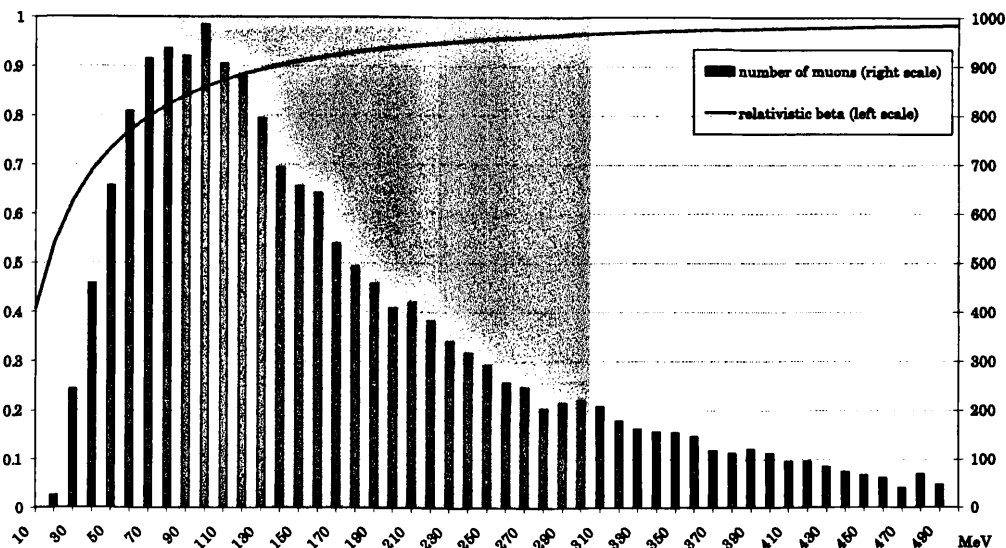## 30 m from target: number of muons / kin. energy histogram

Fig. 5.2a Muon energy histogram at the end of decay channel and corresponding relativistic beta. The energy acceptance of the cooling channel has been lined out grey. The energy range between 100 and 300 MeV has been chosen as a compromise between (still) high muon densities and (already) low debunching due to differences in the relativistic beta.

Mean energy	±50 MeV	±100 MeV
150 MeV	4.7°	12.7°
250 MeV	1.4°	3.3°
350 MeV	0.6°	1.4°

Fig. 5.2b Debunching per meter (in degrees at 44 MHz) as a function of mean energy for two different energy spreads.
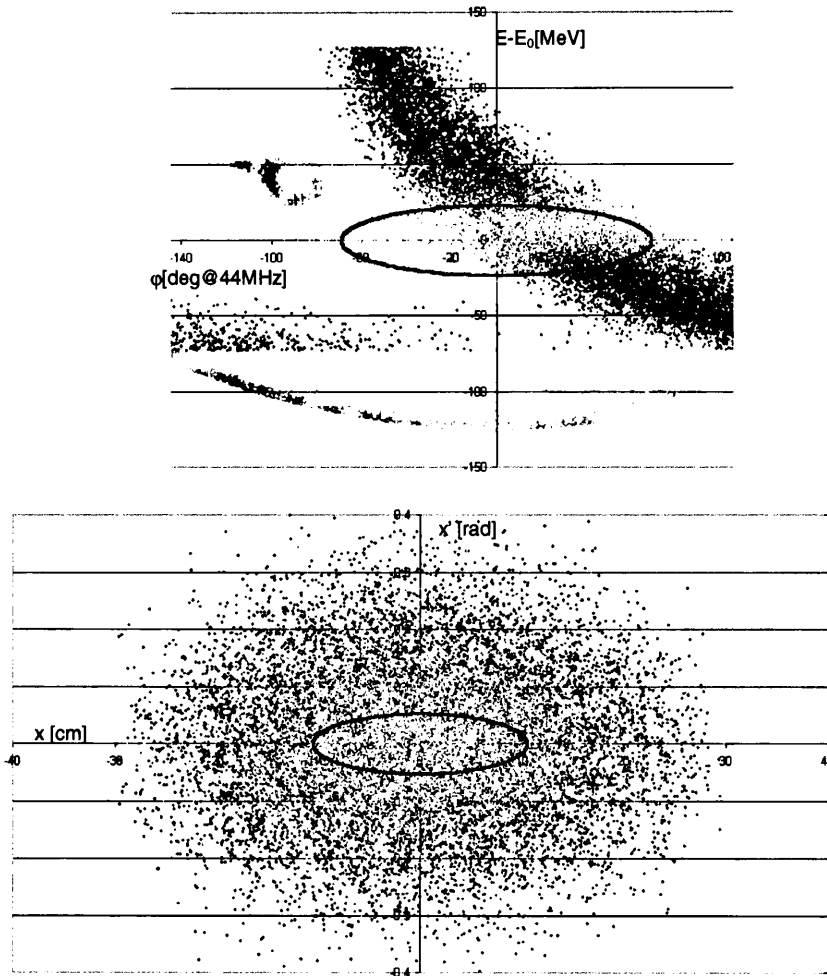

Fig. 5.3 *Upper*: Longitudinal phase plane before (bright) and after (dark) phase rotation. The energy spectrum around $E_0 = 200$ MeV is flattened out. Note the low-energy tail from the previous bucket, that overlaps into the 44 MHz rf bucket. The energy in this graph is given relative to the central energy. The dark circle indicates the 0.1 πeVs acceptance of the RLA1, showing that phase rotation has successfully rotated the most important part of the spectrum into the acceptance.

Lower: Transverse phase planes at the input and output of the phase rotation system. At first sight, no difference can be observed. Calculations show an increase of the transverse emittance of 10% due to rf defocusing. The dark circle indicates the transverse acceptance of the RLA1, showing that cooling is needed in order to fit the whole beam into the RLA.

39

At the end of the phase rotation, the beam still has a 44 MHz structure and can be cooled without further bunching. The fundamental cooling cell (Fig. 5.4) is composed of four 44 MHz cells operating at 2 MV/m on crest. At the end, there are 24 cm of liquid hydrogen (see Fig. 5.4); a solenoid is fitted around the gap of the rf cavity and its field covers the cell almost uniformly. Preliminary Superfish [bil96] runs confirm the feasibility of this structure. The distortion in the longitudinal phase space caused by the sinusoidal variation of the rf can be tolerated as the peak voltage 2 MV/m is small compared to the energy spread 50 MeV.

RF 24 cm gap 1 m long	RF 24 cm gap 1 m long	RF 24 cm gap 1 m long	RF 24 cm gap 1 m long	H$_2$ 24 cm

Fig. 5.4 Cooling cell at 44 MHz, total length 4.24 m

The energy loss/gain per cell is 5.6 MV. The first cooling section consists of 11 such cells and the emittance is reduced by 40% in each transverse plane. The beam is then accelerated to an average energy of 280 MeV by the same set-up (without absorbers). This accelerating section provides also some re-bunching and matching to the next cooling section. A good fraction of the beam (65%) at the end of the first stage of the acceleration fits into an 88 MHz bucket. The cooling process can be continued with 88 MHz cavities that are 0.5 m long with a 15 cm aperture radius and a gradient of 4 MV/m. The 88 MHz cooling cell (reported in Fig. 5.5) is composed of eight 50 cm long 88 MHz cavities and a 40 cm long liquid hydrogen absorber; a solenoid is fitted around the bore of each cavity. There are 25 cooling cells in the 88 MHz section. The longitudinal and transverse beam phase space along the 88 MHz cooling channel is reported in Figs. 5.6 and 5.7. The fraction of muons within the 6D re-circulator acceptance meets the specifications as outlined in the next section. After the beam is cooled, the system is continued with 88 MHz cavities of the same type until the beam has reached 1 GeV where a transition to 220 MHz is possible.

RF 0.5 m	RF 0.5 m	RF 0.5 m	RF 0.5 m	RF 0.5 m	RF 0.5 m	RF 0.5 m	RF 0.5 m	H$_2$ 0.4m

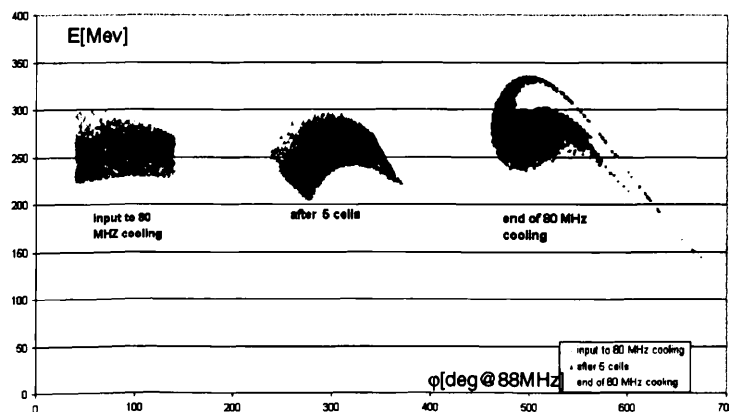**Fig. 5.5** Fundamental 88 MHz cooling cell, total length 4.4 m

Fig. 5.6 Longitudinal beam phase plane along the 88 MHz channel. Three stages have been pictured one beside the other for comparison, with an arbitrary phase shift.
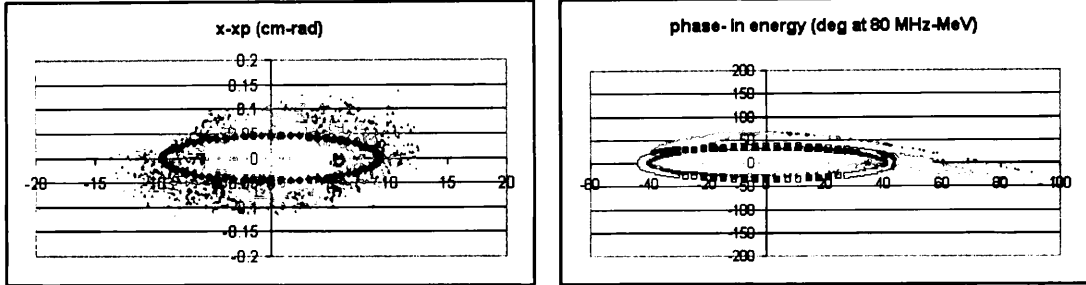
40

Fig. 5.7 The transverse and longitudinal phase space at the end of cooling. The ellipses indicate the acceptances of the downstream RLAs. The normalized numerical values are 1.5π cm rad for the transverse and 0.1π eVs (normalised) for the longitudinal acceptance.

5.3 Particle budget

The particle budget as calculated by PATH [path90] with a hard-edge model for the electric and magnetic field is reported in Fig. 5.8. An additional 20% of losses should be added due to muon decay. As the pion production cross-section is uncertain, it is best to express the particle budget in (surviving) muons per pion. This fraction is 5%.
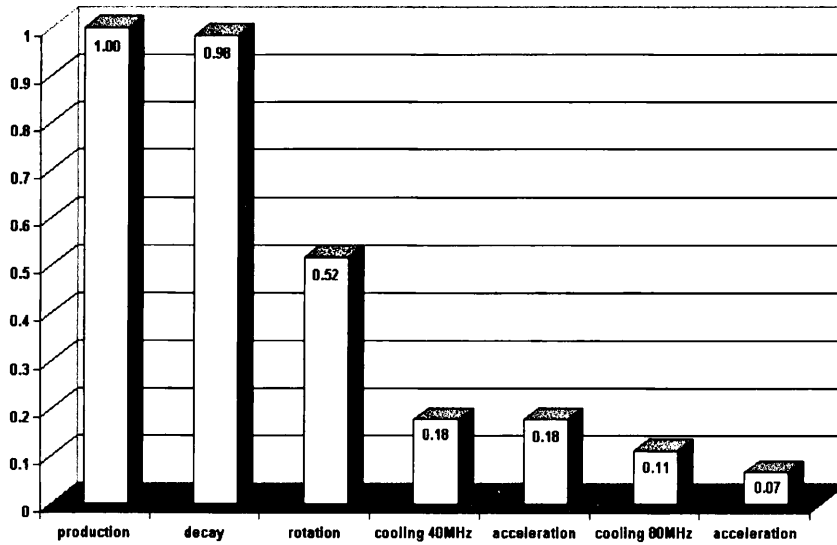

Fig. 5.8 Pions -muons budget along the channel

The total yield of the system can be calculated as follows: The 4 MW proton driver at 2.2 GeV delivers 1.8 mA of current. This is equal to 1.14×10^{16} protons/s. Assuming 10^7 s of run-time per year, a total of 1.14×10^{23} protons are delivered per year. Assuming the particle production as predicted by MARS [mokh95] to be 0.2π/proton at 2.2GeV, a total of 2.28×10^{22} pions/year are produced. After the losses during decay, cooling and acceleration, 1.14×10^{21} muons are counted at the beginning of the recirculators. This leaves some margin for losses in the transfer lines to achieve the design goal of 10^{21} muons per year.

$$\underbrace{1.14 \times 10^{16}}_{protons/s} \cdot \underbrace{10^7}_{s/yr} \cdot \underbrace{0.2}_{\pi/proton} \cdot \underbrace{0.05}_{\mu/\pi} = \underbrace{1.14 \times 10^{21}}_{\mu/yr \; @ \; 2GeV \; \mu \, Energy} \qquad (5.1)$$

41

5.4 Matching the cooling channel to the RLAs

At the end of the second cooling channel, the longitudinal emittance can be calculated as the product of the two half-axes with a ±45 degrees phase spread at 88 MHz and a ±40 MeV energy spread to be 0.0625 eVs. While the RLAs have a similar longitudinal acceptance, their frequency of 220 MHz is 2.5 times higher. That is why the longitudinal phase space has to be rotated to result in a ±200 MeV energy spread and a ±22.5 degrees phase spread at 220 MeV. This phase rotation has not yet been designed.

5.5 Technical challenges and an estimate of the rf power needed

The underlying motivation for this set-up is to plan for hardware with little extrapolation from existing technology. Based on the experience with 40 MHz CERN-PS cavities and based on analysis with Superfish [bi196] encouraging results have been obtained for resonator geometries that fit the needs of the cooling channel. Figure 5.9 shows a typical assembly, with a bore radius of 30 cm and a solenoid fitted inside a cylindrical volume of 22 cm width. A real-estate gradient of 2 MV/m at 44 MHz is obtained with a peak rf power of 1.86 MW per cavity.

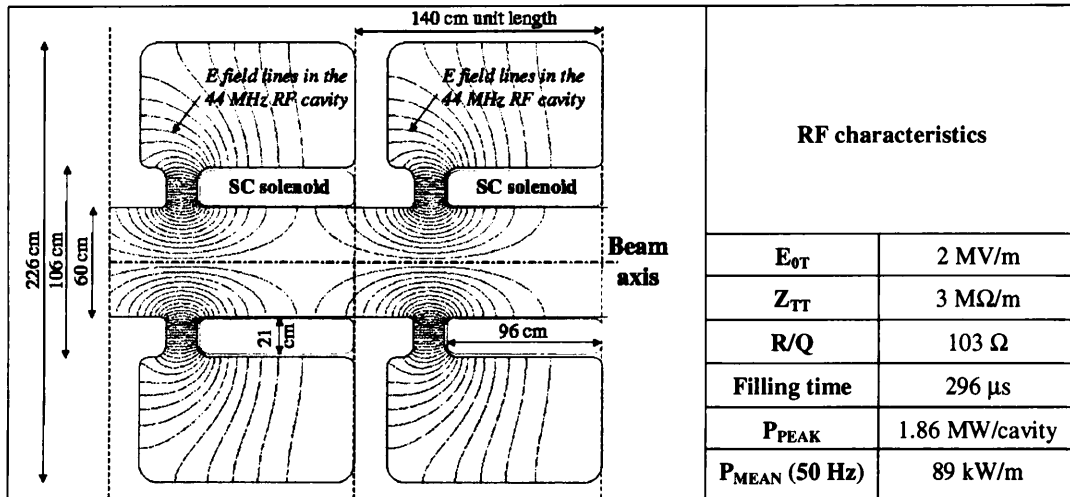| RF characteristics	
E_{0T}	2 MV/m
Z_{TT}	3 MΩ/m
R/Q	103 Ω
Filling time	296 μs
P_{PEAK}	1.86 MW/cavity
P_{MEAN} (50 Hz)	89 kW/m

Fig. 5.9 Sketch of a 44 MHz cavity with solenoid

With a similar design at 88 MHz and having a bore radius of 15 cm (see Fig. 5.10), a real-estate gradient of 4 MV/m is achieved with a peak rf power of 2.04 MW per cavity.

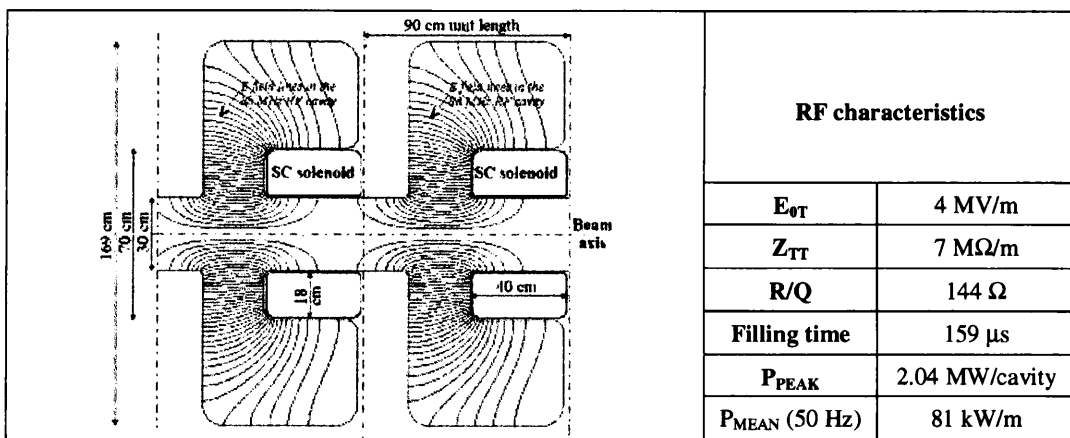| RF characteristics	
E_{0T}	4 MV/m
Z_{TT}	7 MΩ/m
R/Q	144 Ω
Filling time	159 μs
P_{PEAK}	2.04 MW/cavity
P_{MEAN} (50 Hz)	81 kW/m

Fig. 5.10 Sketch of an 88 MHz cavity with solenoid

The mean rf power required to operate all 200 m of the rotation and cooling sections at 50 Hz is consequently estimated to be 19 MW.

5.6 The dependence on the proton bunch length

Since the basic idea of the reference scheme is to make use of the pion beam microstructure in order to avoid re-bunching before cooling, the impinging proton beam longitudinal structure has an influence on the overall performance. The intrinsic spread due to decay and path length through the solenoid is of the order of 1 ns, so a proton beam bunch length below that value would not help. In Tab 5.2 the relative performances at the end of cooling for a square and for a Gaussian proton pulse are reported. An rms bunch length of 1 ns (3 ns total) is achievable as the number of bunches in the compressor ring is large and thus the space charge per bunch low enough to allow such a tight compression.

Tab. 5.2 Muon yield vs. proton bunch length for a square and for a gaussian pulse

Proton pulse total length (ns) (square pulse)	μ/year (10^{21})	Proton pulse rms length (ns) (Gaussian pulse)	Relative yield
0	1.6	0	100
1	1.5	1	89
2	1.4	2	80
3	1.3	3	73
4	1.2		
5	1.1		
6	1.1		
7	1.0		
8	0.98		
9	0.97		
10	0.93		

5.7 Muon front-end without cooling

The possibility of a muon front-end without cooling was examined [han00]. In particular a study was performed on a system using the same rf cavities and re-optimised magnetic fields as the one described above with the exception of the absorbers, which were removed everywhere. This ensures the compatibility of the two options and it gives an estimate of the yield for a potential staging of the front-end. The extra rf power available (as there are no absorbers) was dedicated to longitudinal matching, i.e. providing some bunching during the acceleration phase. The main parameters used in the simulations are shown in Tab 5.3.

Table 5.3 Simulation parameters for no-cooling scenario

	44 MHz section	88 MHz section	220 MHz section
Total length [m]	44	280	224
Solenoid field [T]	2.3	5	6
Aperture [cm]	60	30	20
Frequency [MHz]	44	88	220
Cavity length [m]	1.0	0.5	0.5
Gradient [MV/m]	2.0	4.0	10.0
Phase [deg]	0	±45	0
Kinetic energy [MeV]	200–300	300–1000	1000–3000

The longitudinal optics has been optimised by carefully choosing for each section the frequency and the corresponding synchronous phase. In the first section at 44 MHz, a maximum number of muons is captured in the relatively large bucket and smoothly pre-accelerated. The second section at 88 MHz has an alternating phase at ±45° which allows to accelerate the particles to 1 GeV keeping at the same time the distribution flat in longitudinal phase space. The resulting muon yield at 2 GeV is about a factor 10 smaller than the one obtained with the reference scheme.

5.8 Collaborations

- INFN Frascati collaborates with CERN successfully using the PATH program.

- The MICE (Muon international cooling experiment) collaboration [mice01].

5.9 Research needed

There are several ongoing activities in the phase rotation and cooling domains:

1. An overall optimisation of the proposed system (this includes the study of the decay mechanism in a magnetic field with the aim of reducing the emittance increase, the combination of acceleration and cooling in a super-cell with focus on longitudinal matching), using a hard-edge model for the fields for reasons of computing time.
2. The assessment of the behaviour of the system with engineering constraints (computed field, space for connections, etc.).
3. The definition of a muon cooling experiment to validate the proposal. A study of a possible muon cooling experiment is under way by an international collaboration [Han01]. A preliminary layout exists.

The performance of the overall scheme, as well as the construction (physical length) and operating costs (electricity consumption) depend heavily upon the characteristics of the rf systems. Since these systems operate in unconventional conditions, R&D is especially important, particularly on the following subjects:

- as a first step of investigation, interesting results can be achieved by modifying a PS 114 MHz cavity (formerly used for leptons) into an 88 MHz resonator equipped with a solenoid;
- design, construction and test of a high gradient 44/88 MHz cavity (including rf windows etc.);
- test of the maximum gradient capability in the presence of a solenoid field;
- design, construction and test of the 1.8 T superconducting solenoid;
- study and test of different technological solutions for the beam windows;
- study and development (with industry) of high power, high efficiency rf amplifiers.

5.10 Conclusions

A baseline layout for a phase rotation and cooling channel has been presented. It seems feasible with today's technology. The benefit of adding cooling to the neutrino factory complex is a gain of a factor of 10 in intensity. Further optimisation is needed to make the cooling channel more efficient.

5.11 WWW links

http://nfwg.home.cern.ch/nfwg/nufactwg/nufactwg.html

The CERN Neutrino Factory homepage.

6 Recirculating Linear Accelerators (RLAs)

6.1 Introduction

A major component of the Neutrino Factory is the acceleration of the muons to 50 GeV. There are two criteria to design this part: speed and effectiveness. A synchrotron would certainly be the most effective machine, but it is too slow compared to the muon lifetime. The solution is a Recirculating Linear Accelerator (RLA). This machine has the form of a racetrack, with two long acceleration sections and two short arcs. This setup allows for very high rf gradients over the circumference of the machine, while the expensive acceleration structures are used several times.

The most challenging part of an RLA is the arcs: as it is not possible to ramp up the bending magnets between turns, there have to be separate bends for each energy. As a result, a beam spreader has to guide the beam into the right bending section as a function of the beam energy. Again, as this magnet cannot be ramped up between turns, the spreader has to be passive. The high momentum spread of the beam makes the separation of the turns even trickier. In the case of this study, a clear separation is possible only above 4 GeV. As the first separation is needed after the first passage through a linac, this pushes the injection energy to 3 GeV. An overview of the two RLAs is given in Table 6.1.

Table 6.1 Overview of the Muon RLAs

	RLA 1	RLA 2
Number of full turns	4	4
Kinetic energy [GeV]	3–11	11–50
Length of each linac [m]	350	1900
Acceptance	1500 πcm mrad	1500 πcm mrad

6.2 First recirculator RLA1

The design of this machine is copied from that in Ref. [John00a]. The only difference is that 220 MHz superconducting rf cavities are used instead of 200 MHz ones. As their cut-off pipe is quite large, the limiting factor for the transverse acceptance of the machine is the arcs. Thus there is some more optimisation to be done as the length of the linac could probably be reduced.

The arcs are not made isochronous as in the previous studies [Pal99], because of the strong constraints associated with the design of the spreader. This implies that the bunch length increases during acceleration. Then, either some longitudinal matching has to be done between the two RLAs or the acceleration has to be modified.

6.2.1 Design criteria and parameters

In an RLA, the beam is injected into a linac, accelerated, and returned by arc transports, thereby achieving multiple passes of acceleration through the same linac. Single-pass linac acceleration must be used until the beam is sufficiently relativistic for multi-pass acceleration without phase slip. The longitudinal emittance must also correspond to a feasible RLA design in terms of both machine acceptance and clean separation between the arcs on each pass. At the exit of each linac, the beam is sorted by energy and directed into a separate return arc for transport. At the end of each arc, the separate transport trajectories are recombined for acceleration in the opposing linac. Since the circulation time is of the order of a microsecond, an active kicker system is not considered feasible for sorting. Instead, a passive system based on a dipole field to steer muons as a function of energy into the different channels is used. To separate cleanly in a passive system, the total energy width of the beam must be less than the energy difference between consecutive acceleration passes. This sets the minimum acceleration requirement and, therefore, the maximum number of recirculation turns. The principles of muon RLA acceleration are described in more detail in Ref. [Neuff00].

The difficulty in the design of the lowest-energy re-circulating linac lies in directing a beam with both a large transverse emittance and a large momentum spread into separate arcs on each acceleration pass. Because of the large momentum spreads, the design of the passive beam spreader is so difficult and constraining that it ultimately restricts the parameters and lattice of the lowest-energy re-circulating linac. Preliminary tracking results coupled to practical design issues (realistic magnet apertures and fields) limit the acceptance of the first recirculating linac to the numbers given in Table 6.2.

Table 6.2 Momentum spreads and beam radius in the arcs at the end of each acceleration pass in a 3–11 GeV recirculating linac

Cent. Momentum [GeV/c]	$\delta p/p$ (3σ)	Momentum spread [GeV/c]	Beam radius (3σ), [cm]
3	injection	2.8–3.2	–
4	±5.1%	3.8–4.2	±6.7
6	±4.2%	5.7–6.3	±5.9
8	±3.8%	7.7–8.3	±5.4
10	±3.5%	9.6–10.4	±5.0
11	extraction	–	–

The beam sizes in Table 6.2, which correspond to a normalised rms emittance of 1.5 mm.rad and ±3σ beam size, were determined by initial tracking of the lattice. Both the momentum spreads in Table 6.2, which are given for each acceleration pass, and the acceleration per turn, 2 GeV, are primarily determined by the magnet design and layout of the beam spreader. Below 2 GeV per turn, the energy separation of the beams from different turns is too close to effectively direct each acceleration pass into a separate channel using a passive, fixed-field system. (Even in the current system magnet apertures remain quite large.) The choice of the injection energy of 3 GeV is based partly on maximum possible injected beam size, which decreases with increasing energy (from ±7.5 cm at 2 GeV to ±6.2 cm at 3 GeV), reducing injection kicker aperture and length. The basic lattice design also benefits from lowering the ratio of extracted to injected energy which makes the optics more consistent as a function of energy, and improves machine performance.

6.2.2 RF cells

The rf cells are of FODO type. Two 220 MHz rf cavities are installed between each quadrupole for a total length of 3.1 m. These cavities are scaled from the 200 MHz rf cavities presently under development at CERN [Chiav01], shown on Fig. 6.1. The phase advance of 76.345°, which provides the minimum value of the β-functions, can be achieved with quadrupoles of length 0.7 m with a pole tip field of 0.5 T. The maximum value of the β-functions is 12.7 m. It can be shown easily that the increase of the value of the β-functions with energy, at successive passes, is more than compensated by the adiabatic damping of the transverse emittance during acceleration. Consequently, the normalised acceptance of these cells is that at injection. The radius of the cut-off pipe of the 220 MHz cavity is 172 mm. The normalised acceptance of the rf cells is then 6.6 cm.rad, i.e. larger than that of the arcs.
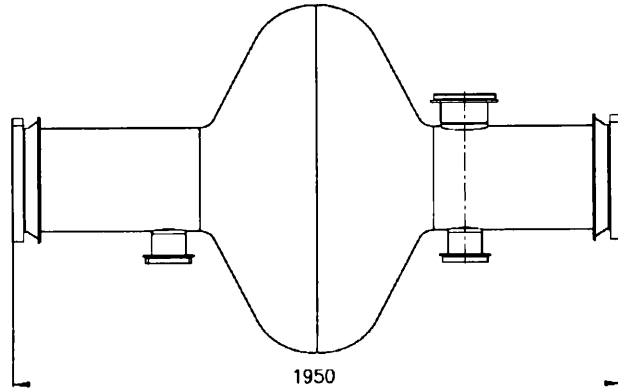
Fig. 6.1 200 MHz superconducting rf cavity under development at CERN

6.2.3 Beam spreader

A passive beam spreader is used to separate the different energy turns of the RLA into independent magnetic channels: 4-, 6-, 8-, and 10-GeV channels on one side and 5-, 7-, and 9-GeV on the opposing side giving a total of seven separate return arcs (the 11 GeV beam may be extracted upstream of the spreader using a kicker). The extremely large momentum spreads of Table 6.2 make a clean separation into individual channels difficult, particularly at the highest energies. If the magnets are staggered between neighbouring channels, at least 0.5 m separation is required for normal-conducting magnets. For superconducting magnets, which share collars/yokes (a multiple bore system), the separation can be decreased to 0.4 m. This decrease requires the arcs to be nested and parallel; the magnets must be aligned radially and encased in a single cryostat crossing all channels. For example, separation of the lowest momentum in the 10-GeV channel (9.65 GeV) by 0.5 m from the highest momentum in the 8-GeV channel (8.30 GeV) using a simple 3 m, 1.5 T dipole followed by a single drift section requires 27 m of drift and generates 5 m of dispersion. For a FODO structure, the transverse beam size increases by more than 30% without intervening quadrupoles, and must be rematched optically into the arc FODO structure. Until fully separated, spreader magnets must accommodate multiple channels. Even in the most efficient spreader designs, magnet apertures greater than 0.5 m are unavoidable, and can reach more than a meter depending sensitively on the details of the spreader layout. With such large magnets, vertical stacking is impractical, so the layout of the spreader and the arcs must be horizontal. Creating vertical dispersion in addition to horizontal dispersion due to the arcs would increase the complexity (and therefore the circumference) of the machine since dispersion must be cancelled before entering the linac section.
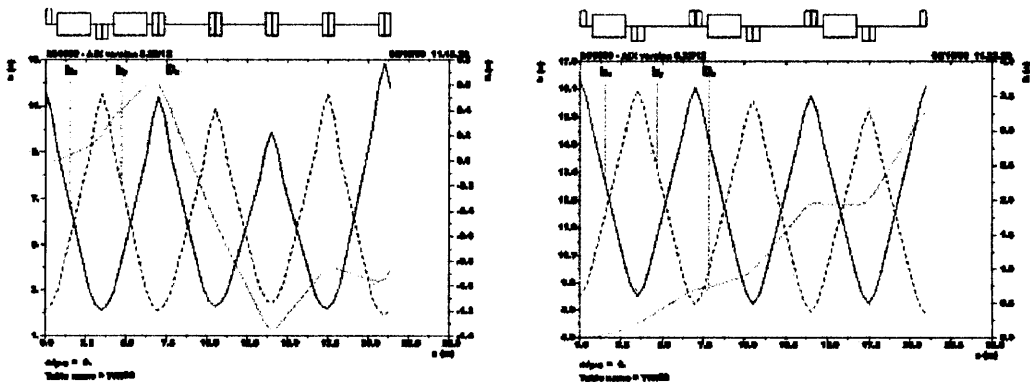

Fig. 6. 2 Lattice functions through the beam spreader for 4 GeV (left) and 10 GeV (right) momentum muons

47

The spreader magnet apertures are minimised when the lowest-energy channels are split off as soon as the minimum spatial separation requirement is met. The length of the entire spreader can be minimised if deflections are sequenced and if the spreader dipoles are embedded optimally in a FODO structure. Sequencing the deflections implies that once a channel is fully separated, another spreader dipole is inserted into the remaining combined channel to increase existing separation kicks. If the spreader dipoles are properly embedded into a FODO structure, the natural peak excursion locations of a FODO structure can be utilised to enhance the channel separation process. To this end the quadrupoles are centred on the highest energy centre orbit (10 GeV). After initial dispersion by a spreader dipole, off-momentum orbits undergo larger off-axis bend fields or kicks when traversing a defocusing quadrupole. Independent channels are then formed at the peak of the off-momentum excursion, or just upstream of every horizontally focusing quadrupole. Septum magnets are inserted prior to a channel split to 'straighten' the rapidly diverging extracted beam, making the newly independent channel parallel to the next highest energy channel and keeping the relative separation between consecutive channels constant. Optimised beam spreader optics for the 4-GeV and 10-GeV channels are presented in Fig. 6.2. Complete separation of all energy channels is achieved in less than 20 m without interrupting the FODO optics of the linac. A list of magnet fields and apertures is given in Table 6.3 based on actual magnet designs. The dipole components in the spreader quadrupoles can be reduced by averaging or smoothing over several quadrupoles since the bends are alternating reverse bend/bend. However, this would require a detailed ray tracing through a physical layout of the spreader magnets. The total bend of the spreader for all channels is 0.294 radians, thus reducing the total bend required in each arc by 0.588 radians.

Table 6.3 Beam spreader and arc magnets: General parameters

Magnet	Number	Length [m]	Dipole field [T]	Quad. gradient [T/m]	Horiz. aperture [cm]	Vert. Aperture [cm]
Spreaders	4	–	–	–	–	–
Spreader dipoles	4 × 3	2	.5–1.9	–	60	10
Spreader septa	4 × 3	2	–1	–	40	10
Spreader quads	4 × 16	0.75	0–4	7.7	25–60	10
Individual arcs	7	–	–	–	–	–
Arc comb. funct	7 × 17	1.5	–	4.3	30	10
Matching quads	7 × 2	1.5	–	4.3	30	10

6.2.4 The arcs

In order to design a machine without an active (pulsed) section to match the different arc channels to the linac optics a suitable periodic structure must be imposed throughout the machine. Short FODO cells have a large energy acceptance and small transverse beam sizes. The structure of the rf cells described in Section 6.2.2 is continued through the spreader. In the arcs the same cell and focal length, i.e. phase advance, is preserved, but longer, combined function magnets are used instead. This has the effect of not only reducing significantly the number of magnets required, but also lowering dispersion and, correspondingly, momentum compaction, or $M_{56} = \int \eta d\theta$.

Table 6.4 Example M_{56} values for $\Phi_s = 30°$ in a 3–11 GeV, 4-turn RLA

Momentum [GeV]	3	4	5	6	7	8	9	10	11
M_{56} [m]	inj.	0.5	0.65	0.8	0.9	1.0	1.1	1.2	1.3 (ext.)

While there is significant flexibility in the RLA bunching scenarios, the RLA arcs must be designed to match the parameters of the bunching scenario in order to obtain the required longitudinal motion. In Ref. [MC96] the scenario has a fixed acceleration phase of 30° with M_{56} increasing from arc to arc, with the first arc (4 GeV) at $M_{56} = 0.5$ m and the last arc (10 GeV) at 1.2 m (Table 6.4). The M_{56} value is

determined by the dispersion or amount of dipole bend per arc cell, so, ultimately it determines the number of cells in an arc. Also, the total length of each arc must be fine-tuned to match an integral multiple of the rf wavelength, which is 1.363664 m at 220 MHz. Not only must the central value of momentum compaction (M_{56}) be specified, but also its derivative with respect to momentum must be zero. Horizontal sextupoles are employed to cancel the first derivative of momentum compaction with vertical ones added to stabilise and balance the off-momentum optics. As a consequence, 90° cells are employed for the lowest energy (4 GeV) primarily because they support strong sextupoles with minimum degradation of transverse dynamic aperture. (Although 90° has the added advantage that the beam size in both planes is minimised simultaneously, the short cell length is the more significant restraint.) For higher energy arc channels, the cell phase advance decreases proportionally.

Cancellation of dispersion and the first derivative can be achieved by requiring an integer phase advance across the arc for all channels. If 24 cells are used (including the beam spreader cells), then 4-, 6-, and 8-GeV arcs have automatically approximately an integer phase advance. The 10-GeV arc gradients have to be gently tuned to the closest integer, representing only a degree change in the individual cell phase advance. Note that the beam spreader sets up an unavoidable, but periodic, dispersion wave through the arc, but, because of the unbroken periodic structure, beta functions automatically match closely. Similarly, on the opposing side, the 5-, 7-, and 9-GeV arcs use 35 cells, with the 9-GeV gradients being adjusted slightly to reach the nearest integer tune. The entire length of the arc with two beam spreaders is 168 m.

As mentioned before, the arcs are nested so that the bend per cell cannot be adjusted to control the central value of M_{56} independently for each channel. To control the value of M_{56} in this scheme, the dipole component (which is approximately equal initially in both combined function magnets) is moved from the horizontally focusing combined function magnet in the lowest energy channel to the horizontally defocusing combined function magnet in the highest channel, with the other channels having intermediate distributions. That is, only the horizontally defocusing magnet in the 10-GeV channel has a dipole bend (0.16 radians in 16 magnets). The 4-GeV channel had 0.08 radians in 33 arc magnets (17 horizontally focusing and 16 horizontally defocusing). The goal is to scale M_{56}, or momentum compaction, proportionally with energy and match the rf bucket. With this technique, momentum compaction varies from 0.012 to 0.07 for the 4- and 10-GeV arc cell unit, respectively. Because this matching technique is linear, using only phase advance, no adverse impact is observed on dynamic aperture. Alternatively, a matching section with properly chosen dipoles can be used for dispersion matching along with additional families of sextupoles to handle the first derivative. The length of such a section and the impact on dynamic aperture would need to be carefully evaluated.

6.3 Second recirculator RLA2

The design of the second RLA is optimised for the normalised acceptance of 15 cm.rad. Its design is copied from that of ELFE at CERN [Burk01] with the notable exception that the final energy is 50 GeV and the energy gain per turn is 10 GeV instead of 3.5 GeV.

6.3.1 Design criteria

The problems associated with the spreader are less serious than for the case of RLA1 described in Section 6.2 thanks to the reduction of both the relative energy spread and the beam emittance. This is why the ELFE design could be used with some modifications associated with the larger acceptance of the RLA.

6.3.2 RF cells

The rf cells are of FODO type. We studied whether triplet focusing was more attractive [Keil01a]. For a given length of the accelerating linac, it is not. Four LEP-type rf cavities are installed between each quadrupole for a total length of 14.5 m. The phase advance of 76.345°, which provide the minimum value of the β-functions, can be achieved with quadrupoles of length 0.5 m with a pole tip field of 0.5 T.

The maximum value of the β-functions is 49.7 m. It can be shown easily that the increase of the value of the β-functions with energy, at successive passes, is smaller than the increase of the energy. Consequently the normalised acceptance of these cells is that at injection. The details of this analysis can be found in Ref. [Keil01b].

6.3.3 The arcs

As in ELFE, the arcs are made of isochronous cells. The optics functions associated with these cells are shown in Fig. 6.3. The value of the average dispersion function can be adjusted by specifying its value at the end of the cell. A complication of the isochronicity problem is introduced by the existence of the vertical spreader. The latter has a huge effect on the path length and the matching of the matrix element M56 over the arc is not easy.
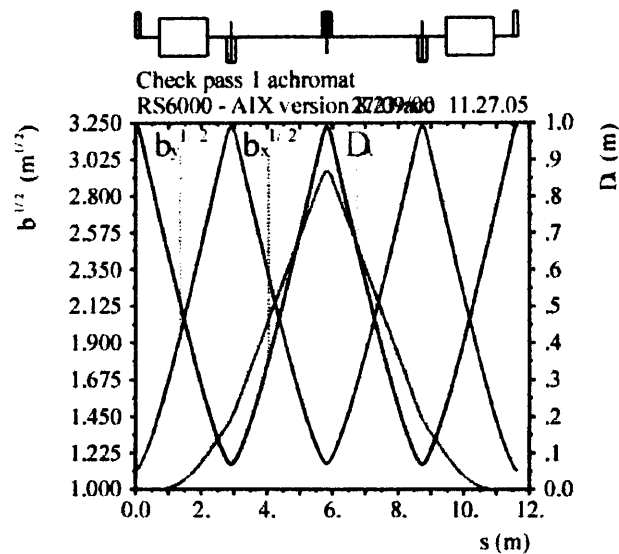

Fig. 6.3. Isochronous cell for the arcs of RLA2

6.3.4 Beam spreader

A passive beam spreader is used to separate the different energy turns of the RLA into independent magnetic channels: 16-, 26-, 36-, and 46-GeV channels on one side and 21-, 31-, and 41-GeV on the opposing side giving a total of 7 separate return arcs. In contrast with RLA1, the separation is vertical as it makes the width of the tunnel the smallest possible. A possible design of this spreader is shown in Fig. 6.4. A design with four dipoles has been chosen to reduce the vertical dispersion created by this system. Here the problem is to pile-up the separation dipoles so that there is no overlap of their yokes, and to obtain isochronicity as mentioned above. The matching of the rf cells to the arc through this spreader can be done. The optical functions in the matching section are shown in Fig. 6.5. The separation of 0.5 m between the central orbit of the arcs is assumed to be sufficient to accommodate the magnet yokes. This distance can be increased by modifying the place of the last dipole of the spreader system and rematch the optics accordingly. The limitation to this process is imposed by the increase in aperture associated with the increase of the vertical dispersion. In order to illustrate this, the acceptance of the machine, obtained after the full arc matching, over the four passes is shown in Fig. 6.6.
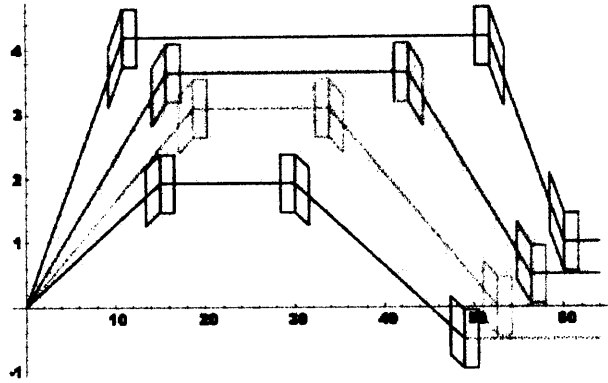
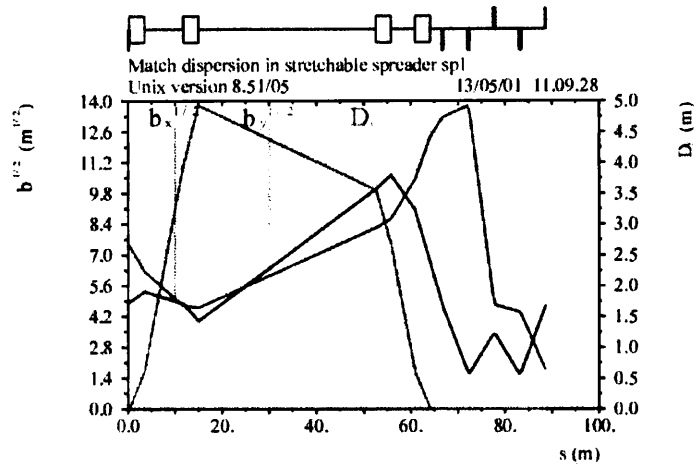**Fig. 6.4** Typical beam spreader for RLA2 (all dimensions in meters).

Fig. 6.5 Matching section between the rf cells and the arcs of RLA2
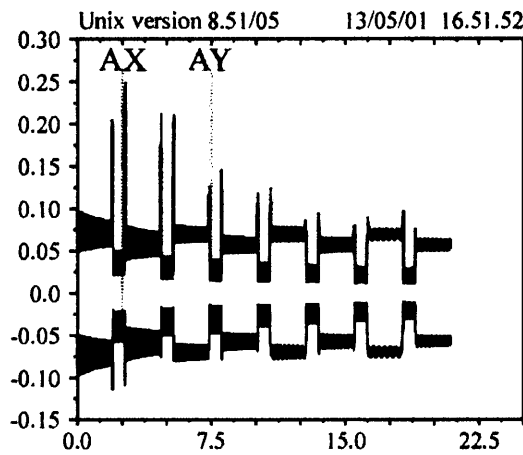

Fig. 6.6 Acceptances of the RLA2 during the four passes. Note that the acceptance is limited by the vertical dispersion. The horizontal acceptance has been plotted as negative in order to make a clear separation from the vertical plot. The ordinate is the aperture radius in meters that allows for 3 rms beam radii. The abscissa is the path length throughout all turns in the RLA in kilometers.

6.3.5 Multi-bunch beam loading compensation in the RLAs

Beam loading in RLA2 can introduce an energy variation between leading and trailing bunches of about ±0.73% [Keil00b] assuming that the cavities are on resonance. The energy shift along the bunch train is larger than the nominal rms beam energy spread in the muon storage ring (0.5%), and it therefore needs to be reduced by a compensation scheme. While in the RLA1 muon beam fills the complete circumference, in RLA2 long gaps between bunch trains may complicate the beam loading compensation in some of the schemes proposed [Keil00b].

A satisfactory beam loading compensation can be achieved by a bunch spacing slightly different from an integer multiple of λ_{rf} [Zimm01c, Ferr01].

This compensation scheme was originally suggested by E. Keil [Keil00b]. In Ref. [Zimm01c] approximate analytical expressions were derived which describe the multi-bunch beam loading in such a scenario. Application to the two RLAs of the CERN Neutrino Factory shows that a bunch spacing shifted in frequency by $\Delta f = -14$ kHz from the rf frequency f_{rf}, combined with an initial phase offset of about $-10°$ with respect to the crest of the rf, reduces the bunch-to-bunch energy variation to less than 0.5% peak-to-peak, or to less than a third of the half-momentum acceptance for the muon storage ring [Zimm01c]. The average accelerating gradient would be 1.66% smaller than the unloaded maximum value. Similar conclusions were obtained in Ref. [Ferr01].

In actual operation, the bunch spacing may stay constant, and the RLA rf frequency will likely be adjusted for varying beam current, assuming that the change required is smaller than typical bandwidths of klystrons and tuning ranges of cavities.

6.4   WWW links

http://nfwg.home.cern.ch/nfwg/nufactwg/nufactwg.html

The CERN Neutrino Factory homepage.

7 Decay Ring

7.1 Generalities

This section describes the design of a 50 GeV muon storage ring that is part of the ongoing study of a neutrino factory in Europe. The Neutrino Oscillations Working Group developed a set of parameters for such a neutrino factory that are desirable from the point of view of neutrino oscillation physics [Blo99]. They are displayed in the upper part of Table 7.1. The lower part shows the accelerator physics parameters of the muon storage ring designed to achieve the desired physics parameters. Parameters of a 30 GeV muon storage ring were given earlier [Pal99]. A feasibility study of another neutrino factory has been made at Fermilab [Fer00]. Its 50 GeV muon storage ring has somewhat different parameters [John01].

Table 7.1 CERN Muon Storage Ring parameters

Design momentum	50 GeV/c
Muon flux at injection	$10^{14}\ s^{-1}$
Distances to far neutrino detectors	1000 and 3000 km
Vertical slopes of straight section	−78.6 and −237.9 mrad
Normalised divergence at σ	0.1
Configuration	Triangle
Normalised emittance at σ	1.667 mm rad
Aperture limit	3σ
Frequency of rf system	352.209 MHz
Bunch spacing	multiple of 0.851178 m
Relative rms momentum spread	0.005

The muon flux is the rate at which muons arrive in the muon storage ring. The fraction of muons that decay in the straight section(s) pointing towards distant detector(s) is less than unity, and determined by the geometry of the muon storage ring. The distances to the detectors determine the vertical slopes of the long straight sections pointing at the detectors. With the usual relativistic factor γ of the stored muons, the normalised divergence $\gamma\sigma'$ is the ratio of the physical rms divergence σ' and the typical opening angle $1/\gamma$ of the decay neutrinos in the straight section(s) pointing towards distant detector(s).

The normalised emittance given in Tab. 7.1 is a design goal, which is not fully achieved at the moment. The purpose of this study, however, has been to produce a consistent scenario of a Neutrino Factory that produces 10^{21} neutrino per year. Even though there are losses between the end of the cooling channel and the acceleration section, this number is achieved. An updated design of RLAs and storage ring with larger acceptances and/or more cooling leaves room for improvement.

It is assumed that an rf system is installed, equipped with superconducting LEP cavities, determining the frequency and the bunch spacing. The nominal rms momentum spread of the muon beam determines the aperture of the storage ring.

7.2 Geometry

In order to achieve a high fraction of muons that decay in the straight section(s) pointing towards distant detector(s), the fraction of the circumference occupied by these straight sections should be large, and the fraction occupied by the arcs joining them should be small. Sending neutrinos to two detectors at different distances implies two long straight sections pointing downwards from the surface of the Earth. Thus, the natural choice is a bow-tie shape, with the two detectors in opposite directions and the muon storage ring in a (nearly) vertical plane. The two long straight sections cross at an angle equal to the sum of the two initial slopes. If this sum is small, long straight sections and compact arcs fit together well.
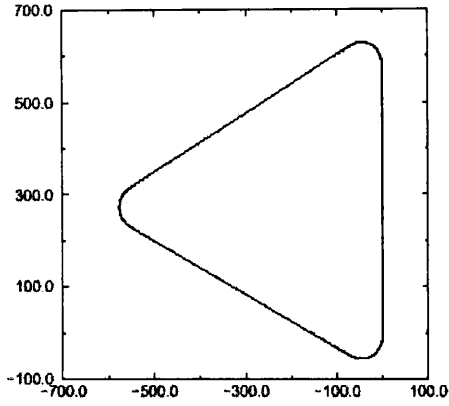
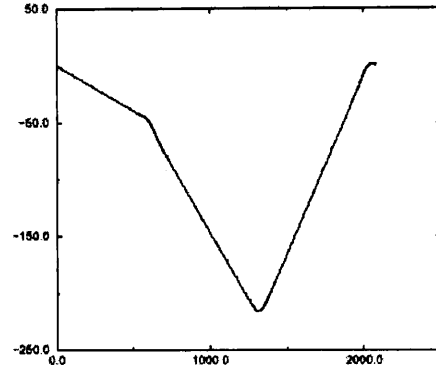**Fig. 7.1** Projection of the muon storage ring on a plane tangent to Earth

Fig. 7.2 Vertical position y along the circumference of the muon storage ring

If one wants to keep the muon storage ring in a nearly horizontal plane, this implies that the directions towards the two detectors are at approximately right angles. In this case, a triangular shape with two long straight sections pointing downwards towards the detectors, and a third long straight section pointing upwards to close the ring, is more attractive than a bow-tie shape. This is because with the triangular shape one can still have long straight sections and compact arcs, while the bow-tie shape with long straight sections crossing at a large angle implies long arcs. The triangular shape is more efficient for plane angles between the directions to the detectors of more than 92° [Gru01].

As an example, it is assumed that the muon storage ring has the shape of an equilateral triangle with rounded corners. It is easy enough to adapt the exact shape later, once the geographical positions of the muon storage ring and the two detectors are known [Ver00]. Figure 7.1 shows the projection of this muon storage ring on a plane tangent to Earth. The reader can verify that the projection is not an equilateral triangle. Figure 7.2 shows the vertical position y along the circumference of the muon storage ring. The origin of y is arbitrary. The total height of the muon storage ring, less than 250 m, is smaller than the thickness of the molasses near the CERN site, which is one of the factors influencing the length of the long straight sections. Figure 7.3 shows the pitch angle ϕ, and Fig. 7.4 the roll angle y along the circumference of the muon storage ring. These angles correspond to MAD definitions [MAD95]. The pitch angles in the first two straight sections are $\phi_1 = -78.6$ mrad and $\phi_2 = -237.9$ mrad, respectively, by design. The pitch angle in the third straight section $\phi_3 = +319{:}6$ mrad is the result of a calculation. The roll angle y does not vanish in the straight sections. Both pitch and roll angle vary rapidly in the arcs. Table 7.2 shows the range of vertical level of the three arcs. They are of the order of 20 metres.
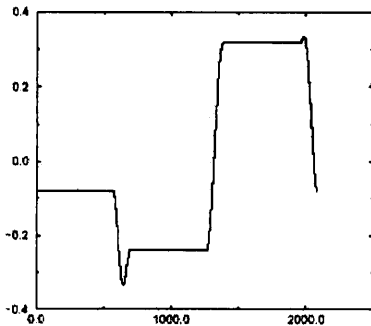

Fig. 7.3 Pitch angle ϕ along the circumference of the muon storage ring
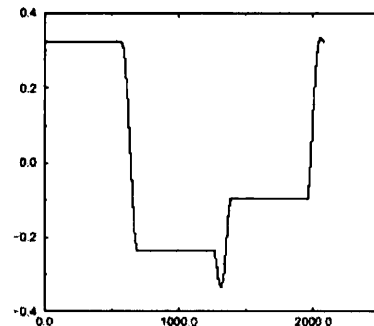

Fig. 7.4 Roll angle y along the circumference of the muon storage ring

Table 7.2 Range of vertical levels y of the three arcs. The origin of y is arbitrary.

Arc number	1	2	3
Top	–45.211m	–202.376m	+0.861 m
Bottom	–73.918m	–216.180m	–21.530 m

7.3 Optical modules

The optical design of the muon storage ring is very modular, and consists of the following modules that will be discussed in detail below:

- FODO cells in the arcs

- Dispersion suppressors at either end of the arcs, consisting of two FODO cells with the same focusing as the arc cells, but modified bending

- Standard long straight section FODO cells in two of the long straight sections, and modified long straight section FODO cells in the third long straight section

- Matching cells between dispersion suppressors and long straight sections

This style of muon ring design was implemented by Keil [NF26] and was previously used [Keil99] for the design of the racetrack muon storage ring.

7.3.1 FODO cells in the arcs

The input parameters for the design of the arc cells are the dipole field, the quadrupole field at the aperture radius, the maximum length of a dipole, the number of dipoles in a half-cell, and the free space, i.e. the space in a half-cell not occupied by dipoles and quadrupoles. A rather conservative dipole field is used, hoping that quadrupoles with this field can be built economically with a single-layer coil. The quadrupole field at the edge of the aperture is lower than the dipole field because of the tungsten shielding between the vacuum chamber and the superconducting coil. The quadrupoles are quite short. The dipoles also are assumed to be relatively short in order to have tight focusing and a small dispersion. A round vacuum chamber is assumed, although an elliptical chamber with a smaller height would also work. An engineering study of the packaging of dipoles and quadrupoles in cryostats, bearing in mind the pitch and roll angles discussed earlier, and a cost estimate are needed before another round of studies of the arc cells. Tables 7.3 and 7.4 show the geometrical and optical parameters of the arc cells, respectively. Figure 7.5 shows their optical functions.

Table 7.3 Geometrical parameters

Dipole field (BA)	6 T
Quadrupole field (QFA, QDA)	3 T
Maximum dipole length	3 m
Quadrupole length	0.5 m
Number of arc cells	3 × 10
Arc cell length	9.703 m
Dipoles per half-cell	1
Dipole length	2.911 m
Bending angle	209.4 mrad
Bending radius	27.797 m
Average radius	46.328 m
Sagitta in dipoles	0.038 m

Table 7.4 Optical parameters

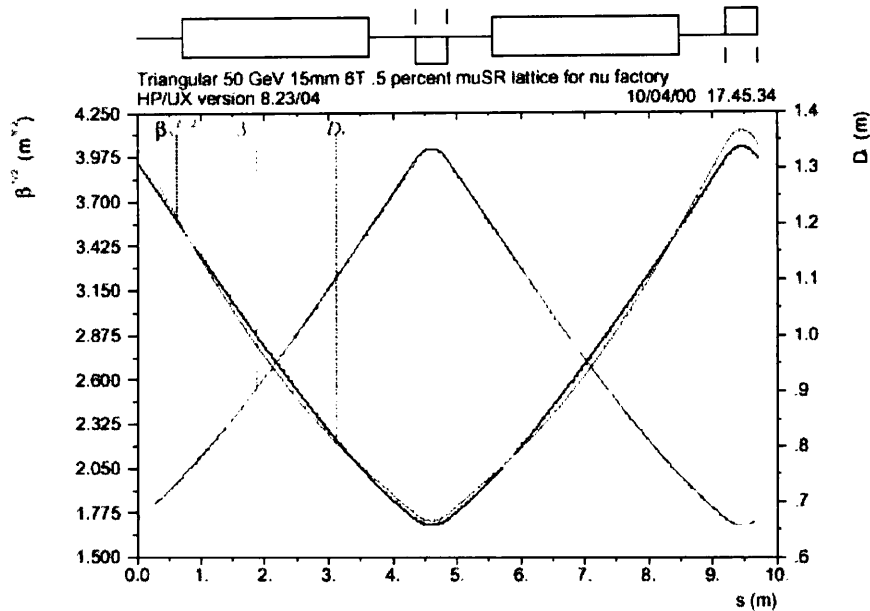|	
Phase advance/2π	0.25
Arc tune	7.5
Maximum β-function	16.56 m
Maximum dispersion	1.375 m
Un-normalised emittance	3.52 μm
RMS beam radius	10.28 mm
Vacuum chamber radius	30.83 mm
Max. half-momentum spread	0.0224
Focal length of quadrupoles	3.431 m
Quadrupole length	0.5 m
Free space in half-period	1.441 m

Fig. 7.5 Optical functions of the arc cells. Note the suppressed zero on the ordinates.

7.3.2 Dispersion suppressors

In order to reduce the dispersion and its derivative to zero in the long straight section, one arc cell at either end of the arcs is replaced by two dispersion suppressor cells each, with modified bending, but the same focusing and period length. In thin-element approximation, neglecting the edge focusing in the dipoles, the average bending in the dispersion suppressor cell is one-half of that in an arc cell, while the distribution between the two dispersion suppressor cells depends on the phase advance [Keil77]. For finite-length elements, neither is true, and MAD does the matching. The data are adjusted such that the total bending angle is 2π, although all the bending angles change. The length of the dipoles in the dispersion suppressors has not been reduced, although their field is only about half that of the arc dipoles.

7.3.3 Long straight section cells

The input parameters for the design of the long straight sections are the total and the period length, the quadrupole field at the aperture radius, and the normalised divergence. The total length of the straight section has to be a multiple of the period length there. Long periods have the advantage that the lever arm for injection is long, and that the number of components in the long straight sections is small. Normalised divergence and period length yield the phase advance, the β-functions, and the focal length of the quadrupoles. These quantities, together with the emittance, yield the rms beam radius, aperture radius, and length of quadrupoles. Since the quadrupole field is low, permanent-magnet quadrupoles look very attractive [Keil00]. There need be neither power nor interlock circuits. Water-cooling would only be needed for the power in the charged muon decay products. Table 7.5 shows the parameters and Fig. 7.6 the β-functions of the long straight-section cells. Figure 7.7 shows the normalised divergence $\gamma\sigma'$ in the whole long straight section, including the adjacent matching cells. It demonstrates that $\gamma\sigma'$ has the design value in the long straight-section cells proper, but larger values in the matching cells at either end. Local minima of $\gamma\sigma'$ occur in all quadrupoles. The plot shows them in those quadrupoles that are split into two halves, but not in the others.

Table 7.5 Long Straight Section Parameters

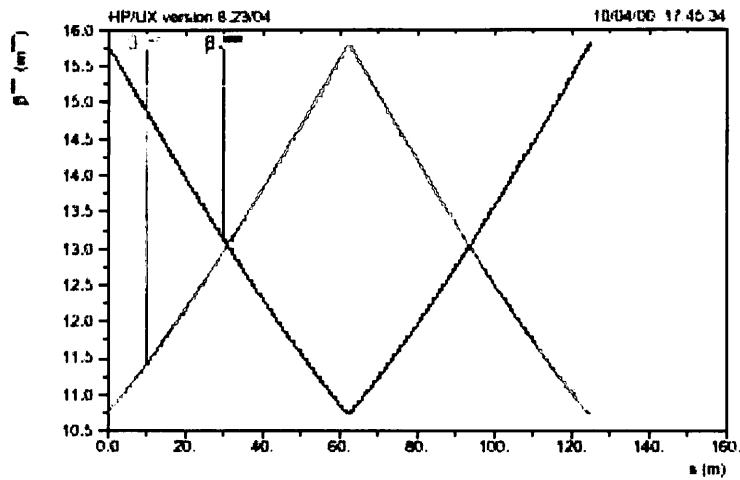| Length of cells	125 m
Quadrupole field (QFS, QDS)	0.5 T
Maximum β-function	249.7 m
Minimum β-function	115.3 m
Maximum RMS beam radius	29.7 mm
Aperture radius	89.0 mm
Focal length of quadrupoles	84.8 m
Length of quadrupoles	0.35 m

Fig. 7.6 Optical functions of long straight section cells. Note the suppressed zero on the ordinate.
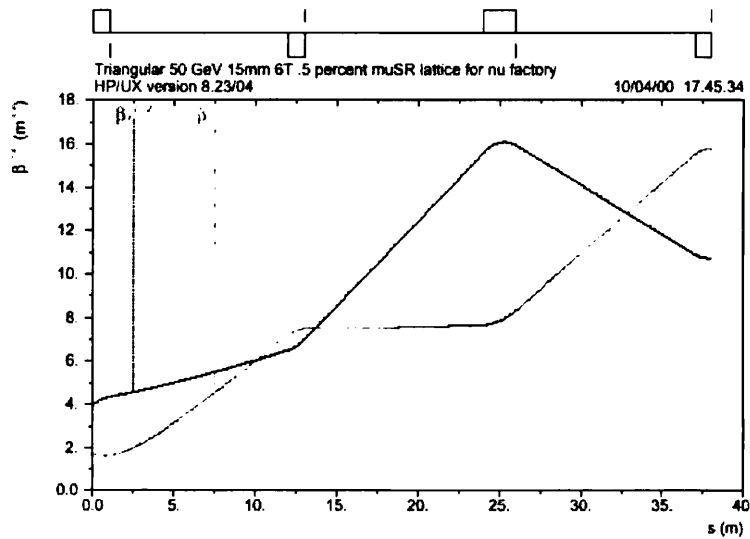

Fig. 7.7 Optical functions of the matching cells

The third long straight section is used for fine adjustments of the tunes. The fractional parts are the same as in the LHC. The geometrical layout is identical to that in the other two long straight sections, but the phase advance and quadrupole gradients in the cells are changed.

7.3.4 Matching cells

The matching cells match the α and β-functions between the dispersion suppressors and the long straight section cells. Four variable quadrupoles, labelled Q1M to Q4M, with three fixed drift spaces between them are used to satisfy these four conditions. At the beginning, their lengths were all arbitrarily set to 1 m. Tracking with COSY-INFINITY [COSY99] for the FNAL design showed a reduction in the dynamic aperture, caused by the fringe fields of quadrupoles in their matching insertion [Zimm00], consequently the lengths of the six quadrupoles Q3M and Q3MT were doubled. Tracking with COSY-INFINITY then showed that the dynamic aperture remains larger than the physical aperture [Zimm00a]. Figure 7.7 shows the β-functions through the matching cells. They vary smoothly between the low values in the dispersion suppressors and the high values in the long straight section. The matching cells surrounding the long straight section for fine adjustments of the tunes have the same geometrical layout, but the gradients of the quadrupoles Q1MT to Q4MT are different from those of Q1M to Q4M.

7.4 Optics of the muon storage ring

Assembling and matching the complete muon storage ring with finite elements yields the geometrical and optical parameters shown in Table 7.6 and the linear optical functions as shown in Fig. 7.8. Tables 7.7 and 7.8 show the parameters of the quadrupoles and dipoles, respectively. Because of the matching with finite elements and edge focusing, the absolute values of the strengths K_1 of the QDA and QFA quadrupoles are not the same, and the bending angles in the BD1 and BD2 dipoles are not equal, and not exactly one-half of that in the BA dipoles.

Tab 7.6 Parameters of the Muon Storage Ring

Length of arcs	347.808 m
Length of matching	228.000 m
Length of straight sections	1498.950 m
Muon decays/detector	0.2774
Circumference	2074.831 m
Revolution frequency	144490 Hz
Momentum compaction	0.00257998
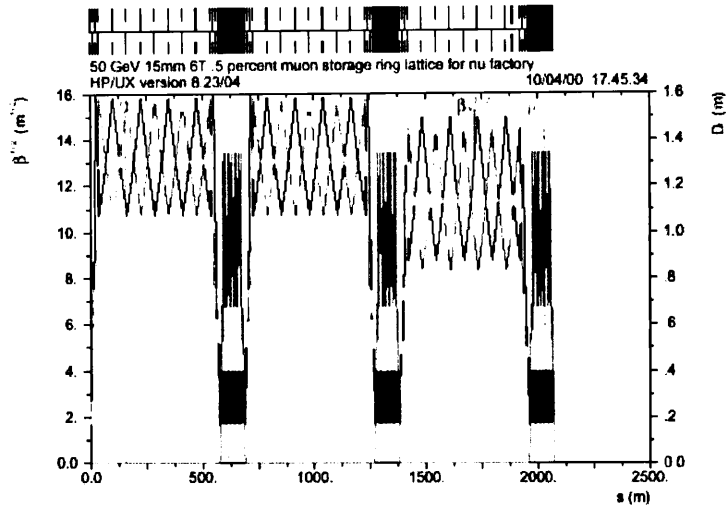
Fig. 7.8 Optical functions of the muon storage ring

Tab. 7.7 Quadrupole Parameters

Name	No.	L/m	K_1/m^{-2}
QFA	33	0.500	+0.603574
QDA	36	0.500	−0.596693
QFS	8	0.350	+0.0337579
QDS	6	0.350	−0.0337579
Q1M	4	1.0	+0.110848
Q2M	4	1.0	−0.0809091
Q3M	4	2.0	+0.0388587
Q4M	4	1.0	−0.0476056
Q1MT	2	1.0	+0.135905
Q2MT	2	1.0	−0.0853225
Q3MT	2	2.0	+0.0388150
Q4MT	2	1.0	−0.0486465

Table 7.8 Dipole parameters

Name	No.	L/m	Φ/r
BA	48	2.911	0.10469
BD1	12	2.911	0.052327
BD2	12	2.911	0.05254

Table 7.9 Sextupole parameters

Name	No.	L/m	K_2/m^{-3}
SDA	24	0.24	−5.040708
SFA	24	0.24	+2.830460

7.4.1 Chromatic effects

Correcting the chromaticity with only two families of sextupoles in the arc cells achieves the chromaticities shown in Fig. 7.9. The tune spread over three rms energy spreads is pretty small. Table 7.9 shows the sextupole parameters. Figure 7.10 shows that the chromatic functions $\beta^{-1}d\beta/d\delta$ (resulting in a neutrino flux uncertainty) and $dD/d\delta$ (leading to debunching) are pretty bad. Their extreme values are much larger than in the arcs and the long straight sections alone. They are driven by the matching cells, and do not change much when the sextupoles are excited.
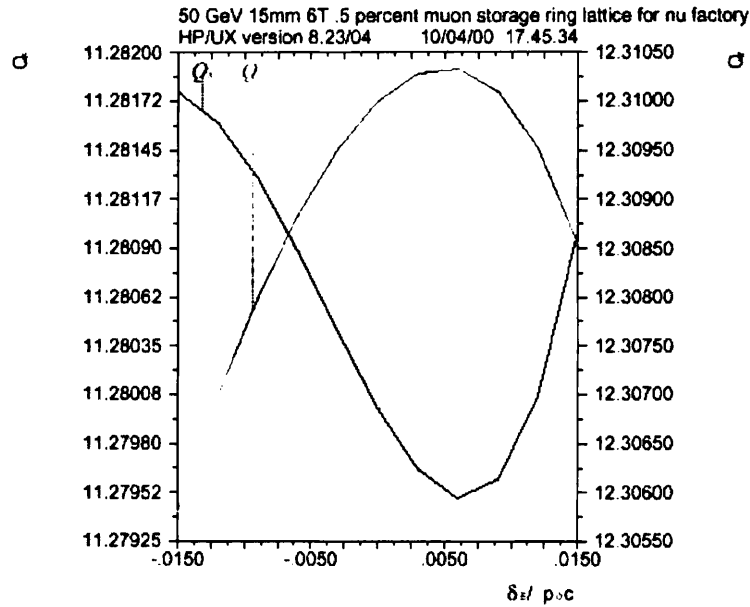
Fig. 7.9 Variation of the horizontal tune Q_x and of the vertical tune Q_y over a momentum spread corresponding to $\pm 3\sigma_e$
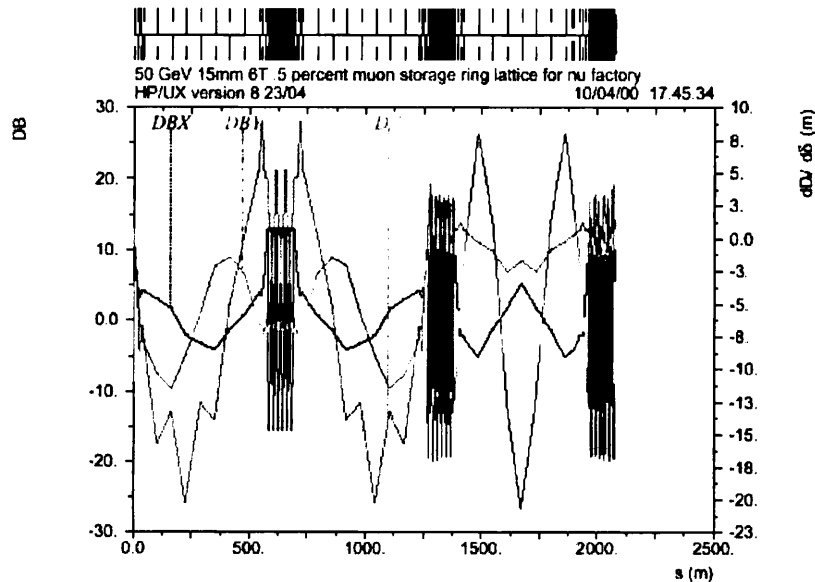

Fig. 7.10 Chromatic functions $DBX = \beta_x^{-1}d\beta_x/d\delta$, $DBY = \beta_y^{-1}d\beta_y/d\delta$ and $D'_x = dD/d\delta$ of the muon storage ring. The sextupoles are not excited.

60

offsets in x and y simultaneously that correspond to 0.1, 0.2, ...,1.0 times the physical aperture, and vanishing momentum error $d = 0$ for 1000 turns, well beyond the muon lifetime. Rectangular collimators at all quadrupoles have half-apertures equal to three standard deviations of the local beam radius. Rectangular collimators are unphysical, but they avoid confusion that could arise by losing large-amplitude particles on a collimator early in the beam line. Figs. 7.11 and 7.12 show the results. Using the TRANSPORT and LIE4 tracking methods, and changing the MAD fringe field definition of the dipoles does not have much effect on the tracking results. Particle no. 10 is lost horizontally. Particle no. 9 is lost vertically.
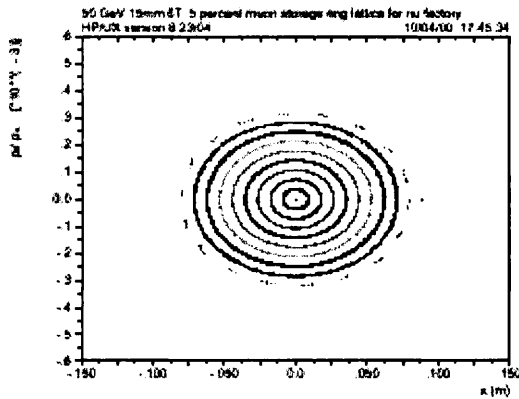

Fig. 7.11 Horizontal tracking results. The physical aperture is ±89 mm at the place where the phase plots are drawn.
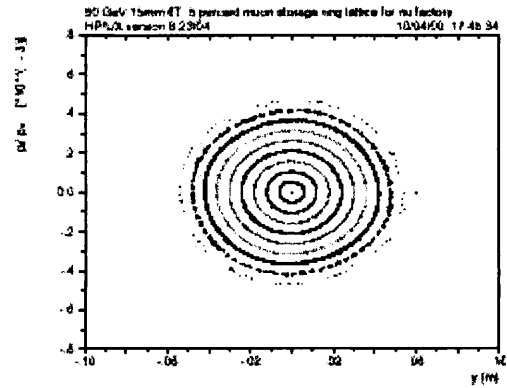
Fig. 7.12 Vertical tracking results. The physical aperture is ±60.5 mm at the place where the phase plots are drawn.

In the second tracking style, typically 30 000 particles are launched with random initial conditions, selected from truncated Gaussian distributions with standard deviations related to emittances, momentum spreads, etc. Typically 100 turns are tracked, comparable to the muon lifetime, and various phase-space projections of the final distributions as well as the distribution of particle losses along the storage ring are observed [Keil99a].

Figure 7.13 shows the horizontal distribution of the 28991 muons surviving after 100 turns at the horizontally focusing quadrupole at the entrance of the long straight section. Figure 7.14 shows the distribution of the 1009 muons lost along the circumference of the storage ring as a function of the turn. Most of the losses occur during the first few turns in the first long straight section. Losses continue to occur during later turns in the arcs. Results obtained with both COSY INFINITY and MAD [Zimm00a] also include tracking with momentum errors and are in good agreement with these results.
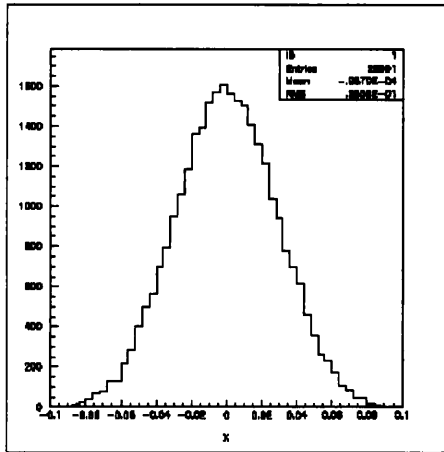
Fig. 7.13 Horizontal distribution of the 28991 muons surviving after 100 turns at the horizontally focusing quadrupole at the entrance of the long straight section. The horizontal aperture is ± 0.089 m.
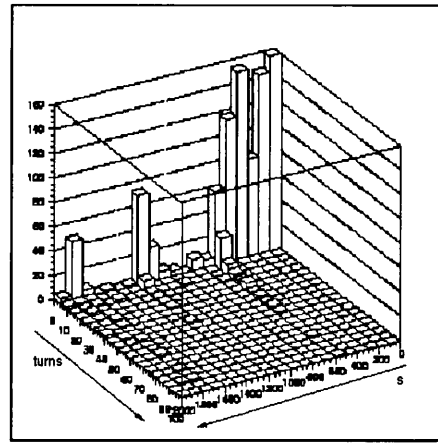
Fig. 7.14 Distribution of the muon losses along the circumference of the storage ring on the right axis as a function of the turn on the left axis

7.5 Injection

The muon beam is injected into a half-period of the long straight section between two quadrupoles. The upstream quadrupole is defocusing and the downstream one is focusing in the plane of injection. Since the muon source is most likely close to the surface thof the earth, the most logical place for the injection system is the upstream end of the first long straight section, pointing downwards. The first element of the injection system is a septum magnet just upstream of the defocusing quadrupole. At that quadrupole, the injected beam and the circulating beam, both with radius 3σ, just touch. The aperture of this quadrupole must be large enough to take both the injected and the circulating beam. A full-aperture injection kicker just upstream of the focusing quadrupole brings the injected beam onto the design orbit. The kicker field drops to zero before the injected bunch train arrives at the kicker in its second turn. This fall time of the kicker magnet determines the number of kicker modules; the shorter the fall time the higher the number of modules. Since the finite lengths of the quadrupoles and injection kicker are neglected, its parameters, shown in Tab 7.10, are optimistic. Longer periods and higher phase advances in the long straight sections make the injection kicker easier.

Table 7.10 Injection kicker parameters

Maximum kicker voltage	60 kV
Characteristic kicker impedance	5 Ω
Kicker fall time	1.0 μs
Width of kicker aperture	177.9 mm
Height of kicker aperture	120.9 mm
Deflection angle	1.934 mrad
Integrated kicker field	0.323 Tm
Length of kicker modules	2.703 m
Number of kicker modules	2
Actual kicker voltage	57.4 kV
Magnetic kicker field	0.0597 T

7.6 RF system

An rf system could be needed in the storage ring for two reasons: (i) to avoid the depolarisation due to the different rate of spin precession of the muons in the beam with an rms energy spread σ_e [Blo99], if the muons are polarised at injection, and (ii) to avoid de-bunching of the muon beam which would make gating in the far detector impossible. It is not yet clear if either of these features will be requested by the physics community.

Table 7.11 shows the parameters of the rf system. It is assumed that superconducting LEP cavities are used. This determines the frequency. With a peak voltage of about 100 MV the bucket height is about $3\sigma_e$. The bunch length σ_s and the bunch area A are those of bunches that would be matched to the rf bucket. The length and area of the bunches arriving in the storage ring depend on the injectors. In the MAD data the rf system was installed at the downstream end of the long tuning straight section, close to the surface of the Earth. The beam port radius of the cavities [Aul99] is well matched to the aperture in the long tuning straight section. Figures 7.15 and 7.16 show the distributions along the beam axis of a train of three bunches, without and with the rf system after 20 turns. For the purpose of this study, the bunches were initially 1.7 m apart, although in the current design the spacing is 6.8 m, corresponding to a 44 MHz bunch structure. Without the rf system, the beam is nearly de-bunched.

Table 7.11 Parameters of the rf system

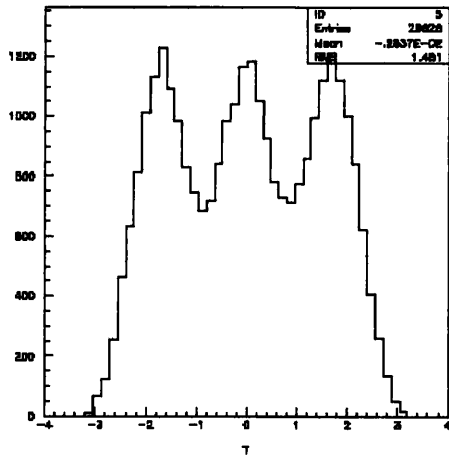|	
Frequency, f_{rf}	352 MHz
Peak voltage, V_{rf}	100 MV
Harmonic number, h_{rf}	2438
Bucket height	0.0145
Synchrotron tune	0.044885
rms bunch length	95 mm
Bunch area $A = 4\pi\sigma_e\sigma_s E/c$	1 eVs

Fig. 7.15 Distribution of three bunches along the beam axis without rf system after 20 turns. The abscissa is in metres.
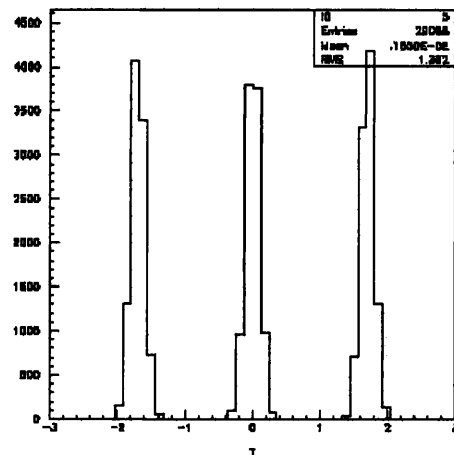

Fig. 7.16 Distribution of three bunches along the beam axis with rf system after 20 turns. The abscissa is in metres.

7.7 Research needed

- The next step should be engineering studies of the components for the arcs. They should take into account that the arcs will be installed with significant and rapidly varying pitch and roll angles.

- The study of the rf system has to be repeated based on the 6.8 m bunch spacing.

7.8 Conclusions

The design of a Muon Storage Ring for a Neutrino Factory at CERN meets the requirements of neutrino oscillation physics. The machine fits into the molasses layer in the neighbourhood of CERN, provided that there are few small-scale perturbations. The modular optical design achieves a dynamic aperture larger than the physical one.

8 Alternative scenarios

8.1 The beta beam

The beta beam is a possible alternative scenario to the whole Neutrino Factory complex. It is based on the idea of using short-lived beta emitters instead of muons for neutrino production. The advantage lies in the low Q-value of the decay of these nuclei, which leads to a low transverse momentum in the decay and thus a better focused neutrino beam. The disadvantage is the low neutrino energy, which has to be compensated by complementary measurements with a neutrino superbeam.

8.1.1 Target station for production of intense beams of short-lived beta emitters

A target station based on the ISOL technique [Ravn98] consisting of a target and ion source unit remotely coupled to a front-end which contains the beam extraction and focusing elements, is illustrated in Fig. 8.1.
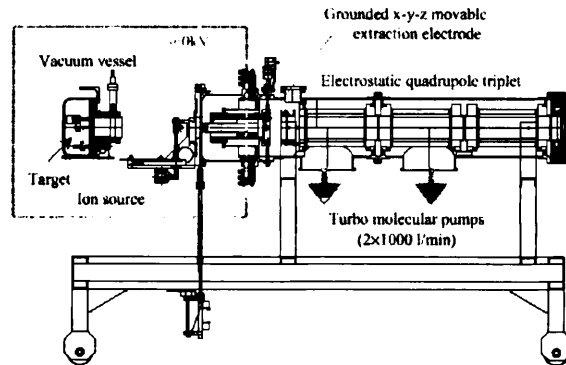

Fig. 8.1 ISOLDE front-end

The nuclide of interest is produced by proton fragmentation of a refractory target kept at high temperature and thick enough to stop the fragments. By means of diffusion and desorption processes the isotopes of the element in question are released and transferred to an ion source. The source emittance is typically in the range of 2–50 πmm mrad. By means of a 60 kV extraction field the singly charged ions are accelerated and may subsequently be electromagnetically mass separated into beams of their individual isotopic components.
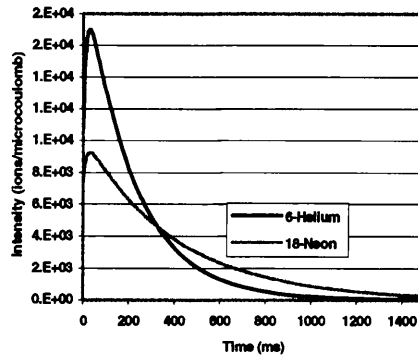

Fig. 8.2 Delay time function for He and Ne released from a MgO target

The very asymmetric pulse shape of the resulting ion current shown, helium and neon in Fig. 8.2, is not determined by the proton bunch and the nuclear reaction but by the relatively slow thermal release and transfer processes [Ravn97, Lettry97b]. This function also controls what is usually the largest loss factor ,the half-life dependent decay losses occurring during the release and transfer processes.

65

The beam intensity that may be obtained from such a target station is determined by Eq. 8.1:

$$I = \alpha \Phi N \varepsilon_1 \varepsilon_2 \varepsilon_3 \qquad (8.1)$$

where α is the formation cross-section for the nuclear reactions of interest, Φ the primary-beam intensity, N the useable target thickness, ε_1 the product release and transfer efficiency, ε_2 the ion-source efficiency, and ε_3 the delay transfer efficiency due to radioactive decay losses.

Table 8.1 gives the ^{6}He beam intensities extracted from the ion source and the target and ion-source parameters using present technology. One can see the expected yields after the successful termination of the development of the EURISOL facility [EURISOL].

Tab. 8.1 Overview of target technologies.

Target element and technique	Target thickness [g/cm^2]	Cross section [cm^2]	Proton driver beam [GeV]	[mA]	Production rate in target [atoms/s]	Transfer efficiency [atoms/s]	^{6}He Beam [ions/s]
MgO target technology presently operating	3	1.0^{-27}	1	0.004	1.8^{+09}	0.025	4.6^{+07}
BeO target improved with known technique	30	1.0^{-26}	1	0.1	4.6^{+12}	0.25	1.1^{+12}
New BeO target technology to be developed	30	1.0^{-26}	2.2	2.5	3.1^{+14}	0.25	7.8^{+13}
Mercury-jet target to be developed	800	2.6^{-26}	2.2	2.5	9.7^{+14}	0.05	4.8^{+13}
Spallation neutron (n, α) reaction							
BeO with converter technology under development	3	6.0^{-25}	2.2	2.5	2.1^{+15}	0.25	5.3^{+14}

8.1.2 Radioactive-ion production system

The generation and extraction of short-lived radioactive ions, which may be useful as precursors for intense, pure electron-neutrino beams, is a well-known technique used in various Radioactive Ion Beam (RIB) facilities, mainly in Europe. A method, very similar to pion production of in-flight capture of charged heavy-ion fragments is the presently preferred production method for high-energy radioactive ion beams in particular for short-lived species.

However, when it comes to the production of high-intensity beams of radioactive nuclei, the technique of target fragmentation by means of an intense proton or neutron beam as practised at ISOLDE [Ravn79] is the method of choice. Such a facility based on the Isotope Separator On-Line technique (ISOL) allows the use of very thick targets in which the fragments are brought to rest before they are re-ionised and accelerated.

An intensive programme for further development of this technique for present and future RIB facilities is actively being undertaken by the EURISOL collaboration [EURISOL]. The possibility of using the MW power of future GeV proton driver accelerators for a RIB intensity increase of 10^3 has already been assessed. For the nuclei relevant to a neutrino source which are formed in high cross-section reactions with half-lives in the range of 100 ms to 10 s the prospects are particularly promising.

This method for the production of electron neutrinos has the following technical advantages over the method for production of muon neutrinos:

1. For a majority of the chemical elements the RIB production is a known technique.
2. No charged-particle collection and cooling system is needed since the products are extracted from ion sources with good emittance.
3. The overall efficiency of transforming the nuclei into a beam of interest is >10%.
4. The MW power of spent protons can be absorbed at a location chosen far from the target and any accelerator component.
5. One may even contemplate using part of the by-products such as pions and 150 GeV/A daughter nuclei for other purposes.

8.1.3 Acceleration and storage of ions for a beta beam

The beta beam requires that ions be accelerated to a Lorentz factor of 150 for ^{6}He and 60 for ^{18}Ne. The neutrino source itself consists of a storage ring for this energy range, with long straight sections pointing at the experiment(s). Such a storage ring does not exist at CERN today, nor does a high intensity proton source for the production of the radioactive ions. Nevertheless, it seems prudent to study whether any part of the existing CERN accelerator infrastructure can be used as this could still represent an important saving for a beta-beam facility. Such a study has been started and has already revealed some important facts. Figure 8.3 shows a possible baseline scheme.
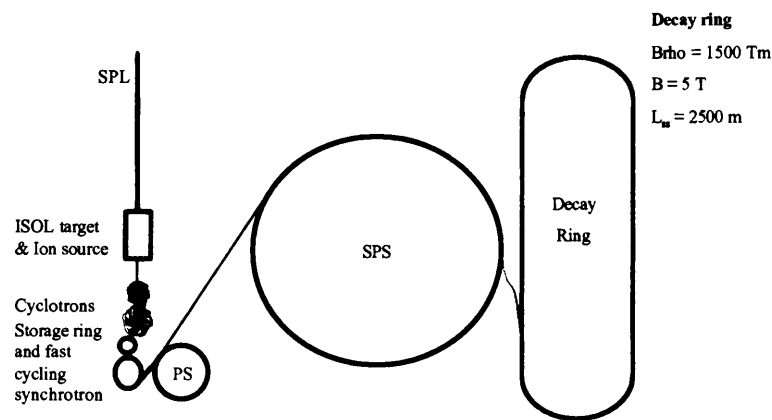

Fig. 8.3: A possible baseline scheme for beta-beam acceleration at CERN. The machines and transfer lines drawn in dashed line will have to be built while the parts marked with a solid line are existing installations. From [BB02].

The essential parameter for such a neutrino source is the longitudinal density of ions in the storage ring. The number of ions per nanosecond must exceed a certain threshold to give a detectable signal above background in the detector. The PS and SPS accelerators were built for fixed-target physics with proton beams of high intensity but distributed in many bunches. Beta beams do not require any intensity records to be broken, but the ions must ultimately be delivered in a single bunch. Consequently, a severe bottleneck arises due to space charge. This precludes the use of the existing Booster to inject into the PS, while, at SPS injection, important modifications to the RF system will have to be envisaged to permit something approaching the required intensities to be handled.

The decay of a radioactive ion changes its charge state, which will cause it to be lost from the accelerator. No acceleration is lossless, but ions are particularly vulnerable due to the potential change of charge state by ionisation or recombination with rest gas electrons. The limiting factor will be the magnitude of all these losses, as they will eventually cause damage to the hardware of the accelerator itself.

After acceleration, the storage ring should ideally hold a single short bunch, which gets 'topped up' at regular intervals to compensate for decay losses. It is clear that any stacking process will lead to phase space dilution. A possible way of counteracting this would be beam cooling. However, there is no technical solution available for beam cooling at the energies required. Electron cooling is the most promising candidate, but the theoretical cooling times are of the order of several minutes, which would make it useless for a beta-beam facility. A brute-force way around this problem would be to use a storage facility comprising multiple rings in which bunches can circulate in parallel.

An interesting new concept to circumvent phase space dilution is asymmetric bunch pair merging [BB02]. It is based on the fact that during the storage time, the phase space density of the ion bunch decreases continuously due to decay and blow-up. If a fresh, densely populated bunch is merged into the centre of the bucket, the phase space density in the centre of the bunch will be increased. This does not violate Liouville's theorem: the total phase space volume is conserved at best, but regions of lower densities are exchanged with regions of higher densities, leading to an overall increase of the density in the

phase space region *of interest*. Technically this is achieved by injecting the new bunch off momentum in a high dispersion region onto a matched dispersion trajectory (Fig. 8.4, middle). Subsequently, the injected bunch rotates a quarter turn until the initial conditions for bunch pair merging are met (Fig. 8.4, right side). The merging itself is performed with a higher-harmonic RF.
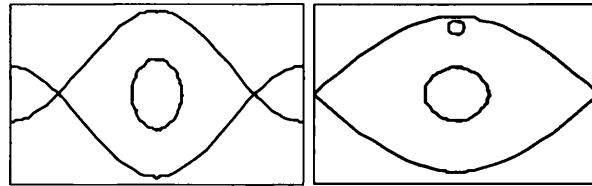

Figure 8.4: Bunch rotation stacking in the storage ring in the energy/phase diagramme. From left to right: big old bunch (green); new small bunch injected with higher energy (red); bunch merging. From [BB02].

At this stage, some scenarios for beta-beam acceleration have been sketched. It is too early to state if any of these will permit the acceleration, stacking, and storage of suitable beams. Still, it is important that this part of the beta-beam concept be studied thoroughly to permit a full and fair comparison with the more traditional muon-based neutrino factory. Furthermore, a 'green-field' scenario free of the limitations imposed by the existing CERN accelerator infrastructure should also be considered for a complete picture of the possibilities offered by this concept.

9 Neutrino Radiation Hazard

Apart from the classical radiation protection issues of the target and the high power proton linac, there is a third source of possible radiation hazards for a Neutrino Factory: neutrino radiation. Owing to the geometry of the decay ring it is impossible to produce only neutrino beams that point towards far detectors. In the case of a triangular decay ring, for example, a third straight section is needed to close the ring. This third straight section produces a neutrino beam that directly points to the sky above the Neutrino Factory site.

A study [Sil02] has been made to assess the radiation hazard associated with the decay ring. The results in the case of 10^{21} muons per year at 50 GeV in the storage ring are as follows:

- To shield against radiation of the muons in the storage ring, 100 m of earth are sufficient.

- Shielding against neutrinos is impossible due to their long attenuation length. The annual dose induced by the neutrinos in the third straight section would be 16 mSv at the surface.

- This dose is above the limit of ionising radiation that can be emitted by CERN beyond its boundaries, which is 1.5 mSv. This means that even if the decay ring could be off-site, the location where the neutrino beam emerges from the ground would have to be on a CERN site.

References

[Apo99]   M. Apollonio et al., hep-ex/9907037

[Aul99]   K. Aulenbacher et al., in ELFE at CERN – Conceptual Design Report, CERN 99-10 (1999).

[Aut 99]   B. Autin, A. Blondel and J. Ellis (Eds.), Perspective Study of Muon Storage Rings at CERN, CERN 99-02, ECFA 99-197, (1999).

[Aut97]   B. Autin et al., PS XXI, A New Synchrotron for the LHC Injector, Part. Accel. 58 (1997).

[Autin01] B. Autin et al., Conducting Target, to be published in the proceedings of NuFACT01, Nucl. Instrum. and Methods A.

[Ball99]   A. Ball, A. Blondel, S. Gilardoni and N. Vassilopoulos, Preliminary Magnetic Horn Studies in the Collection Scheme for a Neutrino Factory (Proc. NuFact'99, Lyon, July 1999), NuFact Note 4

[Bau96]   G. S. Bauer et al., The European Spallation Source Study, vol. III, The ESS Council, ESS-96-53-M, ISBN 090 237 659, (1996).

[BB02]   The Beta Beam accelerator working group, M. Lindroos (Ed.), The acceleration and storage of radioactive ions for a neutrino factory, CERN NUFACT Note 121 (2002).

[Bellone] R. Bellone et al., Beam Tests of a 36 mm Lithium Lens, Proc. EPAC'90 Ed. Frontieres, Nice, 1990, pp. 1303-05.

[Bil96]   J.H. Billen et al., Poisson Superfish, LA-UR-96-1834.

[Blo99]   A. Blondel et al., Beam and Experiments: Summary, presented at v-Fact'99, Lyon, France, 5–9, July 1999.

[Blo99]   A. Blondel, Muon Polarisation in the Neutrino Factory, presented at v-Fact'99, Lyon, France, 5–9 July 1999, also Neutrino Factory Note 7 (1999).

[bnl01]   S. Ozaki, R.B. Palmer and M.S. Zisman, Feasability Study-II of a Muon-Based Neutrino Source, http://www.cap.bnl.gov/mumu/studyii/final_draft/The-Report.pdf

[Bry95]   P. Bryant et al., The Accelerators for the AUSTRON Spallation Source, Proc. 4th EPAC, London, World Scientific, Singapore, 1994, p. 2667.

[Burk99]   H. Burkhardt (Ed.), ELFE at CERN, Conceptual Design Report, CERN 99-10 (1999).

[Capp01]   R. Cappi et al., Increasing the Proton Intensity of PS and SPS, CERN/PS 2001-041 (AE), CERN/SL 2001-032

[Cer00]   A. Cervera et al., Golden Measurements at a Neutrino Factory, hep-ph/0002108.

[Cgg02]   M. C. Gonzalez-Garcia et al., Developments in Neutrino Physics, CERN-TH/2002-021, hep-ph/0202058.

[Chiav01] E. Chiaveri, private communication, March 2001.

[CNGS98]   The Cern Neutrino Beam To Gran Sasso, CERN 98-02, INFN/AE-98/05.

[COSY99]   K. Makino and M. Berz, COSY INFINITY Vers. 8, Nucl. Instrum. Methods A427(1999) 338.

[Debray01] E. Debray et. al., GHMFL Annual Report, chapter 7.1, http://ghmfl.polycnrs-gre.fr/AR2001.htm

[dis]   http://mlm.home.cern.ch/mlm/mucoll/nudis.html

[Dyd99]   F. Dydak, Spokesperson, Proposal to Study Hadron Production for the Neutrino Factory and for the Atmospheric Neutrino Flux, HARP PS-214, CERN-SPSC/99-35, SPSC/P315, (1999).

[ESS96]   The ESS Technical Study, ESS-96-53-M (1996).

[EURISOL] http://www.ganil.fr/eurisol/index.html

[Fabich00] Experimental Observation of MHD Effects and Proton-Induced Shocks. To be published in the proceedings of NuFACT01, Nucl. Instrum. and Methods A.

[Farhat] M. Farhat, Laboratory for Hydraulic Machines, Uni Lausanne, http://lmhwww.epfl.ch

[fer00] N. Holtkamp and D. Finley, A Feasability Study of a Muon-Based Neutrino Source, http://www.fnal.gov/projects/muon collider/nu/study/report/machine report/

[Ferr01] M. Ferrario, V. Fusco and M. Migliorati, Beam Loading Compensation Schemes for the Muon Recirculating Linacs of the CERN Neutrino Factory, CERN-NUFACT Note 076 (2001).

[Gar 99] R. Garoby and M. Vretenar, Status of the Proposal for a Superconducting Proton Linac at CERN, CERN/PS/ 99-064 (RF), (1999).

[Geer 98] S. Geer, 'Neutrino beams from muon storage rings: characteristics and physics potential', FERMILAB-PUB-97-389, 1997; Presented in the Workshop on Physics at the First Muon Collider and Front-End of a Muon Collider, November, 1997, and published in Phys. Rev. D57 (1998) 6989-6997.

[Gru01] P. Gruber, Ionisation Cooling for a Neutrino Factory, CERN-THESIS-2001-029

[Han00] K. Hanke, Muon Front-End Without Cooling, CERN NUFACT-Note 59 (2000).

[Han01] K. Hanke et al., Beam Dynamics Study of a Muon Ionization Cooling Experiment, CERN Neutrino Factory Note 108 (2001).

[Has00] H. Haseroth, Status of Studies for a Neutrino Factory at CERN, Proc. 7th Eur. Part. Accel. Conf. (Vienna, 2000), E.P.S., Geneva, 2000, p. 253 and R.Garoby, HEAC'01 (2001).

[Has01a] A. Hassein et al., RPAH071, PAC 2001, Chicago.

[Has01a] A. Hassein et al., ROPB009, PAC 2001, Chicago.

[Holz01] E. B. Holzer, Simulation of the Pion Decay Channel of a Neutrino Factory, Neutrino Factory Note 92.

[Ibc01] J. Burguet Castell et al., On the Measurement of Leptonic CP violation, CERN-TH/2001-081.

[ICFA00] The ICFA/ECFA Workshop 'Neutrino Factories based on Muon Storage Rings', Lyon, Nucl. Instrum. Methods A 451, No.1 (2000).

[Ili91] A. Iliev and Yu. Senichev, Racetrack Lattices for Low-Medium-Energy Synchrotrons , Proc. 14th PAC, San Francisco, May 1991, IEEE, New York, 1991, p.1904.

[ISAC] P. Schmoor, private communication.

[Jack75] J. D. Jackson, Classical Electrodynamics, Second Edition, J.Wiley & Sons, New York (1975), p. 588.

[John00a] C. Johnstone and D. Neuffer, A 3-11 GeV Recirculating Linac for Muon Acceleration, to be published in NIM.

[John01] C. J. Johnstone, http://www.fnal.gov/projects/muon collider/nu-factory/subsys/ss-stgring/50gevtable.gif

[kaon] http://buchalla.home.cern.ch/buchalla/kaonwww/kaon.html

[Keil00] E. Keil, Permanent-Magnet Quadrupoles for Neutrino Factories, CERN-SL-2000-006 (AP) (2000), also Neutrino Factory Note 15 (Feb 2000).

[Keil00b] E. Keil, private communication (2000).

[Keil01a] E. Keil, Triplet Focusing in Recirculating Muon Accelerators. CERN-NUFACT-Note-058 (January 2001).

71

[Keil01b] E. Keil, Focusing in Recirculating Muon Accelerators, CERN-NUFACT-Note-067 (2001).

[Keil77] E. Keil in Theoretical Aspects of the Behaviour of Beams in Accelerators and Storage Rings, M.H. Blewett Ed., CERN 77-13 (1977), p. 22.

[Keil99] E. Keil, Muon Storage Rings Design with Simple Mathematica Packages, CERN-SL-99-053-AP (1999).

[Keil99a] E. Keil, Histograms of MAD Tracking Results, CERN-SL-Note-99-061-AP, also Neutrino Factory Note 12 (1999).

[Kirk00] H. Kirk et al., 'Target Studies with BNL E951 at the AGS' PAC01

[lep01] LEP Electroweak Working Group, A Combination of Preliminary Electroweak Measurements and Constraints on the Standard Model, CERN-EP/2001-098, hep-ex/0112021

[Lettry97a] J. Lettry et al., Nucl. Inst. and Methods Phys. Res. B 126 (1997), 170.

[Lettry97b] J. Lettry et al., Nucl. Inst. and Methods Phys. Res. B 126 (1997), 130.

[Lom00] A. Lombardi, A 40-80 MHz System for Phase Rotation and Cooling, Proceedings Nufact'00, to be published, CERN NUFACT-Note 20, (2000).

[MAD95] H. Grote and F.C. Iselin, The MAD Program, Version 8.16, User's Reference Manual, CERN SL/90-13 (AP) Rev. 4 (1995).

[Man01] L. K. Mansur et al., J. Nucl. Materials, 296 (2001) 1.

[Mau80] J.M. Maugain, S. Rangod and F. Voelker, Study of a Horn with Integrated Target for a Neutrino Factory, NuFact Note 80.

[MC96] The Muon Collaboration, Muon Collider: A Feasibility Study, BNL-52503, Fermi-Conf. 96/092, LBNL-38946 (July 1996).

[mice01] http://hep04.phys.iit.edu/cooldemo/

[Mokh95] N.V. Mokhov, The Mars Code System User's Guide, Fermilab-FN-628 (1995); N.V. Mokhov, MARS Code Developments, Benchmarking and Applications, Fermilab-Conf-00-066 (2000); N.V. Mokhov, S.I. Striganov, A. Van Ginneken, S.G. Mashnik, A.J. Sierk and J. Ranft MARS Code Developments, Fermilab-Conf-98/379 (1998); LANL Report LA-UR-98-5716 (1998); nucl-th/9812038 v2 16 Dec 1998; O.E. Krivosheev and N.V. Mokhov, A New MARS and its Applications, Fermilab-Conf-98/43 (1998).

[Mor02] Y. Mori, Neutrino Factory in Japan: Based on FFAG accelerators, NuFactJ Note (2002), http://www-prism.kek.jp/nufactj/THALA003.pdf

[Neuff00] D. Neuffer, Fermilab Note, MuCool-75 (2000).

[NIM00] Nucl. Instrum. and Methods Phys. Res. A 451 (2000).

[Pal99] R. Palmer, C. Johnson and E. Keil, A Cost-Effective Design for a Neutrino Factory, presented at Nu-Fact'99, Lyon, 5–9 July 1999, also CERN-SL/99-070-AP (1999).

[path90] Computer Codes for Particle Accelerator Design and Analysis. A compendium. Los Alamos LS-UR-90-1766.

[Pir00] W. Pirkl, Personal communication, 2000.

[Pri00] C.R. Prior and G.H. Rees, Synchrotron-Based Proton Drivers for a Neutrino Factory, Proc. EPAC 2000, Vienna, (2000), pp. 963-965.

[Ravn01] H. L. Ravn, The CERN Target and Horn Concept for a Neutrino Factory Based on Muon Beams, to be published in the proceedings of NuFACT01, Nucl. Instrum. Methods A.

[Ravn79]   H. L. Ravn, Experiments With Intense Secondary Beams Of Radioactive Ions, Phys. Rep. 54 (1979) 203.

[Ravn97]   H. L. Ravn et al., Nucl. Instrum. Methods B 126 (1997) 176.

[Ravn98]   H. L. Ravn, Philos. Trans. R. Soc. Lond. A 356 (1998) 1955.

[Samulyak] R, Samulyak, The Frontier Code, BNL

[Sch00]   H. Schönauer (Ed.), Proton Drivers for Neutrino Factories: the CERN Approach, CERN-NuFact Note 046, (2000).

[Sch00a]   H. Schönauer et al., A Slow-Cycling Proton Driver for a Neutrino Factory, CERN-NuFact Note 30, (2000).

[Sievers01] P. Sievers, A Stationary Target for the CERN Neutrino Factory. To be published in the proceedings of NuFACT01, Nucl. Instrum. Methods A (See also CERN-NuFact-Note 65, 2001).

[Sil02]   M. Silari and H. Vincke, Neutrino Radiation Hazard at the Planned CERN Neutrino Factory, CERN-NF 105 (2002).

[Spa00]   P. Spaminato, Exploration of Solid Carbon Target and High Radiation Facility for Target Area. To be published in the proceedings of NuFACT00, Nucl. Instrum. Methods A

[Stop]   The Stopped Muon Working Group, http://wwwth.cern.ch/stoppedmuons/stoppedmuons.html

[Suk98]   The Super-Kamiokande Collaboration, Evidence for oscillation of atmospheric neutrinos, Phys. Rev. Lett. 81 (1998) 1562-1567.

[Thome]   J. Thome, Laboratory of Heat and Mass Transfer, Univ. Lausanne, http://dgmwww.epfl.ch/ltcm

[Vdm61]   S. Van Der Meer, A Directive Device for Charged Particles and its Use in an Enhanced Neutrino Beam, CERN 61-7.

[Ver00]   A. Verdier, Geometry of the Muon Storage Ring, Neutrino Factory Note 13 (Feb2000).

[Vre 98]   M. Vretenar (Ed.) Report of the Study Group on a Superconducting Proton Linac as a PS Injector, CERN/PS 98-063 (RF-HP), (1998).

[Vre00]   M. Vretenar (Ed.), Conceptual Design of the SPL, a High Power Superconducting H- Linac at CERN, CERN 2000-012, (2000).

[Vre00a]   M. Vretenar, A High-Intensity H- Linac at CERN Based on LEP-2 Cavities, Proc. Linac 2000, Monterey, August 2000, to be published.

[Weg99]   R. J. Weggel et al., Pion Yield vs. Geometry of Target and ~20 T Pulse Solenoid for a Muon Collider Experiment, PAC 99, New York (IEEE Computers Society Press, Piscataway, NJ, 1999), p. 3047-3049

[Zimm00]   F. Zimmermann et al., Fringe Fields and Dynamic Aperture in the FNAL Muon Storage Ring, CERN-SL-2000-011 (AP), also CERN-NUFACT-NOTE-21 (2000).

[Zimm00a]   F. Zimmermann, Fringe Fields, Dynamic Aperture and Transverse Depolarisation in the CERN Muon Storage Ring, CERN-SL-2000-012 (AP), CERN-NUFACT-NOTE-22 (2000).

[Zimm01c]   F. Zimmermann, Beam-Loading Compensation in the Recirculating Linacs of the CERN Neutrino Factory, CERN-SL-2001-006 AP, CERN-NUFACT Note 071 (2001).

[Zuc01]   P. Zucchelli, A Novel Concept for an Antielectron Neutrino Factory, to be published in Phys. Lett. B.